* 7 *

Stability of natural deposits during earthquakes

La stabilité des dépôts naturels lors des tremblements de terre

KENJI ISHIHARA, Professor of Civil Engineering, University of Tokyo, Japan

INTRODUCTION

The title subject envisaged herein embraces a relatively new branch in the field of geotechnical engineering. However, because its coverage is so diffused and because its content is so comprehensive, it appears almost unfeasible to touch on every facet of the recent developments and to give a complete and coherent description on the state of the art in this subject area. It is not the intention of this theme lecture presentation to attempt to carry out such a difficult task. The aim is rather to point out some of the key issues of practical significance and of current interest in the subject area for fostering fruitful and exhaustive discussions in the following sessions of this Conference.

The first subject "Soil liquefaction during earthquakes" has been the focus of primary concern and of considerable discussions among engineers and investigators since the liquefaction of sand has been identified as a major cause of damage to the ground and earth structures during earthquakes. While the early stage of its development was apparently motivated by the dramatic occurrence of liquefaction during the earthquakes in Niigata and Alaska in 1964, the impetus for prompting the study of liquefaction has been supplied incessantly by a series of large earthquakes that have occurred since then throughout the seismically active region of the world.

An important overview on the early stage of developments in the study of liquefaction was made by Yoshimi et al. (1977) on the occasion of the 9th Tokyo Conference. A comprehensive assessment of the state-of-the-art in research and practice in the field of liquefaction was made by Seed (1979) for overall developments until the late 1970's. The subsequent stage of development in this subject area was critically reviewed by Finn (1981), who put an emphasis on the evaluation of research works regarding the factors influencing the liquefaction potential of sand and also on the development of dynamic effective stress analysis.

The state-of-the-art reviews discussed above dealt primarily with the liquefaction of loose deposits of clean sands, reflecting the overwhelming majority of research activities in this direction. However, a growing interest has been created in recent years for elucidating the cyclic behavior of dense sand and of soils other than clean sand. One of the points emphasized in this paper is thus the liquefaction or cyclic mobility characteristics of dense sand and of sands containing fines or coarse-grained gravel.

Evaluation of true behavior of in-situ soil deposits during earthquakes is always essential, more than anything else, for making accurate predictions of the occurrence of liquefaction. The second point raised herein is, therefore, associated with the evaluation of soil properties based on laboratory tests on high-quality undisturbed samples of soils and also based on in-situ penetration tests.

The damage to the ground due to liquefaction such as sand boiling and surface fissuring is brought about when the surface layer composed of unliquefiable soils is sufficiently thin and when the underlying sand deposit develops liquefaction throughout a sufficient depth. In order to identify whether a given site will suffer damage due to liquefaction, it becomes necessary to have a guideline characterizing conditions of soil stratification near the ground surface. This type of problem will be taken up as the third point of consideration in this theme lecture paper.

While the issue of soil liquefaction has been discussed thoroughly and exhaustively in every respect, the problems embraced by the second title subject "Seismic stability of natural slopes" have been left unheeded and have seldom been a target of extensive investigation. However, in view of its potential importance in assessing seismic risk, it is expected that increasing attention will be given to this subject and future research efforts are stimulated in this direction.

Apart from geological and hydrological details, one of the key issues in the stability assessment of natural slopes during earthquakes would be the accurate evaluation of deformation and strength characteristics of slope-forming soil materials under seismic loading conditions. This aspect of the problem will be discussed somewhat in detail based mainly on the outcome of investigations conducted at the University of Tokyo.

The degree of accuracy in soil property evaluation should be matched by an equally accurate assessment of external loads to be applied to the soil during earthquakes. This adds to difficulty in coping with the problem of seismic stability of natural slopes. One of the points to be considered in assessing the seismically induced stress is that topography of hills or mountains where landsliding occurs could exert a profound influence on the modification of motions during earthquakes. Although quantitative field data on this subject are scarce some of the recent developments

will be introduced in this paper. Viewed overall, the subject of seismic stability of natural slopes appears still to be in its infancy of development. The writer hopes this presentation will be of some help in enhancing research efforts on this challenging subject.

SOIL LIQUEFACTION DURING EARTHQUAKES

I DEFINITIONS AND MECHANISM

1.1 Mechanism of Liquefaction

It is widely recognized that the basic mechanism of liquefaction in a deposit of loose saturated sand during earthquakes is the progressive build-up of excess pore water pressure due to the application of cyclic shear stresses induced by the upward propagation of shear waves from the underlying rock formation. Under ordinary conditions prior to an earthquake, a soil element in level ground is subjected to a confining stress due to the weight of the overlying soils. When a series of cyclic stress is applied during an earthquake, the element of loose sand tends to reduce its volume. However, since the duration of the cyclic stress application is so short as compared to the time required for drainage of water, the volume contraction can not occur immediately. In order to keep the contracting loose sand at a constant volume, some change in the existing stress system must take place. This stress change is achieved in the form of a reduction in the existing confining stress and a consequent increase of equal magnitude in the pore water pressure. Therefore, the degree of pore water pressure increase depends, on one hand, upon the state of packing indicative of potential of the volume decrease tendency and, on the other hand, upon how far the sand is sheared to extract the inherent volume decrease characteristics. When the state of sand packing is loose enough and the magnitude of cyclic shear stress is great enough, the pore water pressure builds up to a full extent in which it becomes equal to the initially existing confining stress. At this state, no effective stress or intergranular stress is acting on the sand and individual particles released from any confinement exist as if they were floating in water, as illustrated in Fig. 1(b). Such a state is called liquefaction.

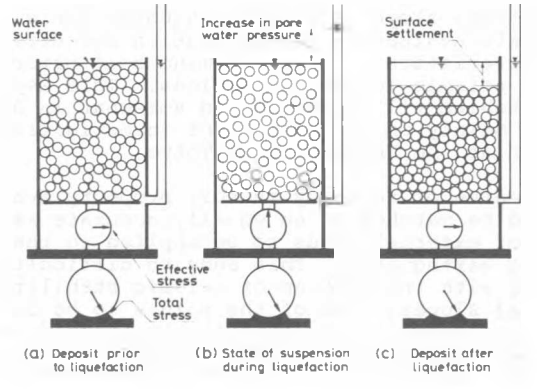

Fig. 1 Transfer of state of deposition via liquefaction

Upon occurrence of liquefaction, individual particles of the sand start to settle in water, thereby expelling pore water towards the surface of the sand deposit and when the sedimentation has taken place throughout the depth of the deposit, the sand is now deposited in a somewhat denser state, as shown in Fig. 1(c). The transfer of the state of sand from the initial deposition to the final dense state via the process of liquefaction is illustrated schematically in Fig. 1, in which the scale inside the box is assumed to indicate the effective stress and the outside scale supporting the sand-filled box indicates the total stress. The length of time for which the liquefied state continues to exist depends upon drainage conditions of the deposit and also on the duration of cyclic shear stress application following the onset of liquefaction. The longer and the stronger the cyclic shear stress application, the longer the state of liquefaction persists; and the thicker the deposit and the finer the sand composing the deposit, the longer the time required to drain the developed excess pore water pressure and therefore the longer is the state of liquefaction.

1.2 Initial Liquefaction and Cyclic Mobility

The above considerations have been concerned with an overall interpretation on the mechanism of liquefaction. A more in-depth understanding of the liquefaction phenomenon can be gained from observation of behavior of sand samples undergoing cyclic stress application in the laboratory test apparatus. This aspect of approach was first explored by Seed and Lee (1966) using a cyclic triaxial test device. Samples of saturated sand were consolidated under a confining pressure and subjected to a sequence of constant-amplitude cyclic axial stress under undrained conditions, until they deformed to a certain amount of peak to peak axial strain. Similar types of cyclic loading tests have been performed since then by a number of investigators. The results of the laboratory tests as above unveiled several common features of cyclic behavior of sand as summarized below.

A set of typical laboratory test records on sand with two different densities is demonstrated in Fig. 2. The tests were conducted on hollow cylindrical samples using a torsion shear test apparatus (Nagase, 1985). The sand used was secured from the bed of the Fuji river in Japan. The mean particle size of this sand is 0.38 mm and the uniformity coefficient is 2.21. The maximum and minimum void ratios are 1.08 and 0.53, respectively. The records of the tests shown in Fig. 2 indicate generally that the pore water pressure builds up steadily as the cyclic stress is applied, and eventually approaches a value equal to the initially applied confining pressure, thereby producing large cyclic torsional deformations. However, the manner of development of the large deformations is different depending upon the looseness and denseness of the sand. If the sand is loose, the pore water pressure increases suddenly to a value equal to the confining pressure, and the large deformations occur rapidly with a shear strain as high as ± 20 %. When the sand will undergo unlimited deformations without mobilizing significant resistance to deformation, the sand is said to have liquefied. The manner in which it occurs suddenly and it is accompanied by unlimitedly large deformation is the characteristic feature of the earth-

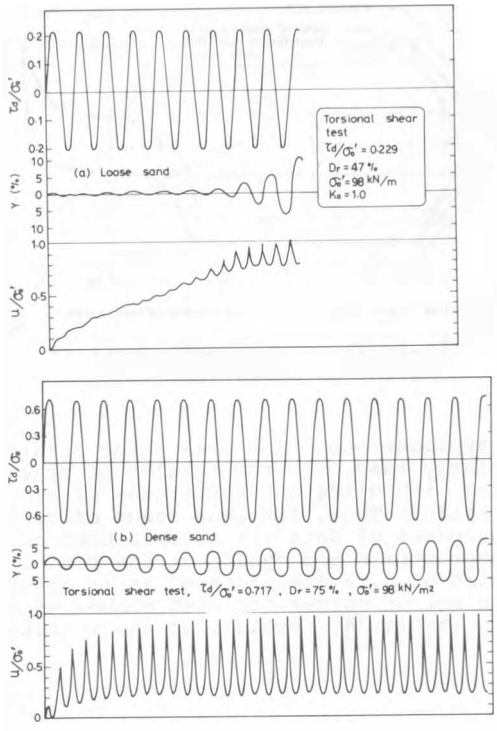

Fig. 2 Records of cyclic torsional shear tests

quake-induced liquefaction. On the contrary, if the sand is dense, the pore water pressure increases more slowly with cyclic fluctuation, and after its peak value becomes equal to the initial confining pressure, its cyclic variation comes to take a steady-state form as can be seen in Fig. 2(b) in which the pore water pressure is cycled with a frequency twice that of the applied load. The torsional shear strain in the dense sand increases steadily with progression of the cycle, but it never becomes larger than a certain limit. The cyclic behavior of dense sand as above in which a peak cyclic pore water pressure becomes equal to the initial confining pressure as a result of cyclic loading and subsequent cyclic stress applications causes limited strains to develop is called "cyclic mobility" by Castro (1975) or "peak cyclic pore pressure ratio of 100 % with limited strain potential" by Seed (1979).

Whether a sand is loose or dense, the pore water pressure builds up steadily in the course of cyclic stress applications and a state is reached after some number of cycles in which a peak pore water pressure in the cyclic fluctuation becomes momentarily equal to the initial confining pressure. Such a state has been referred to as "initial liquefaction". For loose sand, the initial liquefaction coincides with the incipient condition for a state of liquefaction accompanied by large deformations, and accordingly, both terminologies have been used interchangeably. For dense sand, a state of initial liquefaction does not produce large deformations, but since some degree of softening takes place accompanied by a seizable amount of cyclic strain, onset of initial liquefaction may be taken as a measure to recognize a state of cyclic instability in the dense sand.

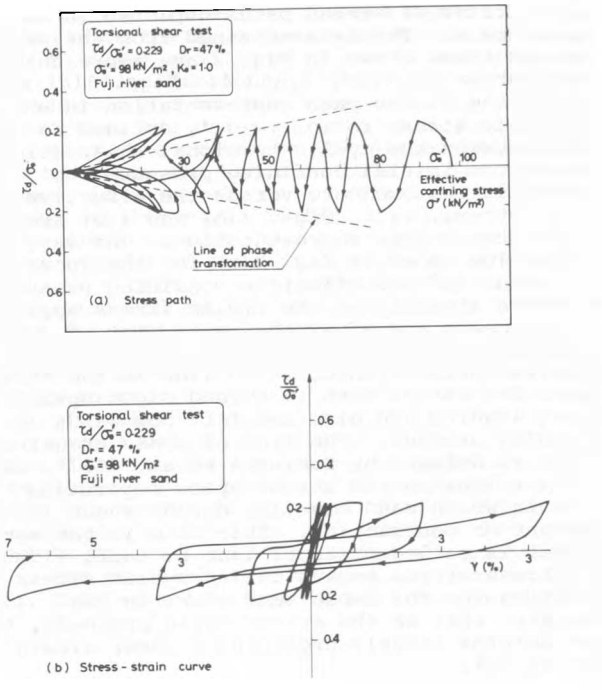

Fig. 3 Stress path and stress-strain curve for loose sand obtained form the cyclic torsion shear test

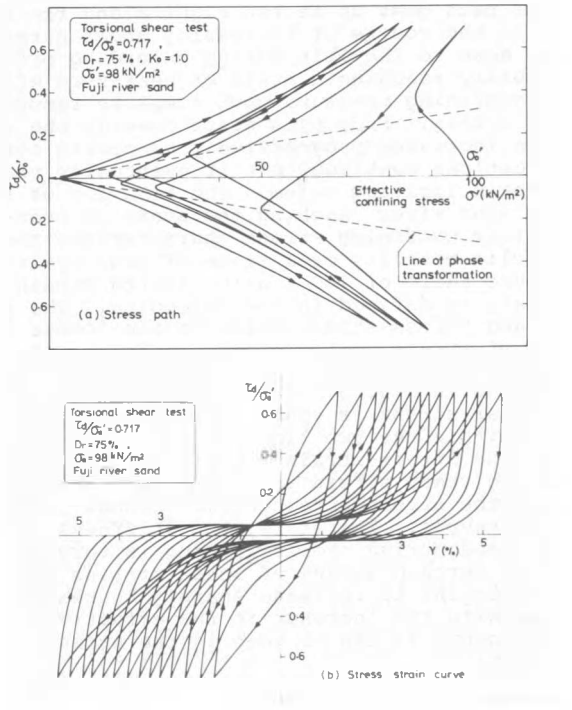

Fig. 4 Stress path and stress-strain curve for dense sand obtained from the cyclic torsion shear test

The characteristic behavior of sand as above will be more clearly understood, if the cyclic behavior is expressed in terms of stress-strain curves and also in terms of stress paths depicted in the stress space. The data obtained from the same tests as those shown in Fig. 2 are represented in this fashion in Figs. 3 and 4. Figs. 3(a) and 4 (a) are the stress path representation in which the cyclic stress ratio, τ_d/σ_0', defined as the ratio between the cyclic torsional shear stress, τ_d, and the initial confining pressure, σ_0', is plotted in the ordinate versus the effective confining stress, σ_0'. Figs. 3(b) and 4(b) are the stress strain type representation. The result of such a plot shown in Fig. 3(a) for the loose sand indicates that the effective confining pressure decreases steadily as the cyclic stress application proceeds and after the peak point of cyclic shear stress touches a point on a line of what is called phase tranformation line in the stress space, the stress path is turned right upwards during loading and directed left downwards in unloading process. The line of phase transformation as defined by Ishihara et al. (1975) is a straight line in the stress space separating two zones in which sand behavior during shear is dilatant or contracting. This line is the same as what is called critical line by Luong (1980). The stress-strain curves during cyclic stress application for the loose sand shown in Fig. 3(b) indicate that as the stress cycle proceeds, the sand deforms largely producing a shear strain as high as 5 %.

The test data on dense sand shown in Fig. 2 are presented in Fig. 4 in terms of stress path and stress-strain curves. It may be seen in the stress space representation that after the stress path passes the line of phase transformation, the stress path goes up to the right along the failure line in the course of increasing shear stress and comes down to the left during unloading process, eventually reaching a state of near-zero effective confining pressure upon complete removal of shear stress. From this state onwards the shear strain increases progressively as cyclic stress applications continue, but it eventually reachs a certain limiting value. The behavior of the dense sand after reaching the state of near-zero effective confining stress characterizes the state of cyclic mobility or a state of peak cyclic pore pressure ratio of 100 % with limited strain potential, as defined in the foregoing. The stress path and stress-strain curve in the course of one cycle of stress application were taken out of the cluster of the curves shown in Fig. 4(b) and demonstrated in Fig. 5. It can be seen that while the shear stress is small, keeping the stress point within the two lines of phase transformation, the stress-strain curve is nearly flat, but once the shear stress is increased above this level, the stress-strain curve becomes increasingly steeper. Therefore, the stiffness of the dense sand during cyclic loading is very small until a certain amount of shear strains develop, but it begins to increase sharply thereafter in unison with the increase in the effective confining pressure as can be seen in the stress path in Fig. 5(a).

1.3 Evaluation of Liquefaction and Cyclic Mobility

In the cyclic stress-strain curve as shown in Fig. 4, it is possible to read off peak values of developed shear strain at each stage of the cyclic

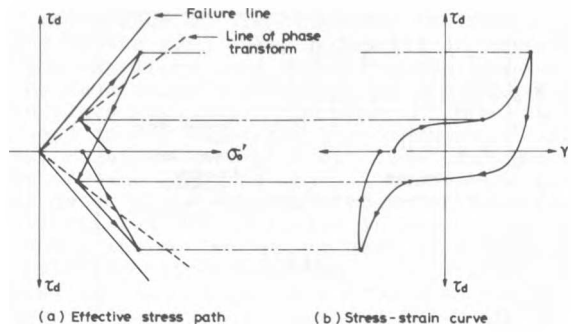

Fig. 5 Illustration for cyclic mobility behavior of dense sand

stress applications. The peak shear strains can be similarly read off from results of other tests conducted with different amplitudes of cyclic stress ratio. Thus, for each stage of cyclic loading, pairs of data can be assembled on the peak shear strain and cyclic stress ratio. When such pairs of data are plotted, it is possible to obtain a set of curves for each number of cycles as shown in Fig. 6. Because of the symmetrical

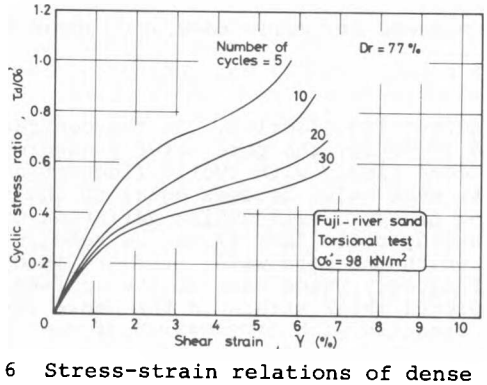

Fig. 6 Stress-strain relations of dense sand for different numbers of cycles

nature of such curves with respect to the origin, only the test data on one side of cyclic loading are demonstrated in Fig. 6. The curve as above may be deemed to represent a stress-strain characteristics of sand under cyclic loading conditions and will be referred to as cyclic peak stress-strain curve. The results of a series of cyclic torsion shear tests on Fuji river sand similarly conducted with different densities are summarized in Fig. 7. It may be observed that, virtually for all relative densities, there exists a convex part in the range of small strains, but it is followed by a concave portion with increasing level of shear strains. Fig. 7 also indicates that for dense sand there appears to be a cyclic strain level beyond which the sand is unable to deform in the given number of cycles without mobilizing an extremely large amount of resistance. This is the characteristic behavior of dense sand in the state of cyclic mobility. In each of the cyclic peak stress-strain curves shown in Fig. 7, an approximate portion is indicated at which the developed pore water pressure becomes nearly equal

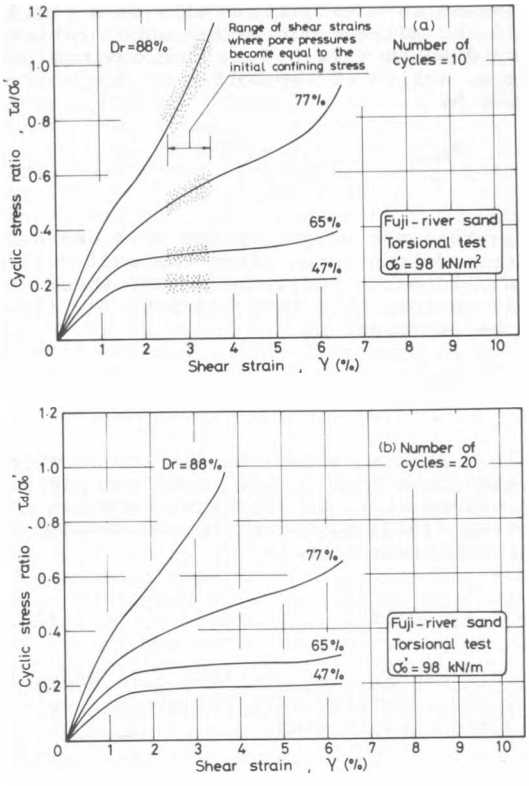

Fig. 7 Stress-strain relations of sand with different densities

to the initial confining pressure for the first time in the course of cyclic stress applications.

For instance, if the cyclic stress is to be applied ten times for a sample with a relative density of 77 %, the cyclic stress ratio required to cause 100 % pore water pressure build-up is somewhere between 0.50 and 0.58 and the peak cyclic strain produced ranges between 2.5 and 3.5% as read off from Fig. 7(a). Interpreted in this manner, it becomes apparent from Fig. 7 that the magnitude of the peak strain at which 100 % pore water pressure build-up takes place lies within a relatively narrow range between 2.5 and 3.5 % in terms of single amplitude, irrespective of widely different cyclic behavior depending upon the density of sand. In the case of loose sand, intolerably large deformation is produced immediately after the inducement of about 3 % cyclic shear strain accompanied by the development of 100 % pore water pressure or initial liquefaction. Therefore, failure of loose sand under cyclic loading conditions may be defined on the basis of development of either 2 to 3 % single-amplitude cyclic shear strain or 100 % pore water pressure. This criterion has been widely used for defining a state of failure in loose sand due to liquefaction, and will be accordingly adopted in this paper in the same context. In the case of dense sand, the development of about 3 % cyclic shear strain does not bring about any state of instability involving intolerably large deformations. Therefore, any level of cyclic shear strain other than 3 % may be considered appropriate to define a state of failure for the dense sand undergoing cyclic loads.

However, a recent trend which has found relatively wide recognition is the use of the 3 % single-amplitude cyclic shear strain as a criterion to define the failure state of dense sand. It may be recalled that the development of about 3 % cyclic strain in dense sand induces concurrently the state of initial liquefaction or 100 % pore water pressure build-up and in this respect it may well be accepted that the onset of initial liquefaction can be used as a criterion to define the start of cyclic mobility and hence a state of failure for the dense sand as well as a criterion to specify the onset of liquefaction for the loose sand. For the above reasons, the 3 % cyclic shear strain will be adopted in this paper, unless otherwise stated, as a criterion to consistently define liquefaction and cyclic mobility of any density of sand from loose to dense state.

In order to represent the liquefaction and cyclic mobility characteristics of sand in a consistent manner, it will be useful to read off values of cyclic stress ratio required to cause a state of initial liquefaction or a certain magnitude of cyclic shear strain and to plot these values against the number of cycles. Such a data arrangement was carried out for the test data presented in Fig. 7, and the results are plotted in Fig. 8 for the sand with a relative density of 88 %. This type of plotting will frequently be

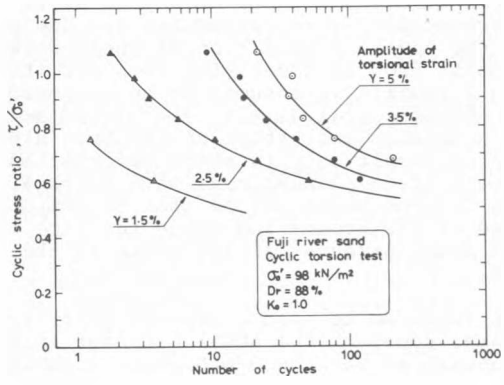

Fig. 8 Cyclic stress ratio versus number of cycles

used in the following pages. Another method of data presentation is to plot the cyclic stress ratio causing a certain magnitude shear strain in a given number of cycles against the relative density of the sand. Such a plot was also made for the above test data and the results are shown in Fig. 9. As may be seen from this figure, the cyclic stress ratio causing a certain magnitude of shear strain in 20 cycles increases with increasing rate as the relative density of sand increases. It is apparent from the data in Fig. 9 that if a value of cyclic shear strain greater than 3 % is adopted as the criterion to define liquefaction or cyclic mobility, the corresponding strength in terms of the cyclic stress ratio is evaluated significantly higher. Therefore, specification of the cyclic strain and number of cycles used for defining liquefaction and cyclic mobility should be clearly stated particularly when the sand is dense.

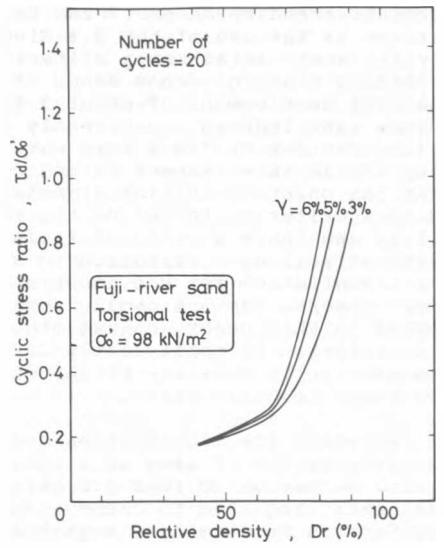

Fig. 9 Relationship between cyclic stress ratio and density causing different levels of shear strains

II CYCLIC SHEAR STRESSES INDUCED BY MOTIONS DURING EARTHQUAKES

The shear stresses induced at any point in the level ground during an earthquake are due probably to the upward propagation of shear waves in the deposit from an underlying rock formation. If a soil profile is assumed to be composed of a series of horizontal layers, the ground motions due to a seismic excitation at the base are considered to result only in shear deformation and the theory of one-dimensional wave propagation through layered media can be used to compute the response of the ground and hence the time histories of shear stresses at any depth in the soil deposit.

Without recourse to such a refined analytical procedure, however, the shear stresses in the soil deposit at shallow depth where liquefaction is most liable to occur can be assessed by means of a simpler procedure proposed by Seed and Idriss (1971). Consider a soil column to a depth, z, as shown in Fig. 10. If the soil column to a depth, z, were assumed to move horizontally as a rigid body and if the maximum horizontal acceleration on the ground surface is, a_{max} the maximum shear stress, τ_{max}, acting at the bottom of the soil column would be

$$\tau_{max} = \frac{a_{max}}{g} \cdot \gamma_t \cdot z \qquad \cdots\cdots(1)$$

where γ_t is the unit weight of the soil and g is the gravity acceleration. Since the soil column moves as a deformable body, the actual shear stress will be less than that given by Eq. (1) and might be expressed by

$$\tau_{max} = \frac{a_{max}}{g} r_d \cdot \gamma_t \cdot z \qquad \cdots\cdots(2)$$

where r_d is a stress reduction coefficient which takes a value less than unity. Seed and Idriss expressed values of r_d in graphical form but Iwasaki et al. (1978) subsequently recommended the use of the empirical formula

$$r_d = 1 - 0.015z \qquad \cdots\cdots(3)$$

where z is in meters. By dividing both sides of Eq. (2) by the effective vertical stress, σ_v', Eq. (2) is modified to read,

$$\frac{\tau_{max}}{\sigma_v'} = \frac{a_{max}}{g} \cdot r_d \cdot \frac{\sigma_v}{\sigma_v'} \qquad \cdots\cdots(4)$$

where σ_v denotes the total vertical stress. The above equation has been used widely to assess the magnitude of shear stress induced in a soil element during an earthquake. One of the advantages for using Eq. (4) is that the vast amount of information on the accelerations ever recorded on the ground surface can be used directly to assess the shear stresses in the ground.

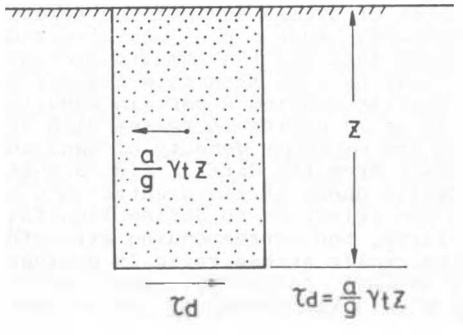

Fig. 10 Relationship between the ground acceleration and the induced shear stress

It is apparent that the type of relation expressed by Eq. (4) can hold valid at any instant of time throughout the time duration of earthquake motions. This implies the fact that any time change in the shear stress in the soil deposit at shallow depths takes place in unison with time variation of the acceleration on the ground surface, the difference being only in the relative magnitude. Therefore, a time history of shear stress in the soil has the same general shape as the time history of acceleration at the ground surface. When performing soil tests in the laboratory simulating the loading conditions during an earthquake, it might be warranted, therefore, that the time histories of shear stress having the same pattern as those of recorded accelerations are applied to soil samples in the test apparatus.

III LIQUEFACTION AND CYCLIC MOBILITY IN IRREGULAR LOADING

3.1 Effects of Load Irregularity of Liquefaction Potential of Loose Sand

It is well-known that the time history of shear stresses induced on a soil element due to motions

of an earthquake consists of an erratic sequence of simple shear mode of stress alteration in the horizontal plane in the soil deposit. On the other hand, most of the laboratory tests used to investigate the liquefaction characteristics of soils under seismic loading conditions have been carried out by applying a sinusoidal or pulsating pattern of shear stresses with constant amplitude. Because of the wide availability of the loading system and the ease in operating the apparatus, the test with uniform cyclic stress applications will continue to be a most commonly used procedure for studying soil characteristics in the laboratory. In view of these circumstances, it is necessary to establish a rule of correspondence in which strength data from uniform cyclic loading test can be converted to a strength parameter indicative of liquefaction or cyclic mobility of soils under actual seismic loading conditions.

In order to evaluate the effect of randonmness on the liquefaction potential of loose sand, multiple series of dynamic triaxial and torsional shear tests were carried out by Ishihara and Yasuda (1973, 1975) by employing several wave forms of acceleration records obtained during recent large-scale earthquakes. The outcome of these tests was summarized in a form of load irregularity factor defined as the ratio between the amplitude of uniform cyclic stress causing liquefaction in 20 cycles, τ_ℓ, and the maximum shear stress, $\tau_{max,\ell}$, in irregular load sequence great enough to induce liquefaction in the sample subjected to the same initial confining stress. It was also shown that the response of loose sand to pore water pressure buildup under irregular loading conditions did not differ appreciably although the load patterns are in full variety in detail, and the response could be classified roughly into two groups according to whether the irregular load time history has an appearance of a constant-amplitude vibration or a single impulse. A simple procedure was then suggested to identify a given time history whether it is of the shock type or of the vibration type. In this procedure, only the wave shape prior to the advent of the maximum shear stress was considered because the wave shape after the passage of the peak exerts no substantial influence on the pore water pressure build-up. Also only the part of the time history on the side of the peak was considered for identification purposes. If the wave form has one or two spikes, before the advent of the peak, whose amplitude is greater than 60 % of the peak, the wave form is identified as being of the shock type. If more than three spikes having the amplitude greater than 60 % of the peak exist in the trace of the time history on the same side of the maximum stress, then the wave is identified as being of the vibration type. Although the above rule is empirical, it has been found satisfactory to identify many existing time histories of earthquake motions into two families, having generally similar pore water pressure response characteristics. For each type of wave form as classified above, the load irregularity factor was established on the basis of a number of test data on loose sand employing a variety of wave forms. The load irregularity factor thus obtained is shown in Table 1. In the Japanese code of bridge foundation design in which the method of liquefaction analysis is specified, the effects of load irregularity are taken into account through a multiplying coefficient, C_2, which is equal to the reciprocal of the load irregularity factor. The value of C_2 is also indicated in Table 1.

Table 1 LOAD IRREGULARITY FACTOR FOR LOOSE SAND

	Shock type	vibration type
$\tau_\ell/\tau_{max,\ell}$	0.55	0.70
$C_2=\tau_{max,\ell}/\tau_\ell$	1.82	1.43

Using the load irregularity factor, the cyclic strength of any sand determined by the cyclic triaxial tests can be converted to the strength which would be encountered if the sand is subjected to an irregular load. Let the cyclic stress ratio causing liquefaction or 3 % axial strain in 20 load ccyles be denoted by, $(\sigma_{d\ell}/2\sigma_0')_{20}$, where $\sigma_{d\ell}$ denotes the amplitude of cyclic axial stress inducing failure in the sample. Then, the maximum stress ratio, $\tau_{max,\ell}/\sigma_0'$, great enough to induce liquefaction or 3 % shear strain in irregular loading may be assessed through the following formula,

$$\frac{\tau_{max,\ell}}{\sigma_0'} = C_2 \left(\frac{\sigma_{d\ell}}{2\sigma_0'} \right)_{20} \qquad \cdots\cdots(5)$$

3.2 Effects of Multi-Directional Shaking on the Liquefaction Resistance of loose Sand

In the preceding section, the motions in a horizontal soil deposit due to an upward propagation of shear waves during an earthquake were assumed to take place under two-dimensional plane strain conditions and, accordingly, the induced cyclic stresses reciprocate in one direction alone, However, actual earthquakes generate much more complicated patterns of motions involving changes not only in amplitude but also in direction. Therefore, the resulting mode of shear stress alteration is an irregular excursion of shear stress over the horizontal plane without any restriction in the direction of motions. The effects of such multi-directional loading on the liquefaction potential of sand were investigated by Pyke et al. (1975) and Seed et al. (1978) using both random loading patterns and almost circular excursions of constant-amplitude cyclic shear stress on the horizontal plane. The results of their studies indicated that the resistance to liquefaction of loose sand under either type of multi-directional shaking is approximately 15 % smaller than the liquefaction resistance obtained in uni-directional loading.

In an effort to study the same aspect of the problem, Ishihara and Yamazaki (1980) conducted a series of multi-directional simple shear tests on loose saturated sand by employing circular and elliptic load paths over the plane of shear stress application. The results of the tests indicated a reduction in the cyclic resistance under multi-directional loading, of 35 % at most, as compared to the cyclic resistance in the one-directional loading tests. It is apparent that when gyratory simple shear is applied to soil with a constant

amplitude, the axis of the major principal stress is spinning with an apex angle of 90 degrees, as illustrated in Fig. 11(a). Since the continuous revolution of the principal stress direction is likely to exert a disturbing influence on the internal structure of sand more drastically than does the cyclic shear without the revolution (Fig. 11b), it is not surprising that the liquefaction resistance was reduced to some extent by the revolution of the principal stress in the execution of the cyclic stress applications.

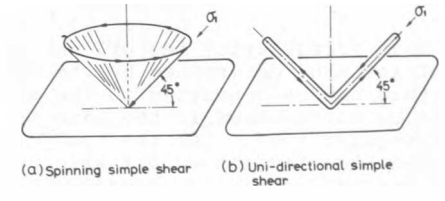

Fig. 11 Mode of cyclic stress changes in simple shear

In order to evaluate the effects of an irregular pattern of gyratory shear stresses, several series of multi-directional undrained simple shear tests have been recently conducted by Nagase (1985) at the University of Tokyo on saturated samples of Fuji river sand by means of a simple shear test device incorporating two pneumatic cyclic loaders in mutually perpendicular horizontal directions. A sample, 3.0cm in height and 7.0 cm in diameter, was consolidated isotropically, and then a set of two components of acceleration time histories obtained during recent earthquakes were applied as an input load in the two cyclic loaders installed in mutually perpendicular directions (Ishihara - Yamazaki, 1980). In conducting the tests, the time scale of irregular shear stress applications was enlarged 8 times the actual time histories in order to accurately reproduce the recorded time histories in the pneumatic loaders. Since the effect of frequency of cyclic loading is known to be inconsequential, the application of irregular simple shear stress with an enlarged time scale would appear not to exert any adverse influence in evaluating the liquefaction and cyclic mobility of sand.

One of the results of these tests on loose sand employing the NS- and EW-components of acceleration time histories recorded in the Niigata earthquake (1964) is demonstrated in Fig. 12. Although the tests were conducted with the enlarged time scale, the time scale of the recorded data was shortened to coincide with the real scale of the original time histories of acceleration. The test data displayed in Fig. 12 were those obtained through such data processing. Shown in Fig. 13 is a trajectory traced on a horizontal plane by a combination of the two components of acceleration time histories obtained in Niigata. The irregular pattern of simple shear stress changes as displayed in this trajectory was applied to loose specimens of sand in the simple shear test device. Since there exist two maximum shear stresses each in the EW- and NS-directions, it is necessary to stipulate which of these two maximums are used to represent the relative magnitude of the combined time histories. In the following,

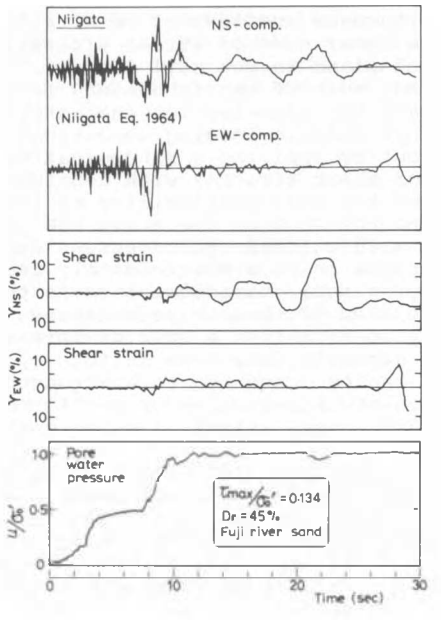

Fig. 12 Recorded pore pressure and shear strains in the multi-directional irregular loading simple shear test on loose sand

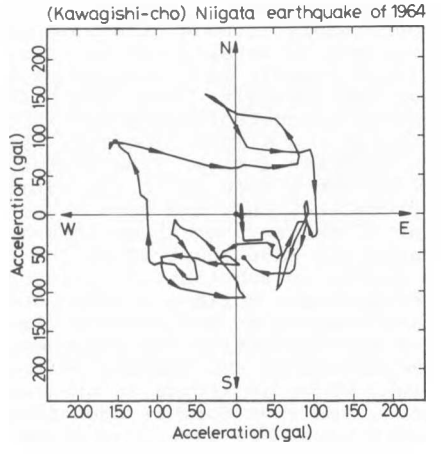

Fig. 13 Trajectory of accelerations recorded in Niigata

the larger value of the two maximum shear stresses will be adopted for this purpose. The maximum shear stress thus defined will be denoted by τ_{max} and the maximum stress ratio is defined as τ_{max}/σ_0', where σ_0' is the effective confining stress applied to the sample during isotropic consolidation. The time histories of shear strains in two directions and pore water pressure obtained from the test are shown in Fig. 12. These are the results obtained in the last step in a series of tests in which the amplitude of the irregular stress histories had been stepwise increased. In the last step in this series, the test was conducted by employing a maxi-

mum stress ratio of 0.134 which was great enough to produce a state of liquefaction in the sample. As shown in Fig. 12, the pore water pressure became equal to the initial confining pressure almost concurrently with the advent of the peak shear stress and remained stationary thereafter even though the sample is still undergoing stress changes. This characteristic behavior is exactly the same as that observed in the test of uni-directional irregular loading. Time changes in shear strains in two directions indicate that the sample deformed largely after the onset of liquefaction producing a shear strain as much as 12 %. The results of the tests in this series are summarized in Fig. 14 in terms of the relationship between the maximum stress ratio, τ_{max}/σ_0' and the shear strain, γ. In the abscissa of this diagram, two strains observed at two different stages of strain development are plotted. One is the strain occurring at the time of initial liquefaction, γ_ℓ, and the other is the maximum shear strain, γ_{max}, which is encountered at a later time. These two strains are defined as the magnitude of vectors in the plot of strain trajectory as illustrated in Fig. 15. Fig. 14 shows that, while the shear strain at liquefaction remains limited, it grows almost indefinitely large in the course of cyclic stress alteration following the peak stress application. Also shown in this figure is the result obtained from the uni-directional cyclic tests with 20 cycles of constant-amplitude shear stress applications using the same simple shear test apparatus. It may be seen in Fig. 14 that the cyclic strength is larger for the multi-directional irregular loading than for the conventional type uniform loading with 20 cycles.

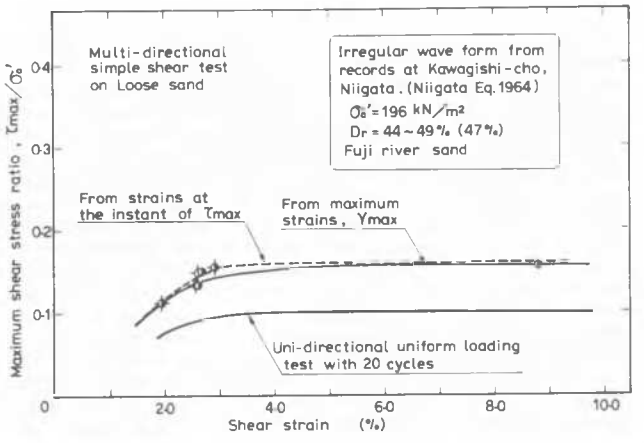

Fig. 14 Relationships between the maximum shear stress ratio and strains in multi-directional irregular loading

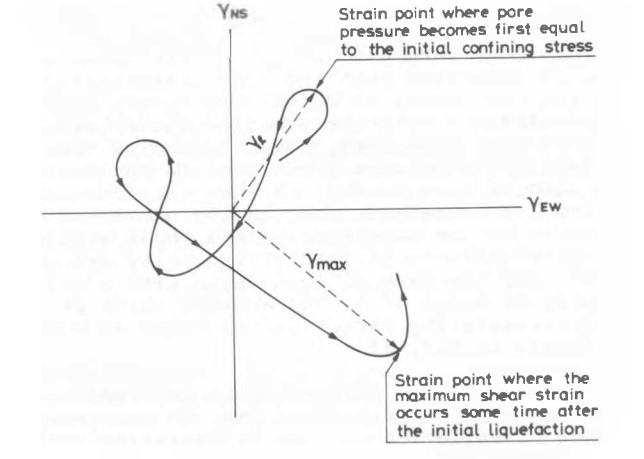

Fig. 15 Definitions of shear strain at initial liquefaction and the maximum shear strain in the multi-directional irregular loading simple shear test

Similar series of multi-directional loading tests were conducted on dense Fuji river sand by employing the time histories of acceleration obtained at

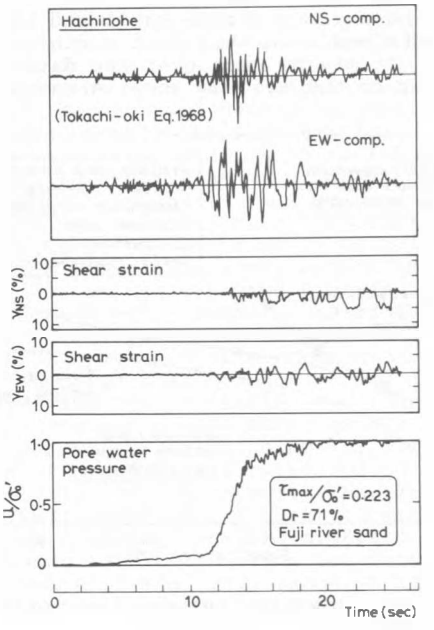

Fig. 16 Recorded pore pressure and shear strains in the multi-directional irregular loading simple shear test on dense sand

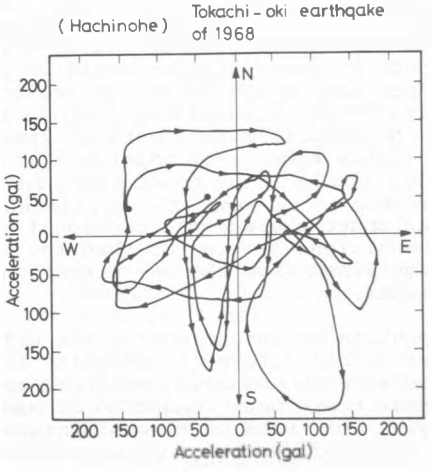

Fig. 17 Trajectory of accelerations recorded in Hachinohe

Hachinohe during the Tokachi-Oki earthquake of 1968. The time histories used as the loads in two directions in the simple shear test apparatus are displayed in Fig. 16 and their trajectory on the horizontal plane for a certain time span of main shaking is demonstrated in Fig. 17. One of the results in this test series is also shown in Fig. 16. The maximum stress ratio, τ_{max}/σ_0', employed in this test was 0.223 which occurs in the time history of the NS-component. It may be seen that the pore water pressure jumped up almost simultaneously with the application of peak stress and remained nearly stationary thereafter, whereas the shear strain began to fluctuate considerably, reaching a value as large as 5 %. It is obvious that the development of shear strain after the attainment of stationary pore pressure is a consequence of the cyclic mobility. The relationship between the maximum stress ratio and the shear strain obtained from this test series is shown in Fig. 18. It may be seen that the data points corresponding to the maximum shear strains lie some

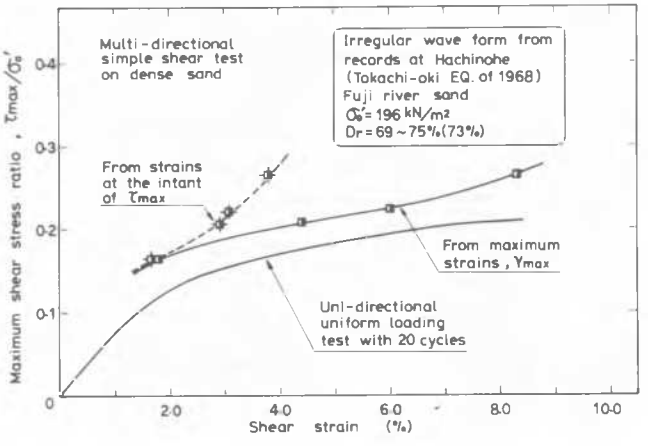

Fig. 18 Relationships between the maximum shear stress ratio and strains in multi-directional irregular loading

distance to the right of the data points plotting the shear strain attained at the instant of peak shear stress applications. This fact indicates that even after the peak shear stress passed by with 100 % pore water pressure build-up, a significant amount of shear strains could be produced in the specimen due to the effect of cyclic mobility. The results of uni-directional uniform loading tests on the samples with identical density using the same simple shear test apparatus are also shown in Fig. 18. It is to be noted that, in the same fashion as for loose sand, the cyclic strength of dense sand under the multi-directional irregular loading conditions is greater than the cyclic strength obtained from the uni-directional cyclic loading tests.

For the prupose of investigating the effects of multi-directional nature of irregular loading on the cyclic strength of sand, multiple series of simple shear tests were conducted by Nagase (1985) by employing five sets of time histories of accelerations recorded in recent major earthquakes. The names of the earthquakes and locations where each acceleration record was obtained are shown in the inset in Figs. 19 and 20. In all sets of

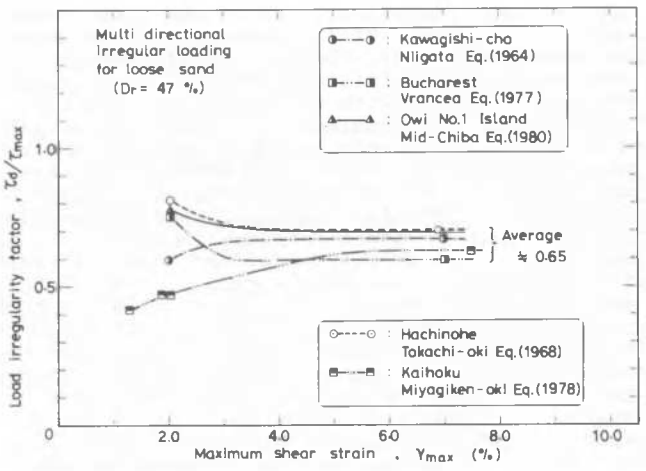

Fig. 19 Load irregularity factor for loose sand in multi-directional irregular loading

these records, time histories in both NS- and EW-components have a wave form which is classified as the shock type according to the rule mentioned in the foregoing section. Therefore, when these records are transferred as the time histories of shear stress alteration in the simple shear test device, the resulting response of the sand is expected to be influenced significantly by the peak. For each set of the time histories, the maximum shear stress ratio versus strain curves such as those shown in Figs. 14 and 18 were obtained for both loose and dense samples of Fuji river sand. Then the maximum shear stress ratio required to produce a given amount of the maximum shear strain, γ_{max}, in the multi-directional loading test was compared with the cyclic stress ratio causing the same amount of shear strain at the end of the application of 20 cycles in the uni-directional loading test. The outcome of such comparison is expressed in terms of the load irregularity factor which is defined as the ratio between the amplitude of uniform cyclic stress and the magnitude of the maximum shear stress required to produce the same amount of shear strain. The load irregularity factor, τ_d/τ_{max}, thus obtained for each of the test series employing different time histories is summarized in Figs. 19 for loose sand and in Fig. 20 for dense sand. Fig. 19 indicates that the load irregularity factor for the five cases of multi-directional loading stays within a relatively narrow range between 0.6 and 0.7 for loose sand, notwithstanding the variety in detail of the wave forms used in the test. It can also be seen in Fig. 19 that the load irregularity factor remains practically unchanged irrespective of the magnitude of the shear strain at which the effects of load irregularity are evaluated. For the case of loose sand with a relative density of about 47 %, the average value of the load irregularity factor may be taken as 0.65, as indicated in Fig. 19.

The outcome of the multi-directional loading tests on dense sand summarized in Fig. 20 indicates trends of variation in load irregularity factor, which are similar to those for loose sand, with respect to changes in load time history and the shear strain at which the factor is evaluated. Although the scatter in the results is larger in this case, an average value of 0.70 may be assigned

to the load irregularity factor for the dense sand.

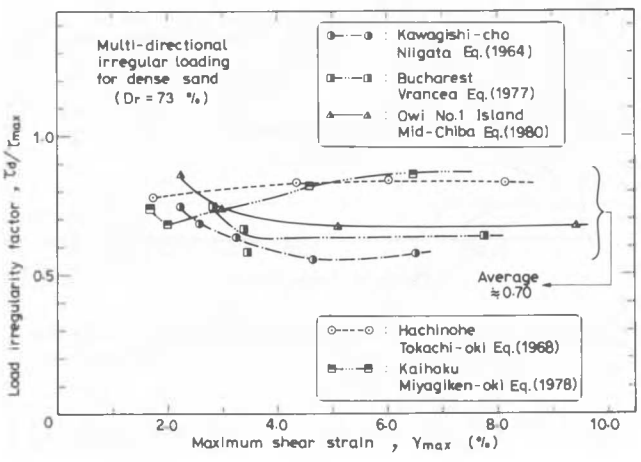

Fig. 20 Load irregularity factor for dense sand in multi-directional irregular loading

For the case of uni-directional loading on loose sand, the assessment of the strength in irregular loading was made using the coefficient, C_2, in Eq. (5). When the multiplicity in loading directions is to be considered, another coefficient needs to be incorporated in Eq. (5). The Japanee design code for bridge foundation design introduces a multiplying coefficient, C_5, to allow for this effect by rewriting Eq. (5) as follows,

$$\frac{\tau_{max,\ell}}{\sigma_0'} = C_2 \cdot C_5 \left(\frac{\sigma_{d\ell}}{2\sigma_0'} \right)_{20} \qquad \cdots\cdots(6)$$

The results of investigations on loose sand by Seed et al. (1978) and Ishihara and Yamazaki (1980) suggested the use of 0.8 to 0.9 for the coefficient, C_5. Thus, for the shock type loading, the coefficient with combined effects of load irregularity and multiplicity for loose sand may be given by

$$C_2 \cdot C_5 = 1.82 \times (0.8 \sim 0.9) = 1.46 \sim 1.64 \qquad \cdots(7)$$

On the other hand, the outcome of the multi-directional irregular loading tests as summarized in Fig. 19 may be regarded as a direct indicator of the combined effects. Thus, by taking the reciprocal of the average load irregularity factor, the coefficient may be given as,

$$C_2 \cdot C_5 = 1/0.65 \fallingdotseq 1.55 \qquad \cdots\cdots(8)$$

The coefficient thus obtained is shown to be in good agreement with the net effect of two multiplying coefficients used in the Japanese code.

With respect to the dense sand, little has been reported on the separate effect of load irregularity and multiplicity in loading direction. Therefore, the results of multi-directional simple shear tests summarized in Fig. 20, which is directly indicative of the combined effects, may be used to obtain the multiplying coefficient. Thus, for the dense sand with a relative density of about 70 %, the coefficient is given by

$$C_2 \cdot C_5 = 1/0.70 \fallingdotseq 1.45 \qquad \cdots\cdots(9)$$

IV LIQUEFACTION POTENTIAL OF FINE-GRAINED SOILS

4.1 General Considerations

Liquefaction is a state of particle suspension resulting from a release of contacts between particles of soil constituting a deposit. Therefore, the type of soil most susceptible to liquefaction is one in which the resistance to deformation is mobilized by friction between particles under the influence of confining pressures. It is a well-known fact that the contribution from the friction to resist deformation generally tapers off as the grain size of soils becomes smaller. It appears likely, therefore, that there is a boundary in terms of the grain size separating potentially liquefiable sandy soils from fine-grained soils which are not vulnerable to liquefaction. Such a boundary curve was proposed by Tsuchida (1970) in terms of a grain size distribution curve as shown in Fig. 21, on the basis of the results of sieve analyses made on a number of soils that were known to have liquefied or not to have liquefied during past earthquakes. On the other hand, it is also widely accepted that coarse-grained materials such as gravel and crushed stones are immune to liquefaction, because of the small amount of volume decrease potential during shear for one thing and because of a rapid dissipation of pore water pressure, if any, for the other. Therefore, a boundary may well exist in the chart of grain size distribution dividing zones of high and low liquefaction susceptibility. Such a boundary is also shown in the chart of Fig. 21. Since it is difficult to

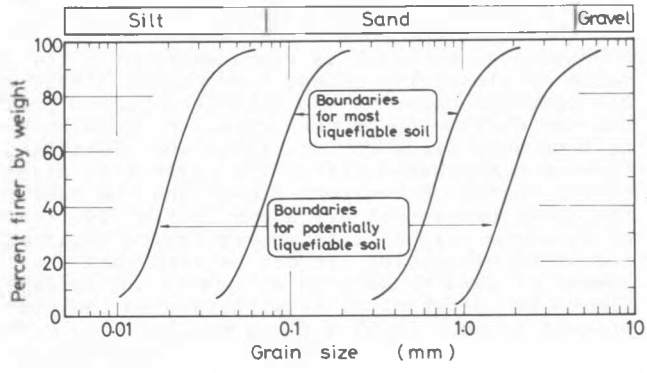

Fig. 21 Limits in the gradation curves seperating liquefiable and unliquefiable soils (Tsuchida, 1970)

establish clear-cut boundaries in the above context, two boundary lines are provided for both the fine-grained portion and for the coarse-grained part of the gradation chart. The set of two inner curves in Fig. 21 is used to identify a soil most likely to liquefy, and the soil with a gradation curve falling in the zones between the outer and

inner curves is identified as being a soil type which is less likely to liquefy.

According to the inner curve on the left in Fig. 21, a soil containing 40 % fines is identified as being vulnerable to liquefaction, where fines is defined as the fine-grained fraction passing the No. 200 sieve with a mesh size of 0.074 mm. Whether or not a soil containing such a large percentage of fines can develop liquefaction would be a subject of concern requiring further investigations. However, it would appear that the liquefiability of soils with high fines contents will depend on the physical characteristics of the fines themselves. In fact, if the fines have a strong cohesion, it will inhibit separation of individual particles when the soil is about to liquefy. Consequently, such a soil will exhibit a strong resistance to liquefaction. In contrast to this, if the fines consist of minerals with dry surface texture free from adhesion, it will easily permit separation of individual grains, and therefore the sand containing such fines will exhibit a large potential of liquefaction.

It has been a common recognition in the expertise of soil mechanics that the cohesiveness of fines can be identified in terms of the plasticity index. The use of the plasticity index of soils as a measure to identify the liquefiability of fine-grained soils was addressed by Ishihara et al. (1980) in connection with investigations of the failure of tailings dams during earthquakes. It is well known that the essential ingredient of the tailings from mines is ground-up rock. Since country rocks do not generally undergo weathering or other natural deteriorating processes, individual particles of rock flour produced by grinding still preserve the hardness of parent rocks with dry surface textures free from adhesion. Therefore, the rock flour, in its water saturated condition, does not possess significant cohesion and exhibits shearing resistance mainly by the mobilization of internal friction. Hence, although a rock flour may be classified as clay or silt in terms of its grain size, its strength and deformation characteristics will closely resemble those of a sand. The fact that the rock flour behaves as if it were cohesionless material is represented by a low value of plasticity index. Casagrande (1933) in his original paper on the Atterberg limits pointed out the difficulty of performing the consistency test on some kinds of rock flour and identified them as non-plastic silt. The grain size distribution curves of the rock flours that he used for the consistency test are shown in Fig. 22, together with the values of Atterberg limits obtained for these materials. It can be seen that the powder of hard rocks such as quartz and feldspar showed no plasticity, notwithstanding the presence of as much as 95 % fines smaller than 0.005 mm in grain size. The powder of mica having inherent cohesiveness showed a plasticity index of 21 although the grain size curve is almost identical to that of the quartz and feldspar powder. The Boston clay, in sharp contract, showed a plasticity index of 16 even though it was composed of much coarser materials with approximately 45 % fines smaller than 0.005 mm in grain size.

From the above considerations it would appear likely that clay- or silt-sized materials such as rock flour having a low plasticity index will exhibit physical characteristics resembling those of cohesionless soils, and hence a high degree of

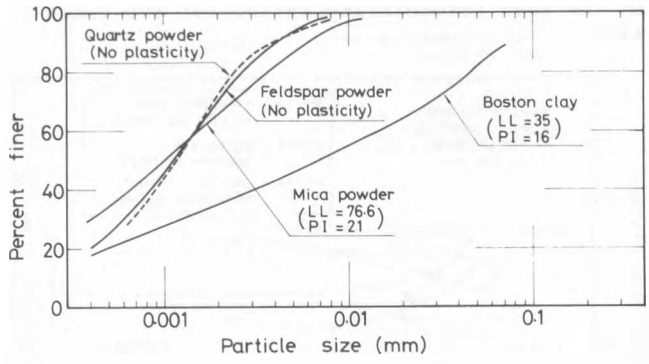

Fig. 22 Gradation curves and plasticity index of rock flours and a clay (Casagrande, 1933)

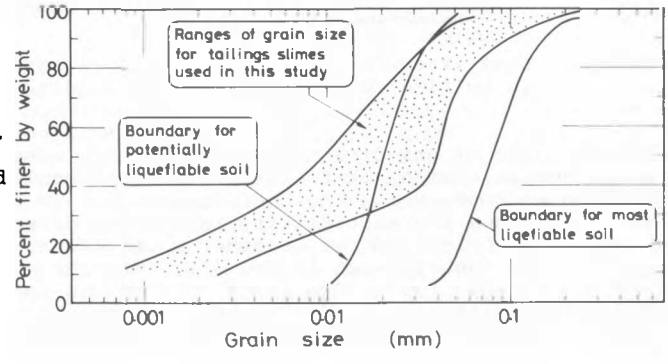

Fig. 23 Comparison of the gradation curves of tailings slimes with the boundary curves

potential to liquefaction. The waste materials deposited in tailings dams are typical of those satisfying the above condition and hence should be considered as substances with a high degree of susceptibility to liquefaction. Shown in Fig. 23 is the range of grain size distribution curves for the fine-grained tailings obtained from several disposal ponds. The gradation curves indicating the boundaries on the left in the chart of Fig. 21 are also cited in Fig. 23. Comparison of these two kinds of curves indicates that the grain size distribution curves of tailings slime do not fall within the domain in which a material has been claimed to be vulnerable to liquefaction. It should be remembered herein that the kinds of soils investigated by Tsuchida (1970) for establishing the above rule were of alluvial and diluvial origin and did not include any particular materials such as the tailings from mine industry. Therefore, the use of the identification rule by Tsuchida ought to be limited to soils containing fines with medium to high plasticity index.

4.2 Cyclic Strength Characteristics of Fine-Grained Soils with Low Plasticity Index

In view of the circumstances described above, a laboratory testing program was implemented, using

a cyclic triaxial test apparatus, in which several silt-sized materials with low plasticity index were tested at varying densities (Ishihara et al. 1980). The grain size distribution curves of the materials used in these tests are shown in Fig. 24. The results of tests on one of these materials are shown in Fig. 25 in which the cyclic stress ratio causing initial liquefaction, 5 % and 10 % double-amplitude axial strain in the

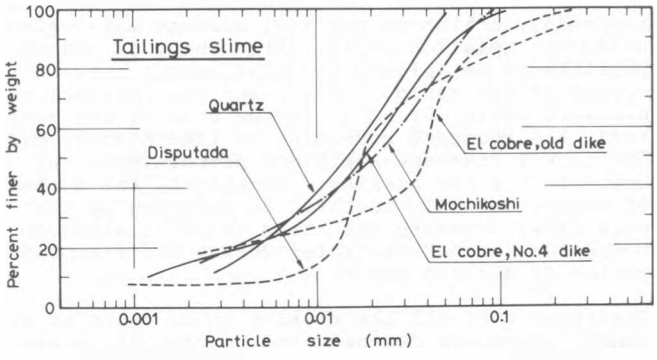

Fig. 24 Gradation curves of the tailing slimes used in the test

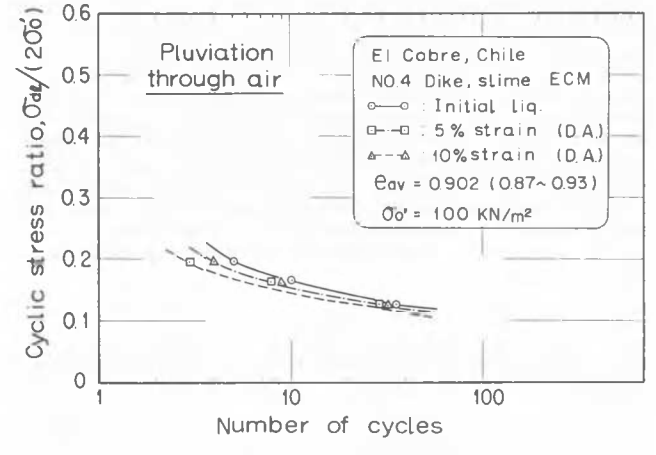

Fig. 25 Cyclic stress ratio versus the number of cycles for a tailings slime

triaxial test specimens is plotted versus the number of cycles. It may be seen that the cyclic stress ratio producing 5 % double-amplitude axial strain in 20 load cycles is about 0.15 which is the same order of magnitude as the cyclic stress ratio obtained with reconstituted samples of clean sand with a relative density of about 40 %. All of the test results are demonstrated in a summary form in Fig. 26 in which the cyclic stress ratio causing 5 % double-amplitude strain in 20 load cycles is plotted versus the void ratio of the test specimens. With reference to the values of plasticity index indicated in the inset, it may

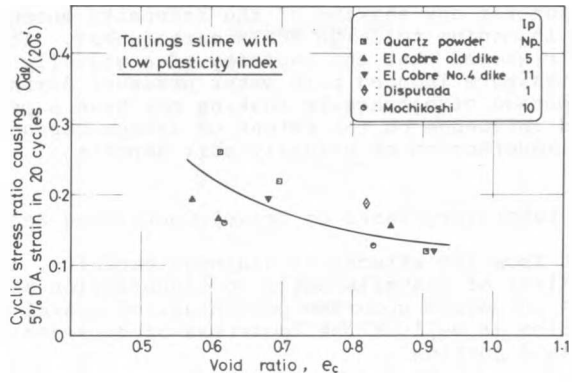

Fig. 26 Relationship between the cyclic strength and void ratio for low-plasticity index tailings slimes

be seen in Fig. 26 that the cyclic strength of low-plasticity tailings is generally small, being on the same order of magnitude as the liquefaction resistance of reconstituted specimens of clean sand. Also noteworthy in Fig. 26 is the fact that void ratios of the samples prepared by the commonly used method of pluviation lie approximately in the same range as the void ratio of clean sand deposited in the same way. This also provides evidence that low-plasticity fine-grained tailings behave as if they were cohesionless sands.

V LIQUEFACTION POTENTIAL OF COARSE-GRAINED SOILS

5.1 General

The hazard associated with soil liquefaction during earthquakes has been known to be encountered in deposits consisting of fine to medium sands and sands containing low-plasticity fines. Occasionally, however, cases are reported where liquefaction apparently occurred in gravelly soils. For instance, at the time of the Fukui earthquake of June 28, 1948 in Japan, signs of disastrous liquefaction were reportedly observed in a gravelly sand in an area of fan deposit near the epicenter of the earthquake. It is also reported by Coulter and Migliaccio (1966) that a major landslide appears to have taken place in a sandy gravel during the 1964 Alaska earthquake. At the time of the Tangshan earthquake on 28 July 1976 in China, a large slide occurred in the saturated sand-gravel protection zone over the upstream slope of the Baihe Dam about 90 Km from Beijing. The cause of the slide is attributed to liquefaction-induced failure which occurred in the protection layer containing 50 - 60 % gravel (Wang, 1984).

In recognition of the importance of the behavior of gravelly soil as above, Wong et al. (1975) performed a series of cyclic tests on gravelly soils with different gradations using a large-size triaxial test apparatus accommodating specimens 30 cm in diameter and 74 cm in height. The results of this study indicated somewhat higher cyclic strength for the gravelly soils as compared to the strength of clean sands, but not so much to a degree completely impeding the occurrence of lique-

faction for any shaking of the intensity encountered in medium to large scale earthquakes. It was also reasoned that the capacity of a gravelly soil to dissipate induced pore water pressure during the period of earthquake shaking may have a profound influence on the extent of damage caused by the liquefaction of gravelly soil deposits.

5.2 Laboratory Tests on Gravel-Containing Sand

Apart from the effects of drainage capacity, the liability of gravelly soils to liquefaction appears to depend upon the percentage of gravel fraction as well as the looseness or denseness of the sand portion.

In order to investigate the effects of the gravel fraction, a series of laboratory tests using a shaking table was conducted by Haga (1984) at the University of Tokyo on artificially prepared sand deposits containing different proportions of gravel. The grain size distribution curves of the sand and gravel used in the tests are shown in Fig. 27. These materials were blended at gravel proportions of 0 %, 30 %, 50 % and 70 %. A sample

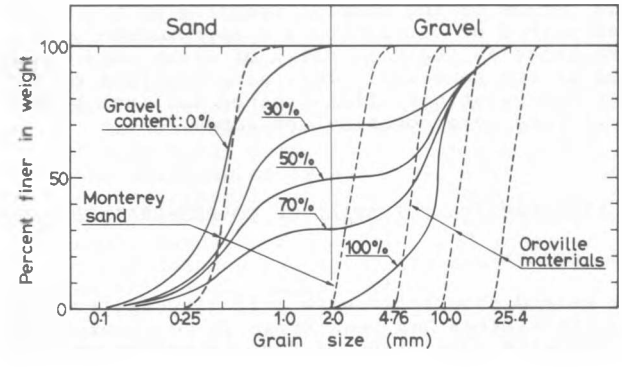

Fig. 27 Grain size distribution curves of gravels and gravel-containing sands

container box having a dimension of 4.0 m in length 0.87 m in height and 1.0 m in width was placed on the shaking table which was operated by an electro-hydraulic system capable of generating a maximum load of 3.0 tons under dynamic load conditions. The mixtures of sand and gravel were poured in the water-pooled container box by means of a movable spreader travelling back and forth over the container. The density of the deposited materials was measured by the gross volume and weight of the material placed in the box. Average values of measured void ratios for each of the test deposits with different gravel proportions are indicated in Fig. 28.

When performing the shaking table tests, horizontal accelerations were measured at the location 10 cm below the surface of the deposit and also at the base of the container box. Pore water pressures were also measured by means of high-precision piezometers embedded at depths 10 cm and 30 cm below the surface of the deposits. The table was shaken by sinusoidal load with 2 Hz frequency. The amplitudes of input acceleration at the base of the container were 100, 150 and 200 gals. In each of the tests employing different intensities of acceleration, the pore water pressure built up and became stationary about 4 seconds after the initiation of shaking. The values of pore water pressures at this instant of time were read off and normalized to the effective overburden pressure to determine the values of residual pore water pressure ratio, Ur/σ_v'. On the other hand, based on the acceleration values monitored near the surface of the deposit, the magnitude of shear stress supposedly acting on the soil element was evaluated using the relation of Eq. (4). Then, it became possible to establish the ralationship between the cyclic stress ratio, τ_d/σ_v', and the residual pore pressure ratio, Ur/σ_v'. In the case of the present test, the recorded acceleration time history did not show a constant-amplitude pattern from the very beginning of the shaking. Therefore, the number of cycles actually involved in building up the pore water pressure was taken to be 7, although the actual number of cycles during the 4-second period of shaking was 8.

The results of all the shaking table tests as arranged above are demonstrated in Fig. 28, where it may generally be seen that the residual pore water pressure increases as the shaking intensity and hence the cyclic stress ratio are increased. Fig. 28(a), showing the test results for sand deposits without gravel, indicates that a state of liquefaction was reached when seven cycles of uniform shear stress have been applied with the cyclic stress ratio of approximately 0.24. This value is in good agreement with the similarly defined cyclic stress ratio causing initial liquefaction in the specimen of clean sand tested in the cyclic triaxial apparatus with a relative density of about 45 %. The test results summaried in Fig. 28(e) indicates that the inclusion of gravel in excess of 30 % acts toward increasing the cyclic strength of the sand, if it is deposited in the identical environment. Since accurate values of density in each test deposit were not known, no definitive conclusion could be drawn from these tests regarding the effects of density of the deposits.

VI EVALUATION OF LIQUEFACTION CHARACTERISTICS OF IN-SITU SOILS

6.1 General

In the preceding sections, several key factors influencing the cyclic behavior of cohesionless soils have been discussed with reference to the results of cyclic loading tests conducted on specimens reconstituted in the laboratory. However, since in-situ soil deposits exist under the influence of many unknown factors which are difficult to evaluate and to duplicate in laboratory-reconstituted specimens, it becomes necessary to recover as perfectly undisturbed samples as possible from in-situ soil deposits and to test them in the laboratory under conditions representative of those prevailing in the field.

6.2 Outline of Undisturbed Sand Sampling Techniques

Attempts to recover high-quality undisturbed

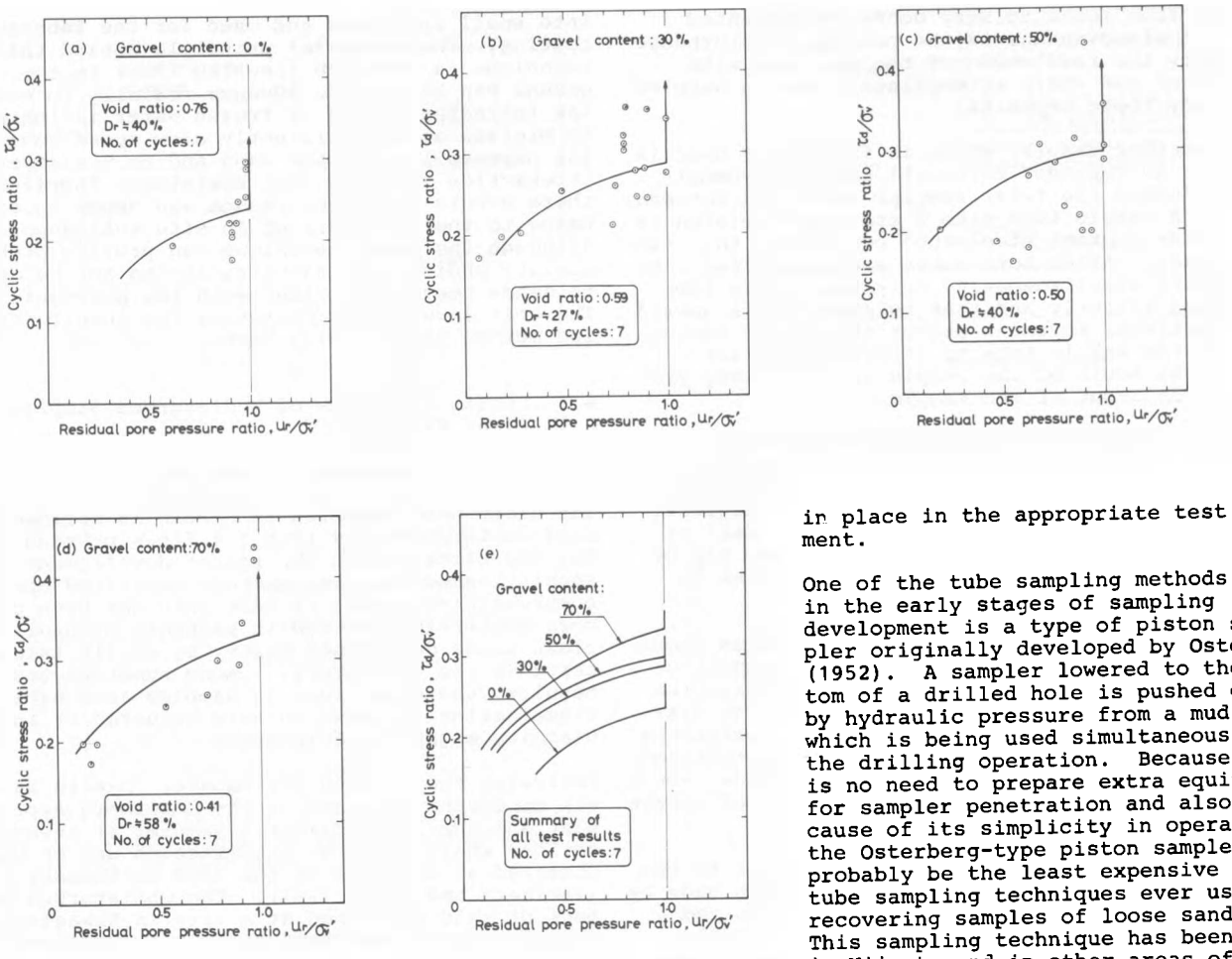

Fig. 28 Pore water pressure buildup characteristics of sand containing different percentages of gravel

samples of sand have thus acquired a renewed importance in recent years in connection with the evaluation of the liquefaction characteristics of in-situ deposits of sands. The in-situ techniques used to recover undisturbed samples from sand deposits may be broken down into three kinds ; tube sampling, block sampling and in-situ freezing method.

In tube sampling, highly sophisticated techniques are required to prevent undisturbed samples from falling out of the sampling tube during the lifting operation. When samples are taken from a loose sand deposit below the ground water table, water in the pores of saturated sand is drained to activate capillary tension within the pores and to develop a small amount of temporary strength necessary for sample handling. The partially saturated sand sample is then frozen at the sampling site with the aid of dry ice or liquefied nitrogen and transported to the laboratory. Since the sample is not fully saturated, the freezing should not produce any volume change and hence disturbance is minimized. In the laboratory, the frozen sample is thawed after it is put in place in the appropriate test equipment.

One of the tube sampling methods used in the early stages of sampling tube development is a type of piston sampler originally developed by Osterberg (1952). A sampler lowered to the bottom of a drilled hole is pushed down by hydraulic pressure from a mud pump which is being used simultaneously for the drilling operation. Because there is no need to prepare extra equipment for sampler penetration and also because of its simplicity in operation, the Osterberg-type piston sampler would probably be the least expensive among tube sampling techniques ever used for recovering samples of loose sands. This sampling technique has been used in Niigata and in other areas of Japan as well to investigate the liquefaction characteristics of in-situ sand deposits (Ishihara et al, 1979).

Another type of tube sampling technique is what is called the large diameter sampler. This sampler has an inner diameter of 20 cm and a length of about 1 m and it is capable of recovering a large chunk of soil from the bottom of a bored hole (Ishihara and Silver, 1977). The cutting bit at the toe of a core tube is equipped with a core catcher consisting of two pieces of stainless steel screen which are folded and held within a narrow space in the wall of the cutting bit. The core catcher screen is stretched transversely across the core tube by means of a cable led to the ground surface. One of the disadvantages of using this type of sampler is that an extra setup is required to provide the large reaction for pushing the sampler into the soil deposit. Also, because of the large scale in every respect, the operating cost is generally high. However, this technique has been used on several occasions in Japan to investigate soil conditions at sites of major engineering importance.

An improved type of Denison sampler, commercially dubbed a triple tube sampler, has also been used in Japan (Mori and Koreeda, 1979) to obtain undisturbed samples of sand from below the ground water table. The triple tube sampler is claimed to have the advantage of being able to retain

samples from loose to very dense and cemented sand. A disadvantage is the probable disturbance caused by the revolution of the core bit with jetting of mud while attempting to obtain samples from very loose deposits.

Still another sampler which is frequently used in Japan is an improved thin-wall sampler, commercially dubbed the twist sampler (Mori and Koreeda, 1979). A sample tube with a stationary piston is put inside another steel tube equipped with a rubber tubing. After both tubes are penetrated into the ground simultaneously, only the sample tube is lifted slightly and then twisted. This upward and rotational movement causes the rubber tubing outside the sample tube to stretch and twist around the mouth of the sample tube, thereby preventing fall-out of the sample.

A type of tube sampler recently developed in Yugoslavia by Kvasnicka (1984) has inner and outer diameters of 70 mm and 98 mm respectively and is equiped with a sharp cutting edge of 10 degrees. Through a small pipe equiped within the wall of the sampling tube, coolant is sent to the tip of the sampler where the soil sample is frozen to provide a plug for preventing fall-out.

Although the techniques of tube sampling as above permit acquisition of samples with a reasonably low degree of disturbance, there is no guarantee that the sample is completely free from any disturbance during all phases of sampling operations. Probably the most important source of disturbance, if it exists in the tube sampling technique, would be the one imparted during the insertion of a tube into an intact deposit of sand,

To eliminate the source of disturbance due to the tube insertion, several attempts have been made by Horn (1978), Espana et al.(1978), Marcuson and Franklin (1979), and Mori and Ishihara (1979), to obtain samples by block sampling. The method of block sampling consists of isolating a column of soil by excavating the surrounding material and of encompassing the soil column by a section of tubing or a square box and of finally cutting the bottom free. This method can be successfully used in all soils provided the true or apparent cohesion is great enough to support the isolated soil column. For carrying out block sampling, the intact surface of the soils to be sampled must be exposed by excavating test pits or exploratory shafts or trenches. Block sampling has the disadvantage of requiring a large amount of excavation sometimes together with a lowering of the elevation of the ground water table. Although the disturbance caused by displacement of soil during driving and pushing a sampling tube can be eliminated, block sampling may still be subject to the disturbance associated with the stress release due to excavation of the test pit or the lowering of the ground water level.

In order to seek for a more complete method of undisturbed sampling, the freezing technique has been developed by some investigators. The most recent attempt to this end was made by Yoshimi et al. (1978). In this method a mixture of ethanol and cruched dry ice is circulated through an open pipe inserted vertically into the ground. After the sand surrounding this pipe has been frozen, the steel pipe is pulled out of the ground by means of a crane together with the huge frozen column of sand. The frozen sand column is cut into small specimens and used for the laboratory testing. The essential principle behind this technique is that the freezing front in the ground can be made to advance radially to enable the increased volume of frozen water in the pores to migrate at a sufficiently slow speed consistent the permeability of the sand and to minimize interaction with the soil skeleton. Therefore, there occurs no volume change and hence no disturbance to the structure of in-situ soil deposit. Although the above technique can provide high-quality undisturbed samples, it can not be applied to sands containing fines with low permeability. The cost involved in operating the in-situ freezing method is generally high.

6.3 Cyclic Strengths of Undisturbed Samples of Clean Sands

6.3.1 Loose to Medium Dense Sand

The clean sand referred to herein is defined as sand containing less than 5 % fines passing the No. 200 sieve. With the recent development of the sophisticated sampling methods described above, a comprehensive amount of test data has been produced concerning the cyclic strength of undisturbed clean sands determined mainly by cyclic triaxial tests in the laboratory. Among numerous test results, those obtained on samples from sites where liquefaction is known to have occurred or in their vicinity might be of interest.

Following the Niigata earthquake, in-situ sampling was conducted by means of the Osterberg type sampler and the large diameter sampler at several locations where signs of liquefaction was or was not observed at the time of the 1964 earthquake (Ishihara and Koga, 1981). The undisturbed specimens of sand recovered at a site in Kawagishi-cho where several appartment buildings surffered severe damage were tested in the laboratory using the cyclic triaxial test apparatus. The results of the cyclic triaxial tests on the specimens obtained by the large diameter sampler are presented in Fig. 29 in terms of the relationship between the cyclic stress ratio versus the number of cycles. The grain size distribution curves of the sand tested are shown in Fig. 30. After finishing the tests on undisturbed specimens, the specimens were completely disturbed and reconstituted so as to have approximately the same density by the method of pluviation under water. The results of the tests on such reconstituted specimens are also indicated in Fig. 29. It may be seen that the cyclic stress ratio causing initial liquefaction or 5 % double-amplitude axial strain during 20 cycles of shear stress application is generally greater for the undisturbed specimens than for the reconstituted specimens. It is also noted in Fig. 29 that this difference in cyclic strengths is more pronounced when the number of cycles in question is small and that as the number of cycles increases, the difference in cyclic strengths tapers off. This is probably because of the disturbing effects of cyclic loading itself imparted to the undisturbed sand specimen. It appears likely that the portion of strength potentially existing in undisturbed specimens due to cemmentation and aging is mobilized to resist externally applied shear only during several cycles in the early stage of cyclic load application, and once the gain in strength due to the cementation or aging is lost, the behavior of undisturbed sand specimens becomes

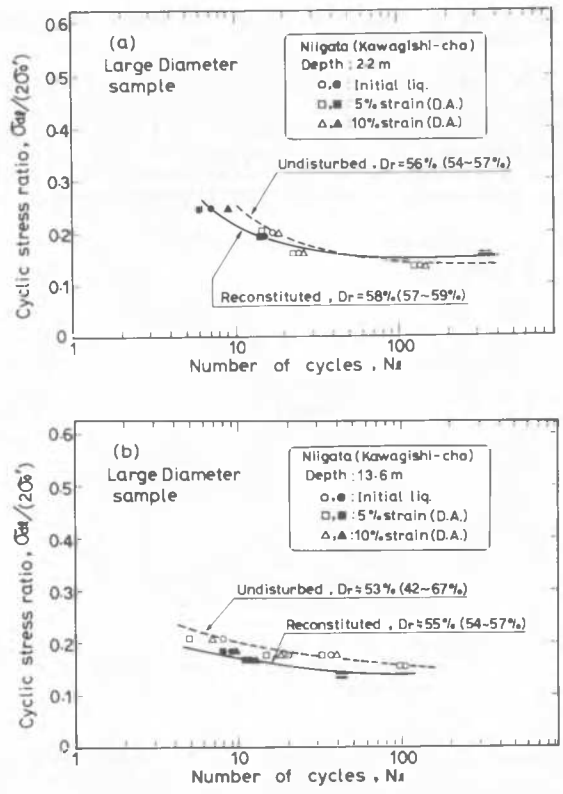

Fig. 29 Comparison of cyclic strength between undisturbed and reconstituted samples of Niigata sand

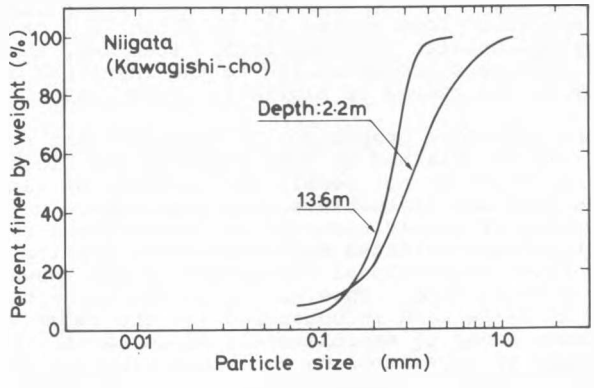

Fig. 30 Gradation curves of Niigata sands used in the test

identical to that of reconstituted specimens.

Fig. 31 shows a similar set of test results on undisturbed sand samples obtained by the large diameter sampler from a site on the right bank of the Shinano river about 3 Km upstream from the Kawagishi-cho site. This site is indicated in Fig. 57 and referred to as the River site. The gradations of the sands tested are approximately in the same range as those of the sand from Kawagishi-cho site. As seen in Fig. 31 the general trend in the cyclic strength of undisturbed

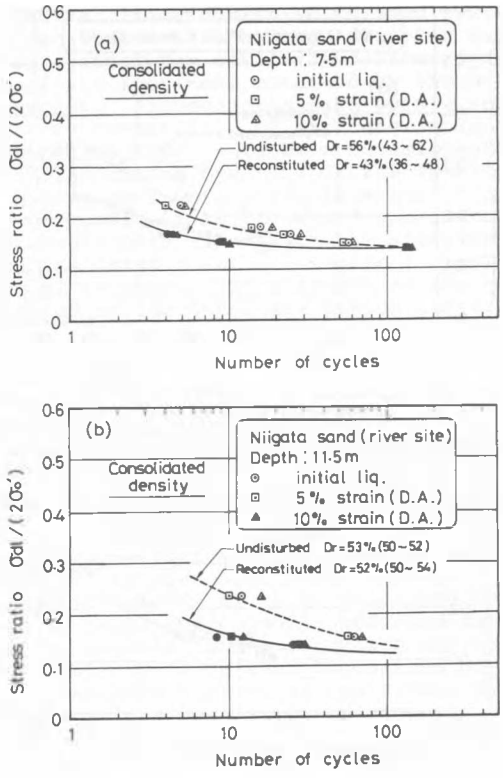

Fig. 31 Cyclic stress ratio versus the number of cycles for undisturbed and reconstituted samples of Niigata sand

specimens relative to that of reconstituted specimens is similar to that observed in the results of tests on the sands at the Kawagishi-cho site.

In the natural deposits of predominantly fluvial origin, loose deposits are generally young and almost free from added strength due to cementation and aging, whereas dense sand deposits might have been exposed to varying degree of strengthing effects such as cementation and aging during a long period of their geological history. Consequently, there are good reasons to believe that undisturbed samples from denser deposits might be more susceptible to disturbance than undisturbed samples from looser sand deposits. It might, therefore, be of interest to see how the density of sand will influence the degree of loss of cyclic strength due to remolding of undisturbed samples. The outcome of the test series conducted on sand samples from the River site in Niigata city will be instrumental to investigate this aspect of the problem. From all the cyclic triaxial test data, those having induced initial liquefaction or 5 % double amplitude axial strain in the course of 3 to 10 cycles of stress application were collected, and the cyclic stress ratio employed in each of these tests was plotted versus the relative density of the specimens at the time the initial confining pressure was applied (consolidated relative density). The result of this data compilation is presented in Fig. 32(a). Similarly those test data producing a state of initial liquefaction or 5 % double amplitude strain in the range of number of load cycles

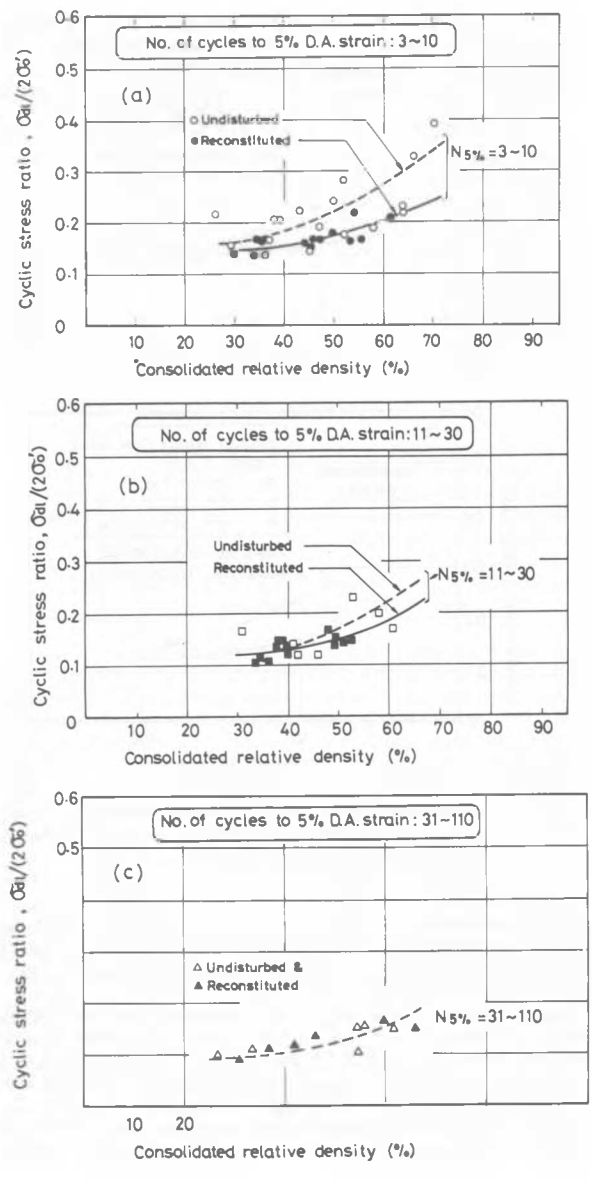

Fig. 32 Cyclic stress ratio versus relative density relationship for undisturbed and reconstituted samples of Niigata sand

between 11 to 30 were assembled and plotted in Fig. 32(b) in terms of the relation between the cyclic stress ratio and relative density. Fig. 32(c) is the plot of test data in which a larger number of load cycles of 31 to 110 was required to cause initial liquefaction both in undisturbed and reconstituted specimens. It is apparent in Fig. 32, that the increased cyclic strength of undisturbed specimens over that of reconstituted specimens is observed in these data when the number of cycles involved is small and when the relative density is large. This consequence appears logical in view of the speculation, as mentioned above, that the inner structure of sand due to cementation or aging is more pronouncedly developed with increasing density and such a built-in structure may be more vulnerable to disturbance with increasing number of load applications.

All the results of cyclic triaxial tests ever performed on both undisturbed and reconstituted samples of sands from the area of Niigata city are assembled in Fig. 33 for comparison purposes of cyclic strength between undisturbed and reconstituted specimens. Except for the block sampling at

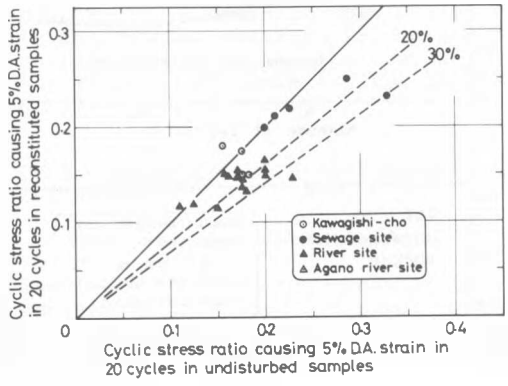

Fig. 33 Comparison of cyclic strength of undisturbed and reconstituted samples of Niigata sand

the sewage treatment site, all the test data are those for samples obtained by means of the large diameter sampler. Although the difference in cyclic strength between the undisturbed and reconstituted specimens depends, as mentioned above, on the number of cycles being considered, 20 load cycles was used to define the cyclic strength comparison shown in Fig. 33. It may be seen that the cyclic stress ratio causing 5 % double amplitude strain in 20 load cycles is, by about 20 % on the average, greater for undisturbed specimens than for specimens reconstituted to the identical density by the method of pluviation under water.

Since the above comparison is based on test results on samples obtained by tube sampling and block sampling, which do not permit the recovery of samples free from any disturbance, the true figure on the increase of cyclic strength of in-situ sand over that of reconstituted specimens under seemingly identical depositional conditions is not known at the present time. However, as far as loose to medium dense sand is concerned (in the relative density range of approximately 40 to 60 %), the methods of tube sampling and block sampling appear to yield the cyclic strength data of in-situ sand deposits with a reasonable degree of accuracy. It is the deposits of loose to medium dense sand that have actually developed extensive liquefaction during past earthquakes and accordingly have been the main target of concern for many researchers and engineers.

Apart from the comparison between undisturbed and reconstituted specimens discussed above, a comparison of the cyclic strengths of specimens obtained from different sampling procedures is also of interest. Most of the data available to the writer concerning the cyclic strength of undisturbed samples are those for samples obtained by means of the large diameter sampler and the Osterberg type piston sampler. In some of the sites investigated,

attempts have been made to recover undisturbed specimens using both sampling techniques at two nearby locations within a few meters from each other. It would, therefore, be of interest to see how the cyclic strengths compare for undisturbed samples taken by these two methods of tube sampling. Fig. 34 shows a comparison, to this

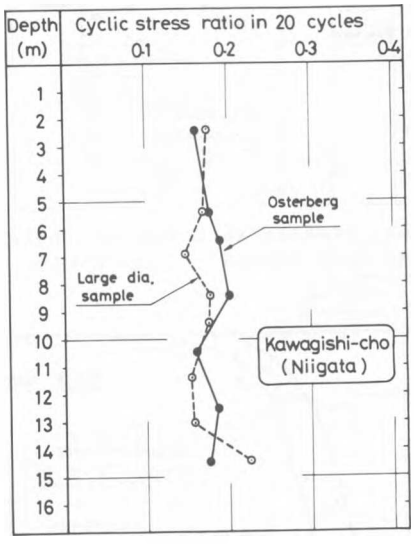

Fig. 34 Comparison of cyclic strength of undisturbed sand in Niigata obtained by the large diameter sampler and Osterberg piston sampler

effect, of the cyclic strength data obtained for samples obtained at the Kawagishi-cho site. It may be seen in this figure that the values of cyclic stress ratios causing initial liquefaction in 20 load cycles are within tolerable limits of variation for the specimens obtained by the two kinds of samplers throughout the depth of the sand deposit investigated. By collecting all test data from other sites, the plot shown Fig. 35 was developed. In this Figure the cyclic stress ratio

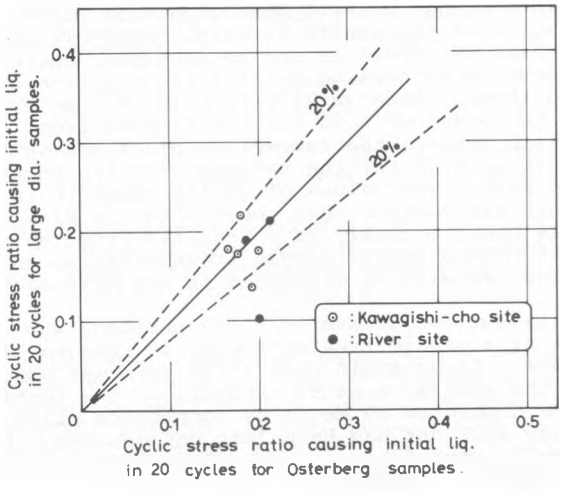

Fig. 35 Comparison of cyclic strength between the large diameter samples and Osterberg samples

causing initial liquefaction in 20 load cycles for the specimens taken by the large diameter sampler is plotted against the similarly defined cyclic strength of the specimens obtained by the Osterberg piston sampler. Although the data points scatter due mainly to variability of strength in individual specimens, there appears to be no consistent trend in Fig. 35 indicating one kind of the specimens to yield a higher or lower cyclic strength than the other. Consequently, it would appear that the cyclic strength determined from the specimens obtained by the large diameter sampler is approximately equal to the cyclic strength of the specimens obtained by the Osterberg piston sampler.

6.3.2. Dense Sand

There has been an increasing need in recent years, in connection with the design of important structures, for a knowledge of the behavior of dense sand deposits subjected to high-intensity shaking of earthquakes. In response to such a demand, some efforts have been made to investigate the cyclic mobility characteristics of dense sands for undisturbed as well for reconstituted samples. The characteristic feature of dense sand behavior indicated by tests on reconstituted samples was described in details in the foregoing section. It was shown that the dense sand is capable of mobilizing a significant amount of resistance to cyclic stress applications even after the induced pore water pressure becomes equal to the initial confining pressure. Such a behavior was called cyclic mobility. Therefore, it has been customary to evaluate the cyclic strength of undisturbed dense sand in terms of the cyclic mobility, i.e., in terms of the cyclic stress ratio required to cause some level of double-amplitude of shear strain.

When recovering undisturbed samples from deposits of dense sand by means of any tube sampler, chances are high for the sand to be loosened due to its dilating nature during penetration of the tube sampler. The samples taken by the large diameter and Osterberg samplers also suffer a varying degree of disturbance depending upon the density of sand, and it would appear that these samplers can not be used to obtain samples without disturbance from deposits with a relative density exceeding about 70 % or with a blow count value of the standard penetration test approximately greater than 15. In recognition of this, the block sampling method has been widely used to obtain high-quality undisturbed samples. The marked difference in cyclic strength between dense samples from the tube sampling and those from block sampling was pointed out by Espana et al. (1978) and Marcuson and Franklin(1979), who showed that the block samples are about twice as resistant to cyclic stress applications as are specimens from the tube sampler. Consequently, it appears that tube sampling should not be used to obtain samples from dense sand deposits.

In order to evaluate the cyclic strength of dense sand, Kokusho et al. (1983a) conducted a series of cyclic triaxial tests on undisturbed sand from a diluvial deposit called the Narita deposit in Japan. The undisturbed specimens were obtained by excavating blocks 30 cm × 30 cm × 30 cm in dimensions. The sand was slightly cemented and contained about 10 % fines. The maximum and ninimum void ratios were 1.345 and 0.824, respectively. Small specimens were trimmed out of the block sample

and tested in the cyclic triaxial test apparatus following the usual test procedure. After finishing the test, the sample was reconstituted to approximately the same density by the method of pluviation in water and tamping and tested again. The results of the tests are summarized in Fig. 36, in terms of the cyclic stress ratio causing

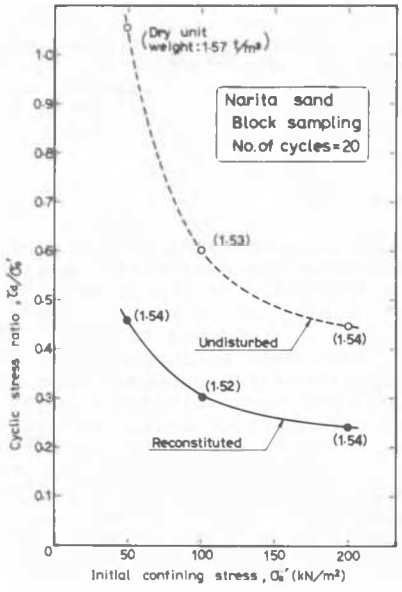

Fig. 36 Effects of initial confining stress on the cyclic strength of dense sand (Kokusho et al. 1983a)

5 % double-amplitude axial strain in 20 load cycles plotted versus the initial confining pressure used in each test. It is of interest to note that the cyclic strength depends significantly upon the initial confining pressure, both for undisturbed and reconstituted states of the sand. Noteworthy as well in Fig. 36 is the fact that the cyclic strength for undisturbed intact sand specimens is about 40 % greater than that for the reconstituted specimens. This increase might well be attributed to the effects of cementation or aging that took place in a long geological time.

Another example of block sampling is the one which was conducted at a site near the east wharf in Ohgishima man-made island, Yokohama, Japan. This site had been stabilized by installing compaction piles at a spacing of 2.0 m about 5 years before performing the block sampling. A section 15 m long and 6 m wide was first enclosed by rows of sheet piles and after lowering the ground water table to a depth of 5.0 m, the ground was excavated to a depth of 4.0 m. The sampling procedure began by carving the exposed intact sand into a column with a diameter and length slightly larger than those of finished samples. A tube was then pushed gently a short distance meanwhile removing the sand around the sampling tube with suitable hand tools. The pushing was continued in this manner until the intact sand was completely encased in the tube. Finally the sample was shaved off by inserting a thin steel plate under the cutting edge. The samples were transported to the laboratory without freezing and tested in the cyclic triaxial test apparatus. The soil profile established by borings prior to the excavation of

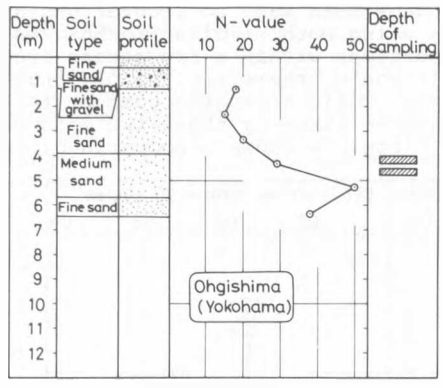

Fig. 37 Soil profile at a site of Ohgishima man-made island

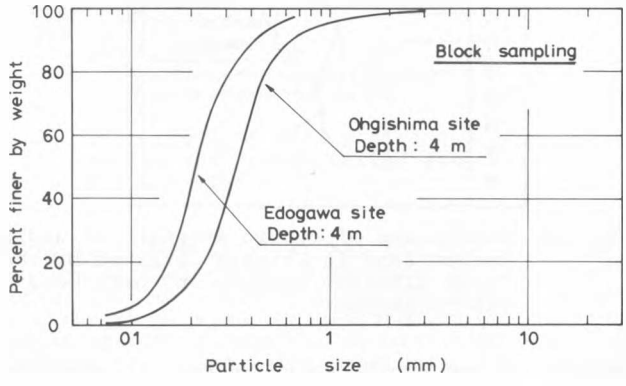

Fig. 38 Gradation curves of two sands compacted by the compaction pile

the ground is shown in Fig. 37. The depths of sampling are also indicated in this figure. The gradation of the sand tested is shown in Fig. 38. The cyclic triaxial tests were performed on two groups of samples, i.e., one from the center of the 40 cm diameter compaction pile and the other from points midway between the compaction piles. The results of the cyclic triaxial tests are presented in Fig. 39, where it may be seen that the cyclic stress ratio causing initial liquefaction or 5 % double-amplitude axial strain in 20 load cycles is on the order of 0.30 for the samples from the points between the compaction piles and on the order of 0.38 for the samples from the points of the pile. The values of cyclic strength in these tests are smaller than those shown in Fig. 36. This might probably have resulted from the sample disturbance during sample transportation and handling, as will be discussed in the next section.

Still another scheme of block sampling was carried out at a sewage treatment site in Edogawa, Tokyo, where a large-scale excavation work was underway. In the general area of excavation, one section had been compacted by means by compaction piles, but other sections had been left uncompacted. Block samples were taken at both sites using the same procedure as described above. The N-value of the standard penetration test was about 27 for the compacted site and about 10 for the uncompacted site. The results of cyclic triaxial tests on

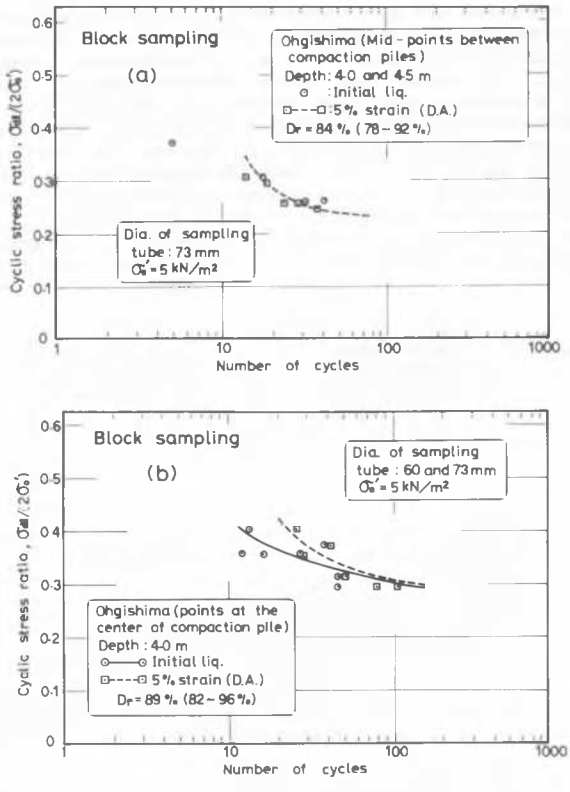

Fig. 39 Cyclic strength of undisturbed sand samples recovered from the deposit compacted by the compaction pile

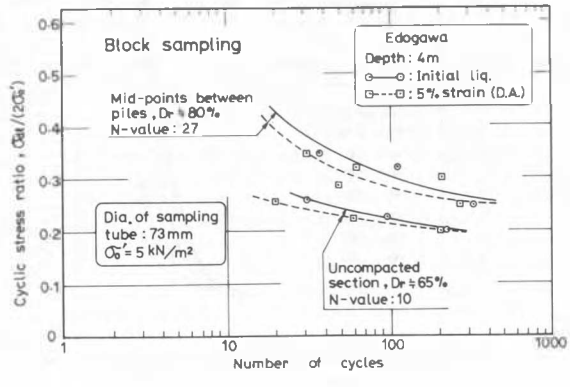

Fig. 40 Comparison of cyclic strength of undisturbed samples obtained from uncompacted deposit and compacted deposit by means of the compaction piles

undisturbed specimens from the compacted and uncompacted sections are presented together in Fig. 40. It may be seen in this figure that the cyclic stress ratio inducing initial liquefaction or 5 % double-amplitude axial strain in 20 load cycles is on the order of 0.4 for the specimens from the compacted section and on the order of 0.26 for the specimens from the uncompacted deposit. From these test results, it may be noted that the resistance to cyclic stress applications is substantially increased if sand is compacted in the ground by means of compaction piles. The relatively small value of cyclic strength for the specimens from the compacted section might have accrued as a result of sample disturbance incurred during sample handling and transportation. This aspect of the problem will be discussed in the next section.

The results of a series of cyclic triaxial tests on specimens taken by the block sampling have also been reported by Frydman et al. (1980). Samples were obtained from a variably cemented sand deposit, known as Kurkar, that is encountered in the area along the coastline of Israel. The sand contained about 5 to 15 % fines and the block samples were frozen after they had been carved in-situ. Cylindrical specimens for cyclic triaxial testing were cored from the frozen block and after thawing they were tested. Although scattered, the test data indicated a cyclic stress ratio of 0.2 to 0.35 required to cause initial liquefaction in 20 load cycles for the intact specimens having a relative density of about 40 to 60 %. In spite of low levels of cyclic resistance, the blow count value of the standard penetration test was high ranging between 25 and 90. The unexpectedly low resistance to cyclic loads was conceived by the investigators to have resulted from the presence of uncemented loose portions in the soil structure of the specimens. One of the interesting outcomes in this investigation was the observation of the influence of the initial effective confining stress on the cyclic resistance of intact specimens of sand. The cyclic stress ratio causing initial liquefaction in 20 load cycles under the confining stresses used in the tests is normalized to the similarly defined cyclic stress inducing initial liquefaction under a confining pressure of 100 kN/m² and shown in Fig. 41 for different confining pressures. Similar data arrangements were also made for the test results shown in Fig. 36 and they are also plotted in Fig. 41. The summary plots in Fig. 41 indicate that the cyclic resistance of cemented sands is significantly weakened as the confining stress increases. The reduction in cyclic strength as above appears to occur due to the overconsolidated nature of dense cemented sand and also as a result of a breakdown of weak cementation bonds with increasing confinement.

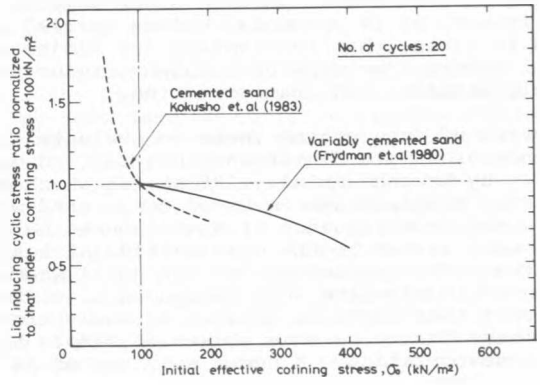

Fig. 41 Effects of confining stress on the cyclic strength of cemented sand

6.4 Effects of Sample Disturbance in Dense Sand

As mentioned previously, specimens of dense sand obtained by block sampling are suspected to suffer disturbance due to stress release during excavation of test pits or lowering of the ground water table. To investigate the effects of the stress release on the cyclic strength of dense sand, Kokusho et al. (1983a) performed several series of cyclic torsion shear tests on densely compacted specimens of Toyoura sand. Specimens were prepared by the method of pluviation in water and tapping. After consolidating the specimens, the confining pressure was reduced and kept at a low level for a period of 1 hour to 3 days. The confining pressure was increased again to the initial level and cyclic loading test was carried out. In another series of tests, cyclic torsion tests were performed on specimens without any such stress release. A comparison of the results of these two types of test indicated that the cyclic strength was virtually the same. In another series of tests, a stress release was imparted to specimens which had undergone some degree of overconsolidation and the cyclic torsion whear tests were run on such specimens. A comparison of the cyclic strength of the overconsolidated dense specimens with and without stress release also indicated approximately the same result. On the basis of the observation as above, Kokusho et al. (1983a) concluded that the effect of stress release is inconsequential at least for the type of dense sand tested in the studies described above.

From the above considerations, it may be that chances are generally small for block samples to suffer a significant degree of disturbance due to the stress release which occurs during the excavation of test pits or the carving of test specimens.

Block samples are sometimes frozen in-situ but not in many cases, particularly when they contain some percentage of fines. In case block samples are not frozen, it is probable, unless special precaution is taken, that the samples are subjected to small shocks from various unknown origins during sample handling and transportation.

A series of interesting tests to evaluate the influence of sample disturbance was carried out recently by Kokusho et al. (1983a), in which artificially prepared specimens of dense sand were subjected to a sequence of small shocks before they were tested in the cyclic triaxial test apparatus. The application of the small shocks was intended to simulate some sequences of disturbing agencies that might be applied to undisturbed specimens during various phases of sample handling and transportation. A dense specimen of Japanese standard sand (Toyoura sand) prepared by the method of tapping in water to a relatively density of about 85 % was made partially-saturated by draining excess water. The specimen enclosed in membrance without external confining stress was taken out of the triaxial pedestal and mounted on a bowl attached to the apparatus of a Liquid Limit testing device. By putting a small bar transversely on the pad, the height of drop was adjusted to become as small as 1.25 mm. A sequence of small shocks was applied to the specimen by dropping the bowl as many times as desired. The specimen was again put in place in the triaxial chamber and tested in the usual manner to determine the cyclic strength. On the other hand, tests were also performed on specimens not subjected to such an artificial disturbance. The results of the tests reported by Kokusho et al. (1983a) are shown in Fig. 42, where the cyclic stress ratios causing 5 % double amplitude strain in the specimens with and without disturbance are plotted versus the number of cycles. Fig. 42 shows that the specimens which had undergone 20 cycles of small shocks exhibited a cyclic strength of about one-half the strength of specimens without disturbance. The extent to which a sand specimen is influenced by the disturbance may depend upon the looseness or

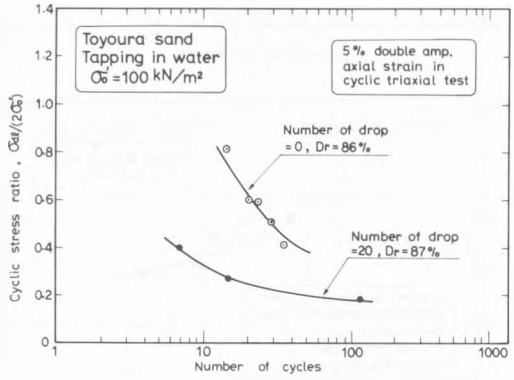

Fig. 42 Decrease in cyclic strength due to sample disturbance (Kokusho et al. 1983a)

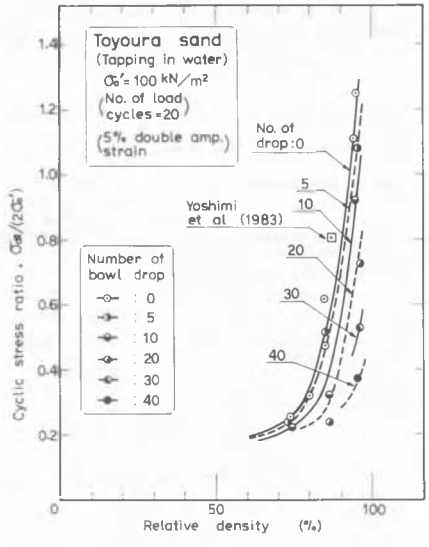

Fig. 43 Effects of sample disturbance on the cyclic strength of sand (Kokusho et al. 1983a)

denseness of the sand. In order to examine this aspect of the phenomenon, multiple series of tests were performed on the Toyoura sand with varying densities by employing different levels of disturbance. The results of these test series are summarized in Fig. 43 in which the cyclic stress ratio causing 5 % double amplitude strain in 20 load cycles in the specimens subjected to different numbers of drops of the bowl is plotted versus the relative density of the sand tested. One of

the most conspicuous features of the test results observed in Fig. 43 is a remarkable drop in the cyclic strength that occurs particularly in dense sand as a result of disturbance caused by the drop of the bowl on which the specimens was mounted. For the specimens with a relative density of about 95 %, the cyclic strength is shown to decrease with increasing number of the bowl drops eventually reaching about one-quarter of the original strength with 40 drops of the bowl . The sharp drop in cyclic strength does not seem, however, to take place in specimens having a relative density less than about 70 %.

In the light of the qualitative demonstration of the importance of sample disturbance as shown above, it may well be mentioned that an undisturbed specimen of dense sand is highly susceptible to any degree of disturbance from various origins, leading to a reduction in its resistance to cyclic loading.

The disturbance due to small shocks during sample handling and transportation will be minimized if samples are properly frozen in-situ. The requirement will be met if sampling is made by the method of radial freezing developed by Yoshimi et al. (1978). Note that this method eliminates the disturbance not only from small shocks but also from the stress release, if any. An attempt was made recently by Yoshimi et al. (1983) to recover a huge block of frozen sand at a site near the railway station in the city of Niigata. The sample was cut into small cylindrical specimens for testing in the cyclic trial test apparatus. The result of the recent test on the dense sand with a relative density of 87 % indicated a value of cyclic stress ratio as high as 0.80 to produce 5 % double-amplitude strain in 20 load cycles in the undisturbed specimens. Similar cyclic triaxial tests were also conducted on specimens reconstituted to nearly the same density by the method of wet tamping. The corresponding cyclic stress ratio in this case was o.48. It was concluded that the cyclic strength of high-quality undisturbed dense sand exhibits much greater resistance to cyclic stress applications than had been previously envisioned. The high value of cyclic strength for dense Niigata sand obtained by Yoshimi et al. (1983) is also plotted in Fig. 43. It may be seen that the point for this test data lies close to the curve of zero disturbance obtained by Kokusho et al. (1983a). It appears likely, therefore, that the cyclic strength of 0.80 by Yoshimi et al. represents the strength of in-situ specimens with least disturbance.

If the effects of stress release are found to be inconsequential for in-situ deposits of dense sand as suggested by Kokusho et al. (1983a), for the laboratory prepared specimens the most economical and reliable procedure would be to recover block samples, freeze them in-situ and test them in the laboratory after thawing. At the present time, there appears no report of such tests conducted on dense deposits of clean sand. Although the study by Frydman et al. (1980) was conducted following the procedure recommended above, it was done on highly stratified sand containing 5 to 15 % fines, and consequently the test results may not be taken as a representative case justifying the usefulness of the above procedure.

As described above, the task of determining a true behavior of dense sand appears much more difficult than that for loose sand, because of the highly susceptible nature of the samples to any sources of disturbance.

Apart from the effects of sample disturbance and the variability of other influencing factors as noted above, one should be reminded of the fact that the cyclic strength of dense sand changes vastly depending on the number of cycles and the amplitude of shear strain by which a state of failure is defined. The definition of failure widely used at present time is a state in which 5 % double-amplitude strain is produced in the sand during the application of 20 cycles of shear stress. This definition is not, however, based on any firm physical background. There is no reason, therefore, to reject any other criteria to define a state of failure. In the writer's opinion, it seems most appropriate to define failure on the basis of careful design considerations.

VII EVALUATION OF LIQUEFACTION RESISTANCE BY IN-SITU PENETRATION TESTS

7.1 General

In view of the somewhat costly operation involved in obtaining and testing high-quality undisturbed samples, and also in view of the generally purported theoretical disadvantages inherent to any laboratory testing technique such as system compliance, membrane penetration and non-uniformity of strain distribution, the merits of having recourse to in-situ penetration tests for assessing the cyclic strength of in-situ deposits of soils have been increasingly recognized in recent years. Such a demand resulted in attempts to correlate the cyclic strength of in-situ soils with values of resistance of any penetration test and to enable the cyclic strength of a given soil deposit to be assessed from a knowledge of the penetration resistance which is generally obtained in the routine practice of soil exploration.

There are basically two types of approach to this end. The first is to collect a great bulk of laboratory test data on cyclic strengths of undisturbed soil samples recovered from deposits of known penetration resistances and to establish an empirical correlation between these two quantities. The second approach is based on observed performances of in-situ soil deposits as to whether or not they have actually developed liquefaction during past earthquakes. With an intensity of shaking estimated by some appropriate procedures, values of cyclic stress ratios believed to have occurred in in-situ soil deposits during the earthquake can be estimated at any depth of the deposit and related to the penetration resistance. Since the occurrence or non-occurrence of liquefaction-induced ground damage is known, it is then possible to establish a threshold relationship between the cyclic stress ratio and the values of penetration resistance.

Although the penetration resistance is most widely available in-situ data at present time, other index parameters such as shear wave velocity (Dobry et al. 1980) or the electrical properties of in-situ sand deposits (Arulanandan et al. 1981) may possibly be used for establishing similar relationships.

7.2 Correlation Based on Laboratory Tests

By assembling a vast quantity of cyclic triaxial test data obtained in Japan, Tatsuoka. et al. (1980) established a correlation as follows,

$$\left(\frac{\tau_d}{\sigma_0'}\right)_{20} = 0.0676\sqrt{N_1} + 0.225\ \log_{10}\left(\frac{0.35}{D_{50}}\right) \quad \text{for } 0.04\ \text{mm} \leq D_{50} \leq 0.6\ \text{mm}$$

$$\left(\frac{\tau_d}{\sigma_0'}\right)_{20} = 0.0676\sqrt{N_1} - 0.05 \quad \text{for } 0.6\ \text{mm} < D_{50} \leq 1.5\ \text{mm} \qquad (10)$$

where D_{50} is the mean particle diameter in millimeters, $(\tau_d/\sigma_0')_{20}$ denotes the cyclic stress ratio required to cause initial liquefaction or 5 % double amplitude strain in 20 cycles of shear stress application and N_1 denotes a corrected blow count value of the standard penetration test (SPT) defined as,

$$N_1 = C_N \cdot N$$
$$C_N = \frac{1.7}{\sigma_v' + 0.7} \qquad \cdots\cdots(11)$$

where N is the blow count value of the SPT and σ_v' is the vertical effective overburden pressure in kgf/cm^2 . The value of N_1 means the N-value of the SPT normalized to an effective overburden pressure of 1 kgf/cm^2 to account for the effect of increasing N-value with increasing confining stress. The normalizing function, C_N, is based on the formula by Meyerhof (1957). Eq. (10) was incorporated in the seismic code for bridge foundation design in Japan (1980).

Field and laboratory observations have shown that the resistance to liquefaction tends to increase with decreasing particle size. Thus for the same penetration resistance, the cyclic stress ratio required to cause liquefaction increases with decreaseing grain size. This effect is incorporated in the above formula in the second term on the right hand side. While the 50 percent particle diameter, D_{50}, is used in Eq. (10) to allow for the effect of particle size, the amount of fines contained in sandy soils may also be used as an index parameter to account for the same effect. A correlation including this effect was also proposed by Tatsuoka et al. (1980) as follows,

$$\left(\frac{\tau_d}{\sigma_0'}\right)_{20} = 0.0676\sqrt{N_1} + 0.0035C \qquad \cdots\cdots(12)$$

where C is the content of fines in percent passing the #200 mesh.

In an effort to identify localities of high liquefaction potential in the bay area of Tokyo, a comprehensive program of undisturbed sampling and testing of subsurface soils was conducted by means of the Osterberg type sampler and by using a cyclic triaxial test apparatus. The results of this investigation were summarized in the following formula (Ishihara, 1979),

$$\left(\frac{\tau_d}{\sigma_0'}\right)_{20} = 0.009\left(N_1 + 13 + 6.5\ \log_{10}C\right) \qquad \cdots(13)$$

where N_1 is defined as

$$N_1 = C_N \cdot N$$
$$C_N = 0.77\ \log_{10}\left(20/\sigma_v'\right) \qquad \cdots\cdots(14)$$

The function to normalize the N-value is based on that proposed by Peck et al. (1974).

The use of fines content as an index parameter to allow for the effect of particle size has some advantages over the use of 50 percent particle size. In the routine practice of physical testing of soils, the gradation of soils is determined mainly by mechanical sieve analysis in which the minimum mesh size is 0.074 mm of #200 sieve, and an elaborate gradation analysis is often omitted for the finer portion. Therefore, in many cases the information on the 50 percent particle size is not available.

It is important to remember that the above empirical formulas were derived on the basis of the results of tests on undisturbed samples obtained mostly by tube sampling. In view of the difficulties in obtaining high-quality samples, using any type of tube sampler, from dense sand deposits with N-values in excess of about 20, the application of the above formulas should be restricted to deposits composed of loose to medium dense sand, or of clayey and silty sand. It is also to be noted that the basic test data leading to the above empirical correlation come from the results of tests on soils from fluvial deposits of alluvium and diluvium. Therefore, most of the fines contained in the sand are of medium consistency with plasticity index values ranging between 20 and 40. As discussed in the foregoing chapter, fine-grained soils with low plasticity indices, such as tailings materials, exhibit as low resistance to cyclic loads as does loose sand. Therefore, the mere presence of such fines does not serve to increase the cyclic strength as much as that evaluated by the formula of Eqs. (12) and (13).

In recognition of these drawbacks, an extensive investigation was undertaken in Japan to determine the cyclic strengths of low-plasticity tailings materials. Undisturbed samples of tailings were taken from 15 tailings dam sites by means of tube samples and tested in the laboratory. The outcome of these tests was arranged in a design formula as follows (Ishihara et al. (1981),

$$\left(\frac{\tau_d}{\sigma_0'}\right)_{20} = 0.0676\sqrt{N_1} + 0.085\ \log_{10}\left(\frac{0.50}{D_{50}}\right) \qquad \cdots\cdots(15)$$

where

$$N_1 = C_N \cdot N$$
$$C_N = \frac{1.7}{\sigma_v' + 0.7} \qquad \cdots\cdots(16)$$

A comparison of this formula with that of Eq. (10) indicates that the increase in cyclic strength with decreasing mean particle size is less pronounced in the case of tailings materials than in soils generally encountered in alluvial and diluvial deposits.

As mentioned in the foregoing chapter, the cyclic strength of sands containing fines depends not only on the amount of fines but also on its consistency characteristics. Fig. 44 shows a summary

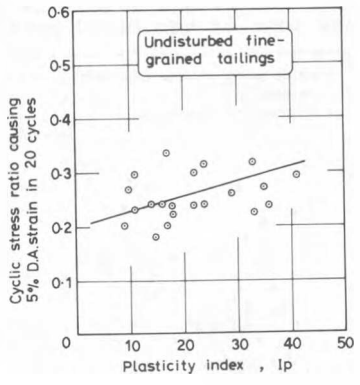

Fig. 44 Relationship between cyclic strength and plasticity index of tailings

of cyclic strength test data on fine-grained tailings plotted versus the plasticity index. The tailings materials tested contained an average of about 30 % fines. With reference to the data in Fig. 44, it may well be assumed that the part of the cyclic strength contributed by the presence of fines increases approximately in direct proportion to the plasticity index of the fines at a rate of Ip/35 for a sand containing about 30 % fines. If this rate of increase in cyclic strength is assumed to hold approximately valid for any percentage of fines over 30 %, the factor of Ip/35 may be incorporated into the above empirical formula as a correction factor to allow for the effect of consistency of the fines. Thus, Eqs. (12) and (13) will be modified as,

$$\left(\frac{\tau_d}{\sigma_0'}\right)_{20} = 0.0676\sqrt{N_1} + 10^{-4}\cdot I_p\cdot C \qquad \cdots\cdots(17)$$

$$\left(\frac{\tau_d}{\sigma_0'}\right)_{20} = 0.009(N_1+13)+1.67\times10^{-3}\cdot I_p\cdot\log_{10}C \qquad \cdots\cdots(18)$$

Still other series of comprehensive investigations was carried out by Kokusho et al. (1983b) by using a large-scale test box 2 m in height and 2 m in diameter. A sand from the bed of the Tone river called Tonegawa sand was compacted to different densities in the box, and standard penetration tests were conducted under varying surcharge pressures which were applied through an air-inflated rubber bag placed over the compacted sand fill. After the penetration tests were over, small specimens were excavated and carried carefully to the soil testing laboratory located about 50 m distant without imparting any disturbance whatsoever. The cyclic triaxial tests were conducted undrained on these specimens to determine the cyclic strength. The results of these tests are presented in Fig. 45, where it can be seen that

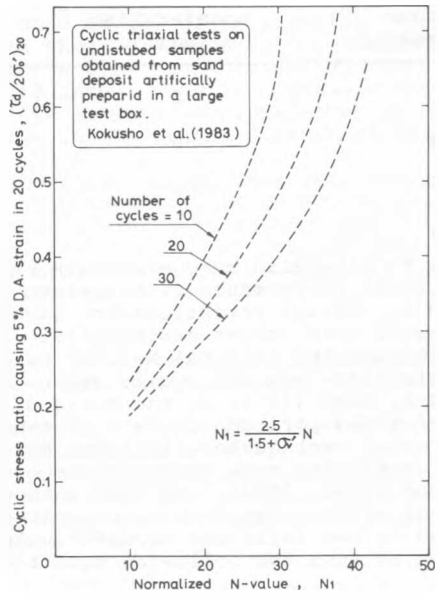

Fig. 45 Relation between the cyclic strength and N-value

the cyclic strength increases sharply with increasing N-value. Note that a new formula showr in Fig. 45 was used to compute the normalized blow count, N_1 in plotting the test data. This formula gives about the same value of N_1 as the formula indicated in Eqs. (11) and (14)

7.3 Correlation Based on Field Performances

Following the Niigata earthquake of 1964, the areas where liquefaction had and had not occurred were investigated by Kishida (1966), Koizumi (1966), and criteria for differentiating between soil conditions of liquefaction and non-liquefaction were developed based on the standard penetration resistance of the sand deposits. These criteria were established, however, on the tacit assumption that the intensity of shaking is on the order of 150 to 160 gal in terms of the ground acceleration as recorded in the city of Niigata.

On the other hand, field studies of liquefaction had also been underway in China, leading to the development of an empirical criterion which was incorporated into the Chinese seismic code in 1974 (Xie. 1979). According to this criterion, the critical blow count value, N_{crt}, differentiating between the occurrence and non-occurrence of liquefaction is given by

$$N_{crt} = \bar{N}\left\{1+0.125(d_s-3)-0.05(d_w-2)\right\} \qquad \cdots(19)$$

where d_s is the depth of the sand layer under consideration and d_w is the depth of the water table below the ground surface. $\bar{N}$ indicates the

reference N-value which is specified in Table 2 as a function of the intensity of shaking.

Table 2 REFERENCE BLOW COUNT VALUE IN CHINESE CODE

Chinese Intensity	Acceleration (gal)	$\bar{N}$
7	75	6
8	150	10
9	300	16

In order to establish more elaborate criteria, several field performance correlations have been proposed by several investigators, based on experiences of more recent earthquakes. A method of determining the critical N-value as a function of liquefaction-inducing cyclic stress ratio was proposed by Seed (1979) on the basis of a vast amount of field performance data of sand deposits during recent earthquakes, followed by a renewed version containing more comprehensive performance data (Seed et al. 1983). In this method, an equivalent cyclic stress ratio conceived to have developed in the field due to earthquake shaking is estimated from the following equation,

$$\frac{\tau_{av}}{\sigma_{v}'} = 0.65 \frac{a_{max}}{g} \cdot r_d \cdot \frac{\sigma_v}{\sigma_{v}'} \qquad \cdots\cdots(20)$$

This equation is similar to Eq. (4) except that a correction factor,0.65, is introduced to compute the average shear stress, τ_{av}. The next step in this method is to collect information on the N-value of the SPT and to calculate the N_1-value corrected to an effective overburden pressure of 1 kgf/cm^2 by the formula,

$$N_1 = C_N \cdot N \qquad \cdots\cdots(21)$$

The function to normalize the measured N-value is shown in Fig. 46. Having compiled a set of data

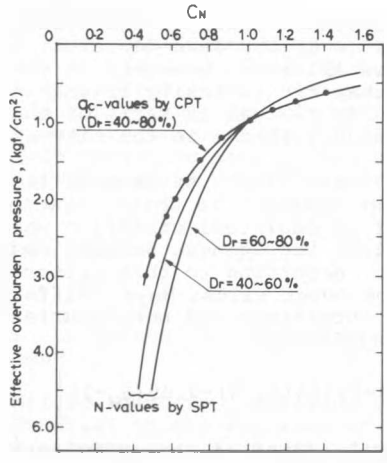

Fig. 46 Chart for the coefficient, C_N, (Seed et al. 1983)

as above, it becomes possible to plot values of the cyclic stress ratio known to be associated with some evidence of liquefaction or with non-liquefaction in the field versus the normalized penetration resistance, N_1, of the sand deposit being considered. Then, a line can be drawn through the plotted data points giving the lowest cyclic stress ratio known to cause liquefaction for any given N_1-value. This line is regarded as a boundary line differentiating between conditions in which liquefaction can and can not occur. The result of the most recent data compilation in the above vein by Seed et al. (1983) is shown in Fig. 47(a). Since most of the field performance data

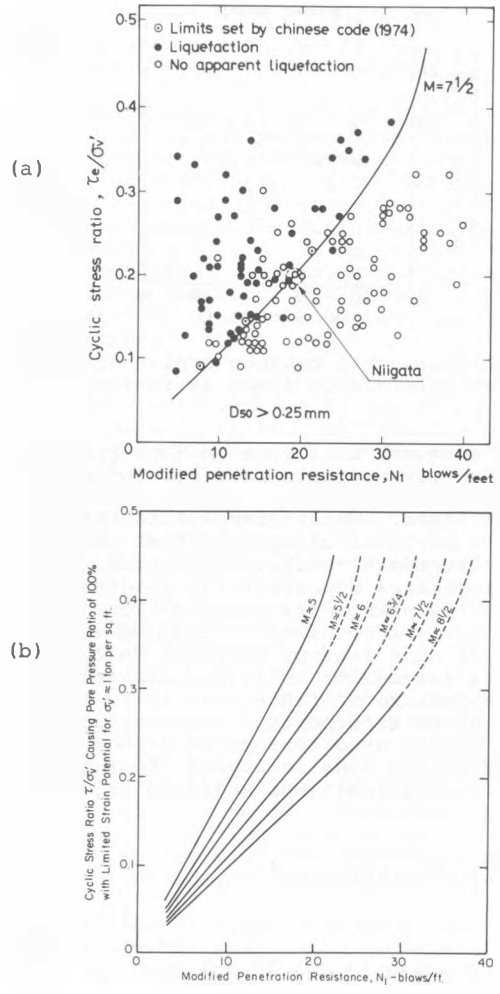

Fig. 47 Correlation between the cyclic stress ratio and the standard penetration resistance (Seed et al. 1983)

compiled in this figure are those from experiences of earthquakes with a magnitude around 7.5, it is so indicated in Fig. 47(a). Without accummulating more field data, it appears difficult to obtain different field performance curves for other magnitude events. However, the curve in Fig. 47(a) has been extraporated to other magnitude events on the basis of the numbers of cycles associated with these other earthquakes leading to the family of curves shown in Fig. 47(b).

In arranging the performance data shown in Fig. 47(a), it appears that a certain layer of sand at some depth representative of a site in question was taken up for consideration. If such a sand layer is located fairly deep overlaid by a thick non-liquefiable surface soil, there will be no visible sign of liquefaction on the ground surface even if the sand layer developed liquefaction deep in the ground. In such a case, the site is identified as a site of no-liquefaction and indicated accordingly with a white circle in Fig. 47(a). The occurrence of liquefaction within some layers at a given site is not uniquely associated with its visible manifestation at the ground surface, and, therefore, many of the data points of no-liquefaction are plotted in Fig. 47 in the zone above the boundary line. It is to be noted, therefore, that the boundary line in Fig. 47 simply implies a genuine soil characteristic identifying whether or not the soil itself can develop liquefaction under a given intensity of shaking which is expressed in terms of the cyclic stress ratio. In this sense, the boundary line curve in Fig. 47 has the same implication as the curve which can be depicted by the empirical formulae such as Eqs. (10), and (13).

Another comprehensive study in the same vein was made by Tokimatsu and Yoshimi (1983), who had accumulated a body of field performance data from past earthquakes mainly in Japan. Results of the data compilation were presented in the form of an empirical formula containing a parameter allowing for the effect of shear strain amplitude to define failure. The boundary line separating the occurrence and non-occurrence of liquefaction obtained from this formula for a failure condition of 3 % shear strain development is demonstrated in Fig. 48, where it may be seen that, while the curve lies approximately in the same zone as the others for a small blow count value, say, less than 20,

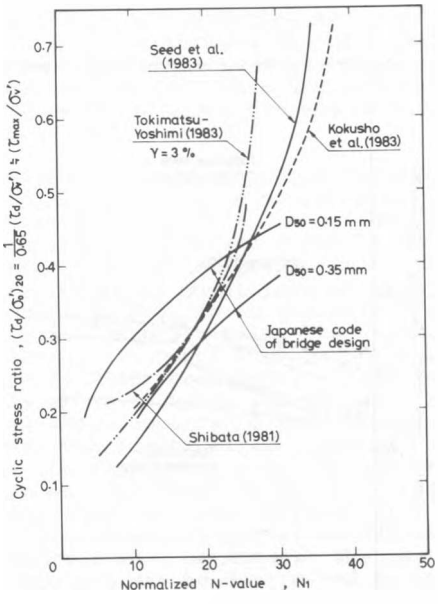

Fig. 48 Summary chart for evaluating the cyclic strength based on the normalized SPT N-value

the curve rises very sharply for a blow count value larger than 20. The boundary curve in Fig. 47 due to Seed et al. (1983) is also replotted in Fig. 48 by converting the cyclic stress ratio into the maximum stress ratio. The conversion was made simply by dividing the cyclic stress ratio by 0.65. Fig. 48 indicates that the boundary curve by Seed et al. gives a smaller cyclic stress ratio than that by Tokimatsu and Yoshimi in the ranges of the blow count value, N_1, which is smaller than 17 and larger than 25. These differences are probably due in part to differences in measuring the N-value in the United States and Japan.

A threshold curve in the same vein was also proposed by Shibata (1981) based on the data of field performances during past earthquakes. As indicated in Fig. 48, this curve gives slightly higher values of cyclic strength as compared to the curves by other investigators.

7.4 Summary of Correlations between Blow Count Values and Cyclic Strength for Clean Sands

The correlations between the cyclic strength and N_1-value established thus far are all plotted together in Fig. 48 for comparison purposes. In compiling the data from different sources, the following assumption is made which seems to hold approximately valid:

$$\left(\frac{\tau_d}{\sigma_0'}\right)_{20} \doteqdot \frac{1}{0.65}\left(\frac{\tau_d}{\sigma_v'}\right)_{20} \doteqdot \left(\frac{\tau_{max}}{\sigma_v'}\right) \qquad \ldots\ldots(22)$$

It may be noted that the laboratory-established curve by Kokusho et al. (1983) lies close to the curves by Seed et al. (1983), Tokimatsu and Yoshimi (1983), and Shibata (1981), which had been derived from field performances. It is surprizing to notice that, unlike the laboratory test results by others, the cyclic strength values determined by Kokusho et al. (1983b) shows much higher values particularly for dense sand. This appears to accrue as a result of having nimimized sample disturbance, as mentioned before, by carefully transporting the undisturbed samples. As demonstrated experimentally in Figs. 42 and 43 by Kokusho et al. (1983a), a series of small shocks likely to be imparted to samples during transportation and handling could exert deleterious effects on the quality of undisturbed samples particularly when the sand is dense. Therefore, the results of the laboratory tests by Kokusho et al. (1983b) would probably reflect real field performances, as evidenced by the comparison with other studies based on field performance data.

The formula used in the Japanese code for bridge design is also shown in Fig. 48. In view of the limitation when using these formulae for dense sand deposits, the curves derived from these formulae are shown only for a range of the normalized blow count value less than 30.

Looking overall at the cluster of curves in Fig. 48, one may conclude that for medium to high values of the SPT blow-count, all curves yield approximately the same cyclic strength, whereas variable cyclic strength values are obtained in the range of N_1-value less than about 10.

When using any curve in Fig. 48, it should be born in mind that the dependence of the cyclic strength on the confining stress is not taken into account. As indicated in Figs. 36 and 41, the laboratory-determined cyclic stress ratio at failure exhibits a relatively strong dependence on the confining stress particularly when the sand is dense and cemented. The charts shown in Fig. 48 have all been established on the basis of data obtained with effective overburden pressures or confining stresses of approximately 100 kN/m^2. Consequently, when the overburden pressure of a sand layer being considered deviates greatly from the above value, appropriate modifications should be made to values read from the chart.

7.5 Correlations for Fine-Grained Soils

The effects of fines contained in sand may be evaluated either in terms of the average grain size or in terms of the percentage of fines passing the #200 mesh. Because of the advantages of the use of the fines content, as explained before, this measure will be employed in the following discussion as an index parameter.

Two methods have been used to consider the effects of fines content on the correlation between the cyclic strength and N_1-value. One method is to assess an apparent increase in N_1-value so that it gives the same amount of cyclic strength as do clean sands without fines and, with this increased N_1-value, to enter the chart in Fig. 48 established for clean sand. The apparent increase in N_1-value is expressed as a function of fines content. Such an approach was suggested by Tokimatsu and Yoshimi (1983) who proposed the use of the relationship shown in Fig. 49 to compute the increment of N_1-value. Similar manipulation can be applied to the relationship of Eq. (13) by considering the term $6.5 \cdot \log_{10} C$ as being

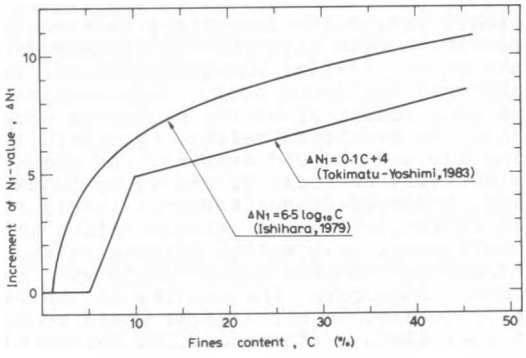

Fig. 49 Increment of N-value to evaluate the cyclic strength by the chart in Fig. 48, allowing for the effect of fines content

an increment of N_1-value due to the presence of fines. This relationship is also shown in Fig. 49. The other method is simply to establish an empirical relationship such as Eq. (12) on the basis of laboratory tests or field performance data during earthquakes for soil deposits containing fines.

The results of the investigations as outlined above are displayed in Fig.50 in terms of the cyclic stress ratio versus the normalized blow

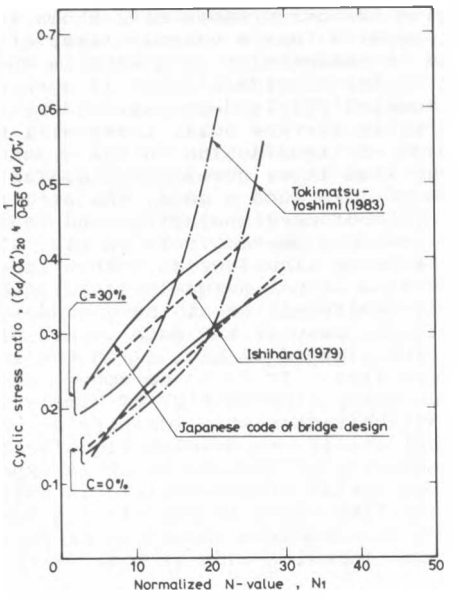

Fig. 50 Increase in cyclic strength due to inclusion of fines

count value, N_1. It may be seen that for a fines content of 30 %, the cyclic strength is increased about 30 % on the average for deposits with N_1-value up to about 20. Fig. 50 also shows that the curve by Tokimatsu-Yoshimi gives slightly lower cyclic strength for smaller N_1-values but higher cyclic strength for larger N_1-values as compared to the other curves. In order to examine the effects of fines, the cyclic strength estimated by the three methods is plotted in Fig. 51 versus the content of fines for blow count values of N_1=10 and 15. The figure shows that the formula by the

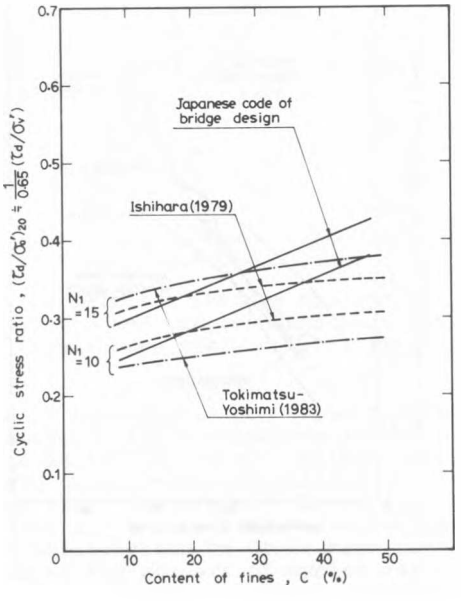

Fig. 51 Effects of fines content on the cyclic strength of fines-containing sand

Japanese bridge design code gives a higher rate of increase in cyclic strength with increasing fines content than do the other two formulae.

The presence of fines as a factor influencing the relationship between the cyclic strength and blow count values has been a topic of considerable discussion among engineers in China and many empirical formulae have been proposed in recent years to incorporate a correction for the generally authorized formula of Eq. (19). It is generally recognized that the present form of the Chinese code can be applied only for soils having a plasticity index less than 3. It is also accepted in China that soils with a plasticity index greater than 10 are almost immune to liquefaction and can be put aside in discussing code specifications. Therefore, the kind of fine-grained soils under consideration as potentially liquefiable in China are soils having a plasticity index between 3 and 10. In addition, the effects of fines are allowed for in most of the proposed formulae by considering the content of clay with a grain size smaller than 0.005 mm. Among many formulae proposed, the following two purporting to be most interesting are cited here for reference sake (Shi, 1984)

$$N_{cri}=\bar{N}\left[1+0.125(d_s-3)-0.05(d_w-2)-0.1(p_c-3)\right] \quad \cdots(23)$$

$$N_{cri}=\bar{N}\left[1+0.125(d_s-3)-0.05(d_w-2)\right]\left(\frac{3}{P_c}\right)^{0.5} \quad \cdots(24)$$

Where P_c is the content of clay in percent. It may be seen that the effects of clay content are incorporated in both of the above two formulae in such a way that the critical blow count value by the present code is decreased with increasing percentage of clay content.

7.6 Correlations for Gravelly Sands

Because of difficulties encountered in undisturbed sampling and laboratory testing and also because of ambiguity in interpreting the blow count value of the standard penetration test, attempts have seldom been made to correlate the cyclic strength of gravelly sands or sandy gravels with any parameter measured in the field.

One of the possible breakthroughs to this end would be to obtain the blow count value at some sites consisting of sand in the neighborhood of a gravel deposit in question which is conceived to have been formed under geologically and environmentally identical conditions and then to enter into the chart in Fig. 48 to evaluate a datum value of cyclic strength using the N-value as obtained above. It might also be possible to locate, in the same bored hole, a sand layer immediately above or below the gravelly layer in question which appears to have been formed under conditions identical to those of the gravel layer. If the blow count value of such a sand layer is known, the datum value of cyclic strength may be determined from the chart of Fig. 48. In any case, the content of gravel contained in the gravelly deposit must be known. The percentage of gravel content may be determined by measuring the quantity of gravel remaining on the #10 sieve with 2.00 mm mesh size or in the #4 sieve with a mesh size of 4.76 mm. The next step in this procedure would be to establish a correlation between the cyclic strength and the gravel content. A chart for this purpose could be established, if the resistance to liquefaction of gravelly sand is known by some means for deposits with different gravel contents but formed under identical depositional conditions. Once this kind of chart is established, it becomes possible to estimate the liquefaction potential of the gravelly deposit in question, with the known datum value of cyclic strength from the nearby sand deposit (zero gravel content) and also with the known percentage of gravel content. A chart of this type was established as shown in Fig. 52 on the basis of the results of the shaking table tests summarized in Fig. 28(e). It may be noted that the shaking table tests were conducted on sand deposits with different gravel contents propared under identical depositional conditions.

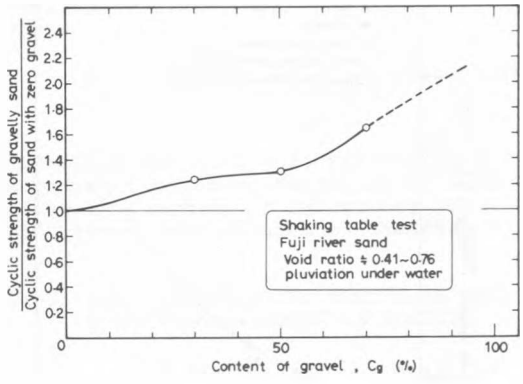

Fig. 52 Effects of gravel inclusion on the cyclic resistance of gravel-containing sand

7.7 Correlations between the Cyclic Strength and Cone Penetration Test

Several types of the cone penetration device have been developed, but the most commonly used would be the one called Dutch cone test in which a cone with a 10 cm base area with an apex angle of 60° is penetrated statically by means of a hydraulic or mechanical jack at a speed of approximately 2 cm/sec. In what follows, the data presented refer, unless otherwise mentioned, to those obtained by the Dutch cone. Although it has in the past been less widely used than the standard penetration test, the cone penetration test has the advantage that it can provide a high degree of resolution for identifying soil properties particularly in soft deposits of clayey or silty soils where the SPT N-values of less than one are encountered. The other unequalled advantage lies in its high level of capability for delineating stratigraphy of soil deposits.

A correlation between the cone bearing and the cyclic strength may be established based on the same general principles as those used for the SPT correlation. Seed (1981, 1983) suggested the modification of the cone bearing, qc, to that corresponding to an effective overburden pressure of 1 kg/cm^2 using the relations, C_N, such as those of Eqs. (11) and (14), or Fig. 46. Then, the normalized cone bearing, q_1, is defined as

$$q_1 = C_N q_c \quad \cdots\cdots(25)$$

If test data of cyclic strength is available together with the cone bearing data for the same soil deposit, a correlation between these two sets of soil parameters can be established. Fig. 53 shows the results of data plotting in the above contest using test data on alluvial sands in the reclaimed land in Tokyo Bay and in the city of Niigata (Ishihara and Koga, 1981). The cyclic strength of the sandy soils in Tokyo Bay was obtained from the cyclic triaxial tests on undisturbed samples recovered by means of the Osterberg-type tube sampler. Although there is considerable scatter in the data points, a line was drawn through the entire data set, which may be used as a boundary line seperating conditions in which liquefaction can and can not occur.

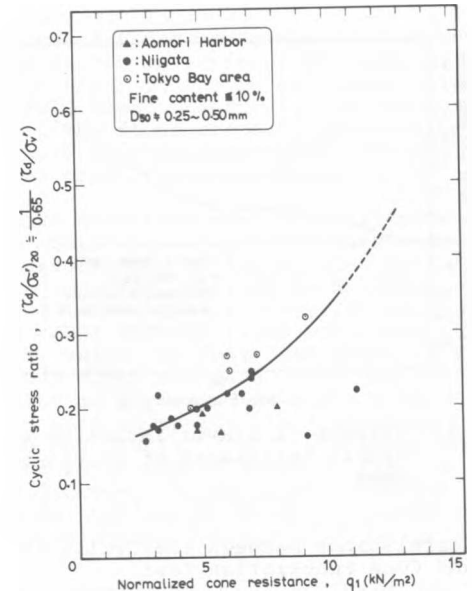

Fig. 53 Correlation between cyclic strength and normalized cone resistance for clean sands

When soils contain fines greater than about 10 % by weight, the curve shown in Fig. 53 is no longer usable. Since the presence of fines appears to exert a similar influence on the cone bearing as it does on the SPT resistance, it would be reasonable to introduce a correction factor into the correlation established for clean sands. The easiest way to achieve this correction is first to determine an increment of q_1-value in accordance with the manner in which the content of fines is accounted for in Eq. (13). In the case of the standard penetration test, the effect of fines is viewed in Eq. (13) as being allowed for by using an equivalent N_1-value which is increased by an amount $6.5 \log_{10} C$. However, since the cone bearing in the CPT has been known to take a value approximately four times the SPT N-value for silt to sand-sized soils, it would appear appropriate to introduce a correction factor of $4 \times 6.5 \log_{10} C = 26 \log_{10} C$. Thus, a corrected cone resistance, q_2, may be evaluated by

$$q_2 = q_1 + 26 \log_{10} C \qquad \cdots\cdots (26)$$

The in-situ cone bearing data for silty sands obtained in the reclaimed lands in Tokyo Bay were corrected through Eq. (26) and they are plotted in Fig. 54 versus the cyclic strength test data on undisturbed samples recovered by the Osterberg sampler. Also indicated in Fig. 54 is a curve quoted from Fig. 53. It should also be noted, based on the comparison in Fig. 54, that the effects of decreasing cone bearing or increasing cyclic strength caused by the presence of fines may be taken into account by correcting the q_1-value through Eq. (26) and then using a chart such as that of Fig. 53 established for clean sands with very little fines content.

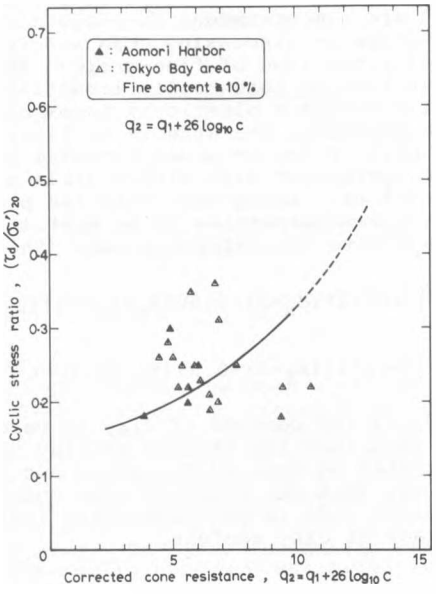

Fig. 54 Correlation between cyclic strength and Dutch cone resistance corrected for fines content

VIII SIMPLE METHOD OF ANALYSIS FOR LIQUEFACTION IN LEVEL GROUND

8.1 General

A general method of analysis to assess a possibility of liquefaction or cyclic mobility occurring in the level ground was proposed by Seed and Idriss (1971). In this method the cyclic stress ratio induced in a soil deposit by earthquake shaking is estimated from a knowledge of the magnitude of acceleration at the ground surface and compared against the corresponding cyclic strength expressed in terms of the cyclic stress ratio causing liquefaction or cyclic mobility in the soil deposit in question. Similar methods of liquefaction analysis were suggested by Ishihara (1977) and Iwasaki et al. (1978), but these are somewhat different from the analysis method developed by Seed and Idriss. The essential difference between these two types of approach , however, appears to lie in the way the effects of the irregular time history of shear stress applications is taken into account in the framework of the analysis.

In the method of Seed and Idriss, the irregular nature of earthquake loading is allowed for by

converting a given load time history into a sequence of uniform loads with specified amplitude and number of cycles. The specification of the amplitude is made by taking 65 % of the maximum stress ratio as defined by Eq. (4). The number of cycles is specified as a function of the magnitude of the earthquake in question. For a typical event of 7.5 magnitude, the number of cycles is chosen to be 15. Thus, the irregular nature of load applications is taken into account in the framework of enviromental conditions in which external forces are created. The corresponding cyclic strength to be compared against is determined either from the results of cyclic load tests on undisturbed samples or from a correlation chart between cyclic loading resistance and the penetration resistance of the soil. If the externally applied cyclic stress is greater than the cyclic strength, liquefaction is judged to occur, but otherwise no liquefaction takes place.

On the other hand, the method of analysis by Iwasaki et al. is based on the characteristics of soils responding differently depending upon the type of irregular wave forms. The effects of the irregularity in seismic shaking is allowed for in terms of the material reponse by introducing some correction factors which are to be applyed to the failure-inducing cyclic stress ratio determined typically by the cyclic triaxial tests under uniform loading conditions. Generally, the cyclic stress ratio causing liquefaction or 5 % double-amplitude axial strain in 20 load cycles is used as a measure to represent the cyclic strength of soils. This cyclic stress ratio is corrected by multiplying the load irregularity factor, C_2, discussed in Chapter 3. The external shear stress induced by seismic shaking is expressed in terms of the maximum shear stress ratio as given by Eq. (4) and this is compared against the strength as determined above.

A somewhat different method of analysis was proposed by Dobry et al. (1980) by considering the threshold level of strains at which pore water pressures in the sand start to build up. The magnitude of ground surface acceleration great enough to initiate a build-up of pore water pressure on the soil was correlated with the threshold strain for the soil determined by laboratory tests. Because this method is based on the onset condition of pore water pressure buildup, it will generally yield somewhat conservative predictions for the occurrence of liquefaction. However, this method of analysis appears of interest in that it incorporated the use of in-situ shear wave velocity measurements which are sometimes executed in the hope of obtaining soil property data for certain kinds of soil with a higher level of accuracy than can be obtained with any kind of penetration test.

8.2 A Method of Liquefaction Analysis

The simple method of liquefaction analysis adopted in the following pages is essentially the same as that proposed previously by Ishihara (1977) and Iwasaki et al. (1978). It gives results very similar to those obtained by the method proposed by Seed and Idriss (1977). The external shear stress is evaluated in terms of the maximum shear stress ratio, τ_{max}/σ_v', given by Eq. (4). It will be stipulated that the value of τ_{max} is determined by using the greater value of the maximum accelerations which are generally measured in EW-and NS-directions on the ground surface. The cyclic strength corresponding to the above conditions is given by,

$$\frac{\tau_{max,\ell}}{\sigma_v'} = C_1 \cdot C_2 \cdot C_5 \left(\frac{\sigma_{d\ell}}{2\sigma_0'} \right)_{20} \qquad \cdots\cdots(27)$$

where $C_2 \cdot C_5$ expresses the combined effect of load irregularity in multi-directional loading. On the basis of the exhaustive discussions in Section 3.3, the combined coefficient, $C_2 \cdot C_5$, will be assume to take a value shown in Table 3. The coefficient, C_1, allows for the effect of K_0-condition and is assumed to be given by

$$C_1 = \frac{1+2K_0}{3} \qquad \cdots\cdots(28)$$

The adequacy of using this relationship for the wide range of relative densities of sand has been verified by a series of laboratory tests using the torsion shear test apparatus (Yamazaki, 1984).

Table 3 LOAD IRREGULARITY FACTOR IN MULTI-DIRECTIONAL IRREGULAR LOADING

	Loose sand $D_r = 40 \sim 60\%$	Dense sand $D_r = 60 \sim 80\%$
$C_2 \cdot C_5$	1.55	1.45

The liquefaction potential of sand deposits is evaluated in terms of the factor of safety, F_ℓ, which is defined as

$$F_\ell = \frac{\tau_{max,\ell}/\sigma_v'}{\tau_{max}/\sigma_v'} \qquad \cdots\cdots(29)$$

If the factor of safety is equal to or less than unity, liquefaction is said to take place. When liquefaction does not occur with a computed factor of safety greater than unity, the extent of pore water pressure buildup relative to the initial overburden pressure can be estimated by using the curve indicated in Fig. 55. The relationship shown in this chart was established by observing the residual pore water pressures in the laboratory test specimens subjected to irregular loads with varying levels of the maximum shear stress ratio.

IX CASE STUDIES OF LIQUEFACTION

9.1 General

Cases of liquefaction-induced damage during earthquakes have been reported by many investigators,

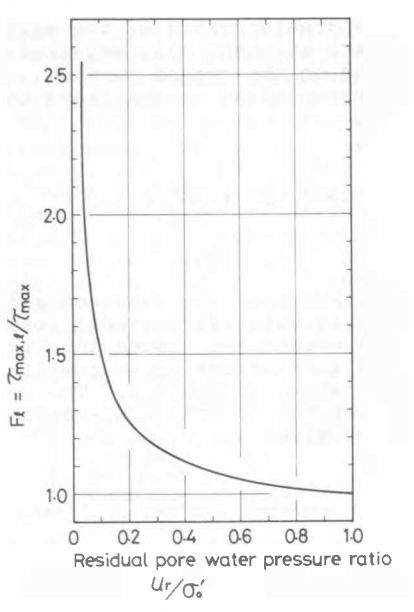

Fig. 55 Relationship between the residual pore pressure ratio and factor of safety against liquefaction

since the events in 1964 in Niigata and Alaska. Several features of ground damage characteristics during the 1964 Niigata earthquake were disclosed by elaborate studies by Kishida (1966), Koizumi (1966) and Ohsaki (1966). Subsequently, some studies were made on the cause of the liquefaction in Niigata by Ishihara et al. (1978, 1979, 1981). The failure of the Lower San Fernando dam during the earthquake of 1971 was described in detail by Seed et al. (1975). The failure was attributed to the liquefaction which occurred in the loose deposit of sandy soils in the dam constructed by the hydraulic method. The cause of landsliding in the Joseph Jensen Filtration Plant at the time of the San Fernando earthquake was atributed by Dixon et al. (1973) to the liquefaction of the natural deposit of saturated alluvium underlying a thick layer of compacted fill. The rupture of the ground resulting from the liquefaction of fluvial deposits during the Tokachi-oki earthquake was reported by Tohno et al. (1981). The ground failures such as landsliding and liquefaction of sand deposits which occurred during the Vrancea earthquake of 1977 was reported by Mandrescu (1978, 1981), Botea et al. (1980), Perlea (1981), and Ishihara and Perlea (1984). The liquefaction-induced damage during the Monte Negro earthquake of 1979 was described by Talaganov et al. (1981). The results of investigations made after the Guatemala earthquake of 1976 (Magnitude 7.6) in the area of La Playa near the edge of Lake Amatitlan were described by Seed et al. (1981). Youd and Bennett (1983) presented results of comprehensive in-situ investigations at sites where liquefaction took place at the time of the Imperial Valley earthquake of 1979.

From the number of liquefaction cases outlined above two cases, viz., the Niigata earthquake of 1969 and the Monte Negro earthquakes of 1979 will be taken up for somewhat detailed discussions.

9.2 Intensity of Ground Shaking Associated with In-Situ Liquefaction

The intensity of earthquake shaking large enough to cause liquefaction depends, needless to say, on the looseness or denseness of soils comprising the ground. The soils in the field are deposited, in many cases, however, with a density greater than a certain value, say, about 40 % in terms of relative density, whether they have been artificially placed or naturally deposited. Therefore, there appears to be a certain lower limit in the magnitude of ground acceleration during an earthquake which can barely bring about liquefaction in actual field deposits. Such a minimum value of acceleration would be discovered by examining motions of the ground recorded during major earthquakes in the past. Listed in Table 4 are the maximum horizontal accelerations on the ground recorded at sites where liquefaction is known to have occurred in their neighborhood within a distance of about 5 Km. Table 4 indicates that the minimum value of ground acceleration ever monitored with the liquefaction occurring in its vicinity was 116 gal and this was on an old landfill at Aomori Harbor in Japan at the time of the Nihonkai-Chubu earthquake of May 26, 1983.

Table 4 VALUES OF MAXIMUM ACCELERATION RECORDED AT SITES IN THE NEIGHBORHOOD OF LIQUEFIED GROUND DURING THE RECENT EARTHQUAKES

Earthquake	Date	Magnitude	Site of recording	Epicentral distance (km)	Max.acc.(gal)		Ground conditions
					NS	EW	
Niigata (Japan)	1964 June 12	7.5	Kawagishi-cho	55	155	159	Artificial sand fill
Tokachi-oki (Japan)	1968 May 16	7.9	Aomori harbor	280	213	180	Alluvial sand
Tokachi-oki (Japan)	1968 May 16	7.9	Hachinohe harbor	210	235	188	Alluvial medium dense sand
Vrancea (Romania)	1977 March 4	7.2	Bucharest	120	213	178	Loess (Silty loam)
Nihonkai-chubu(Japan)	1983 May 26	7.7	Akita harbor	107	190	205	Artificial sand fill
Nihonkai-chubu(Japan)	1983 May 26	7.7	Aomori harbor	156	95	116	Alluvial sand
Miyagiken-oki (Japan)	1978 June 12	7.4	Ishinomaki	100	289	200	Rock
Monte Negro (Yugoslavia)	1979 April 15	7.2	Herceg-Novi	73	228	255	Soft rock

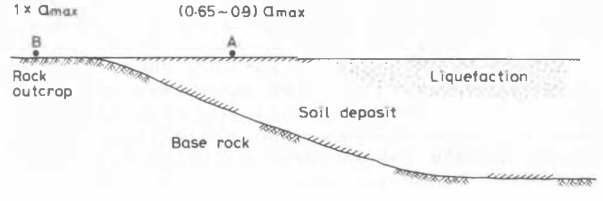

Fig. 56 Illustration of ground conditions for sites where acceleration records are obtained

In order to compare the magnitude of accelerations recorded at sites with different ground conditions such as those illustrated in Fig. 56, the data in Table 4 are classified into two groups ; those on rock outcrops and the others on soil deposits both in the free field. Among the several records obtained on soil deposits, the motions at Niigata

were obtained right on the site of liquefaction, but all others were acquired at the sites where liquefaction occurred in their neighborhood. It may be seen in Table 4 that the ground accelerations recorded on the soil deposits lie in the range between 116 gal and 235 gal, but the majority are in the range of 200 gal to 235 gal. Table 4 also shows that the accelerations recorded on the rock outcrops near the place of liquefaction were somewhat higher than those recorded on the soft deposits. This may be understood if one is reminded of the fact that soils exhibit much higher damping than rock materials especially when the shaking is strong thereby inducing large shear strains. Although the available data are scarce, it may roughly be mentioned that, whenever the intensity of shaking is stronger than about 260 gal on the rock outcrop and whenever it is greater than approximately 200 gal on the soil deposit, it appears likely that liquefaction can take place in their vicinity if the sand is a loose deposit of alluvium or man-made fill. It may as well be argued that the ratio of acceleration on the soil deposit to that on the rock outcrop causing liquefaction in their vicinity is approximately in the range of 0.65 to 0.9 with an average of about 0.8. This ratio will be useful when roughly assessing ground accelerations on soil deposits from known values of accelerations on rock outcrops in connection with making analyses of liquefaction.

9.3 Niigata Earthquake of 1964

At 1:01 p.m. on June 16, 1964, a violent earthquake rocked the Niigata prefecture in Japan, inflicting considerable damage in the city area of Niigata. In the area along the Shinano and Agano rivers where sand deposits were widespread, the damage was primarily associated with the liquefaction of loose sand deposits. Buildings not enbedded deep in firm strata sank or tilted towards the direction of the center of gravity. Underground installations such as septic and storage tanks, sewage conduits and man-holes floated up a meter or two above the ground surface. In flat fields, sand flows and mud volcanos ejected water and sand 2 to 3 minutes following the main shaking of the earthquake. Sand deposits 20 to 50 cm thick covered the entire city area, as if the whole area were inundated by a flood.

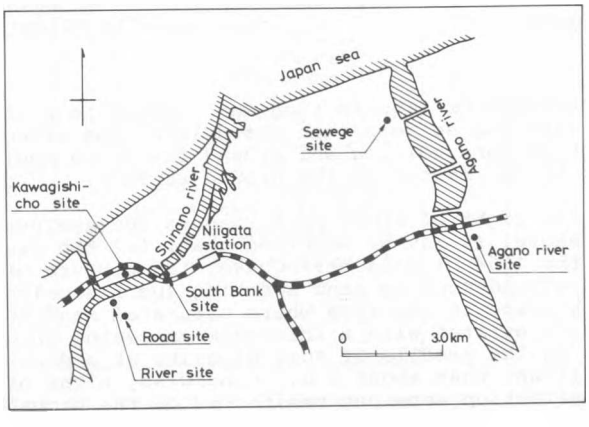

Fig. 57 Sites of in-situ investigations in Niigata area

The area affected by the hazardous liquefaction was mainly located along the Shinano river indicated in Fig. 57. About 15 years after the earthquake, a series of detailed investigations was undertaken to clarify the cause of the liquefaction. The investigations included the standard penetration test, Dutch cone test, sampling of undisturbed specimens from sand deposits below the ground water table and testing undisturbed samples in laboratory cyclic triaxial tests to determine the cyclic strength of the intact samples. The locations of six sites thus investigated are shown in Fig. 57, and the items of in-situ investigations conducted at each site are listed in Table 5.

Table 5 ITEMS OF IN-SITU INVESTIGATIONS IN THE CITY OF NIIGATA

Site	Method of Sampling	Penetration test	Signs of Liq. or non-Liq.	Formation of deposits
River site	Large Dia. Sampling Osterberg sampling	SPT	Liq.	Reclaimed and alluvium
Road site	Osterberg sampling	SPT	No. Liq.	Alluvium and diluvium
Kawagishi-cho site	Large Dia. Sampling Osterberg sampling	SPT CPT	Liq.	Reclaimed deposit
South bank site	Large Dia. Sampling Osterberg sampling	SPT CPT	No. Liq.	Diluvium
Sewage site	Block Sampling in an excavated pit	SPT	Liq.	Alluvium
Agano river site	Large Dia. Sampling	SPT	Liq.	Alluvial riverbed

The soil profiles and SPT N-values obtained at each site are shown in Figs. 58 to 63, together with the results of the cyclic triaxial tests. On the basis of the cyclic strength data, analysis of liquefaction was performed using the simple procedure described in the foregoing chapter. In making the liquefaction analysis, the maximum horizontal accelerations of 158 gal and 155 gal in EW-and NS-directions, respectively, monitored at the basement of the Kawagishi-cho apartment were used for all deposits of the sites analyzed. These sites are all located within 10 Km from the Kawagishi-cho site and the values of acceleration as above may well be regarded as representative of the intensity of shaking in the respective site. In the analysis, the K_0-value appearing in Eq. (28) was taken as 0.5. The cyclic strength values used in the analysis were those obtained from the cyclic triaxial tests conducted on undisturbed samples of sand.

The results of the analysis are presented in Figs. 64 to 69. Of six cases being considered, four sites are known to have undergone ground damage due to liquefaction. The observation of the soil profile data on these four sites indicates that the ground water table was in all cases located at a depth shallower than 2.0 m and that deposits of clean sand with SPT N-values less than about 10 exist down to a depth of about 6 to 10 m. The cyclic strength data for these sand deposits are shown to lie in the range between 0.1 and 0.2. The results of the analyses all indicate, in coincidence with the observed in-situ performances during the 1964 earthquake, that the liquefaction could occur in the deposits of loose sand as described above. In contrast to the above, the soil profile data

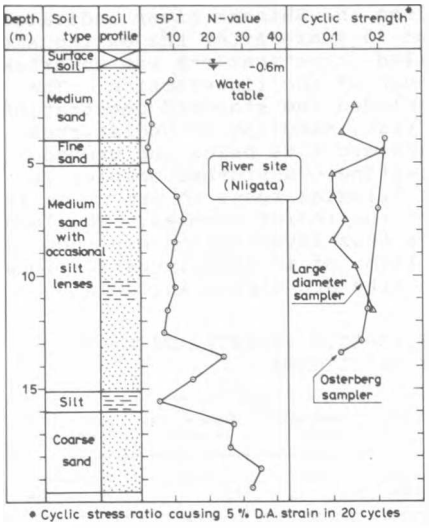

Fig. 58 Soil profile at River site in Niigata

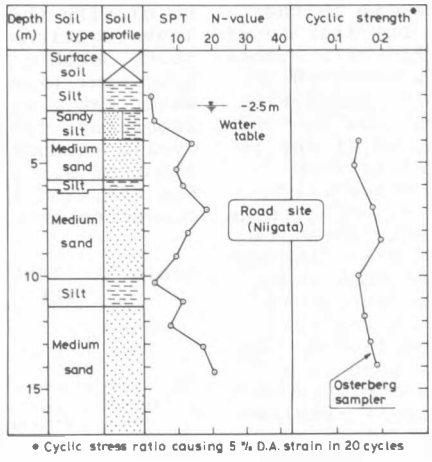

Fig. 59 Soil profile at Road site in Niigata

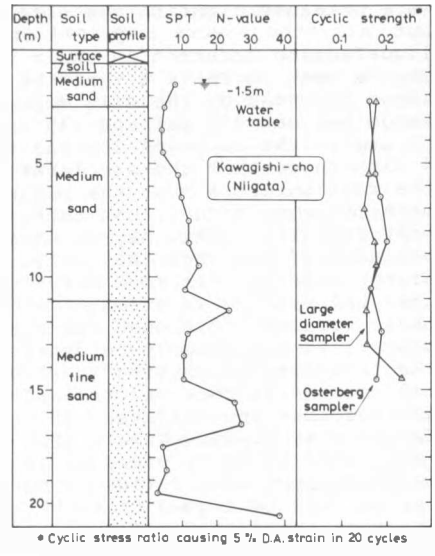

Fig. 60 Soil profile at Kawagishi-cho site in Niigata

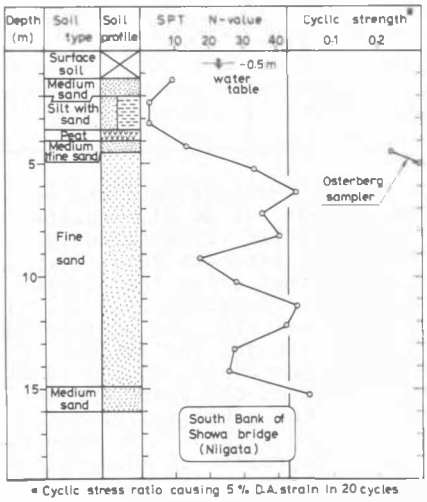

Fig. 61 Soil profile at South Bank site in Niigata

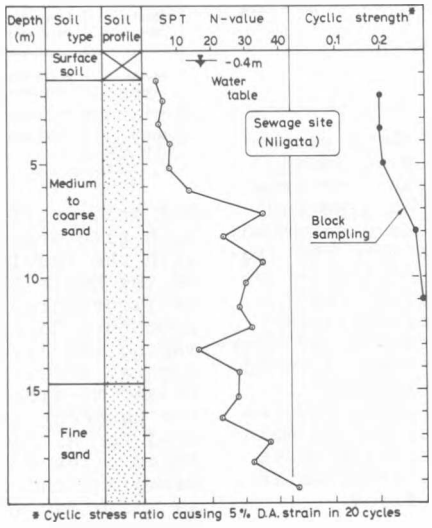

Fig. 62 Soil profile at Sewage site in Niigata

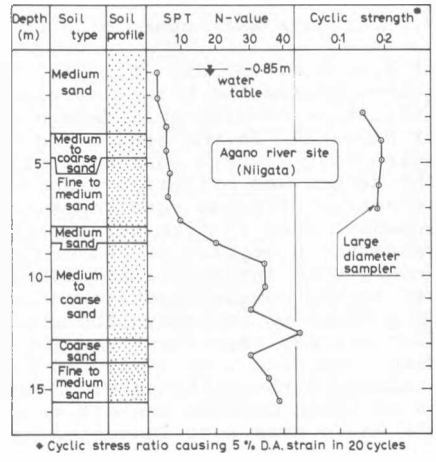

Fig. 63 Soil profile at Agano river site in Niigata

at the two sites (the Road site and the South Bank site) where surface evidence of liquefaction was not observed indicate commonly that there exists a surficial layer to a depth of 4 to 5 m consisting of what is called surface soil and underlying silt or sandy silt. The surface soil implies a man-made fill composed of a potpourri of various kinds of soils or stones which are immune to liquefaction. It is also observed that the liquefaction-immune surficial layers are underlaid by deposits of loose sand but their thickness is limited to about 2 to 3 m. The results of the analysis shown in Figs. 65 and 67 indicate that liquefaction might probably have developed locally in the sand deposits underlying the surficial layer but its extent was limited to a few meters in thickness. Therefore, it would appear likely that the occurrence of liquefaction was limited to a layer so thin and so deep that its deleterious effects such as sand boiling and ground fissuring could not be manifested on the ground surface.

In the light of field performances and analyses as above, it may be observed that, for the case of the 1964 Niigata earthquake, the rupture of the ground such as sand spurting and fissuring took place in the area where saturated sand deposits existed with a thickness exceeding about 3 m in the profile of soil deposits at a depth shallower than about 3 m. Otherwise, signs of liquefaction were not manifested on the ground surface, although the liquefaction might have locally occurred in some thin layer located sufficiently deep in the deposit.

9.4 Monte Negro Earthquake of 1979

A disastrous earthquake of magnitude 7.2 took place in Monte Negro, Yugoslavia, at 7:20 a.m. April 15, 1979, affecting the widespread area along the coast of the Adriatic sea from Croatia to the northern part of Albaria. Its epicenter was located in the Adriatic sea about 15 Km off the coast of Ulcinj and the focal depth was 25 Km, as shown in Fig. 70. Fig. 71 shows an isoseismic map of this earthquake developed by the Yugoslav Association of Seismology (Petrovski and Paskalov, 1981). Fig. 70 indicates the maximum ground accelerations in three components recorded at several

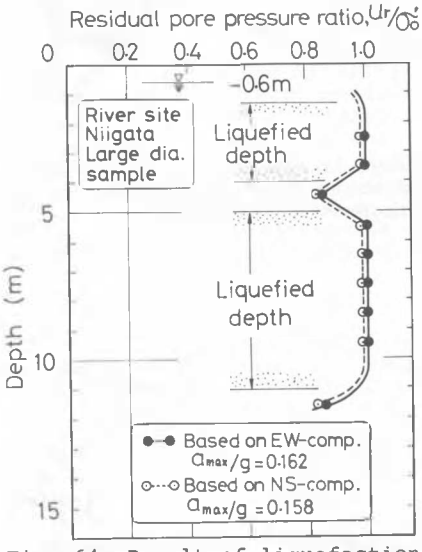

Fig. 64 Result of liquefaction analysis for River site in Niigata

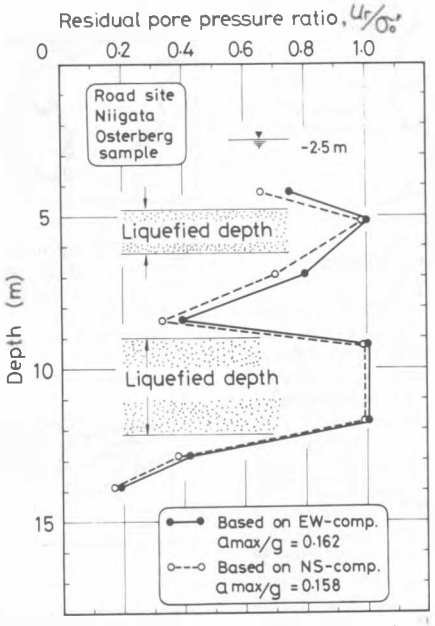

Fig. 65 Result of liquefaction analysis for Road site in Niigata

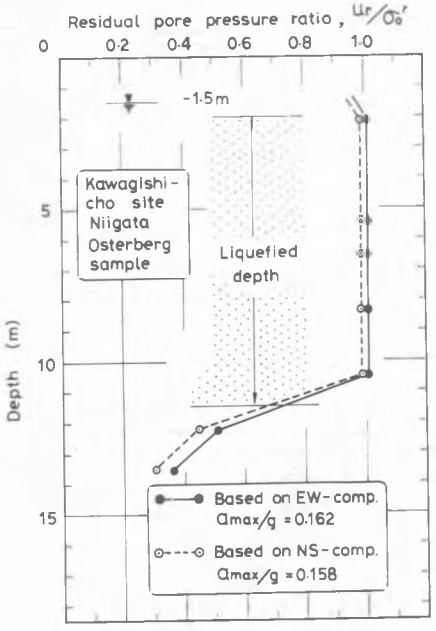

Fig. 66 Result of liquefaction analysis for Kawagishi-cho site in Niigata

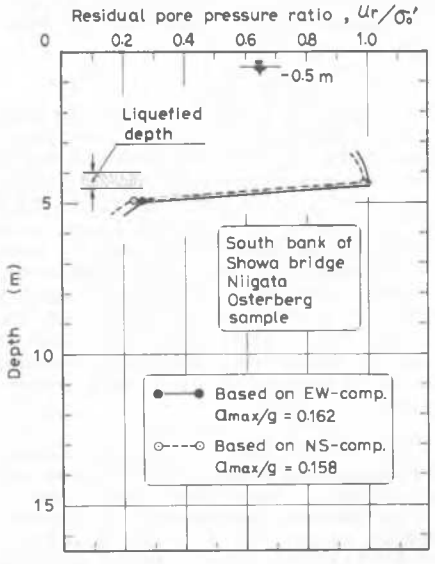

Fig. 67 Result of liquefaction analysis for South Bank site in Niigata

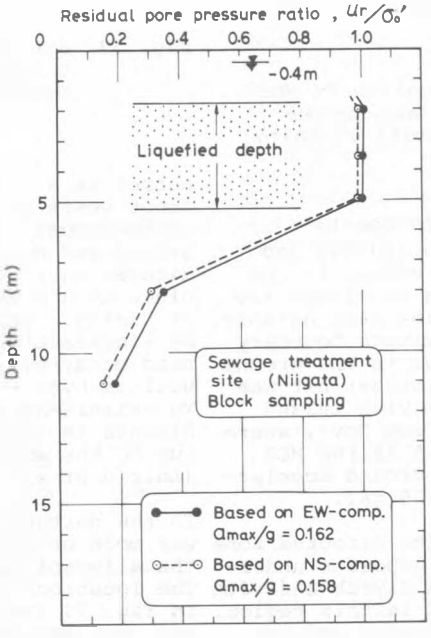

Fig. 68 Result of liquefaction analysis for Sewage treatment site in Niigata Niigata

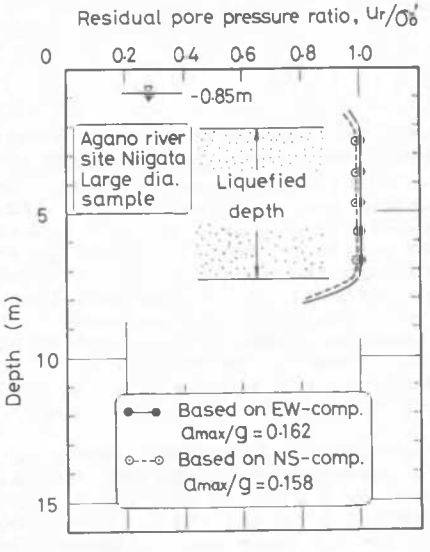

Fig. 69 Result of liquefaction analysis for Agano river site in Niigata

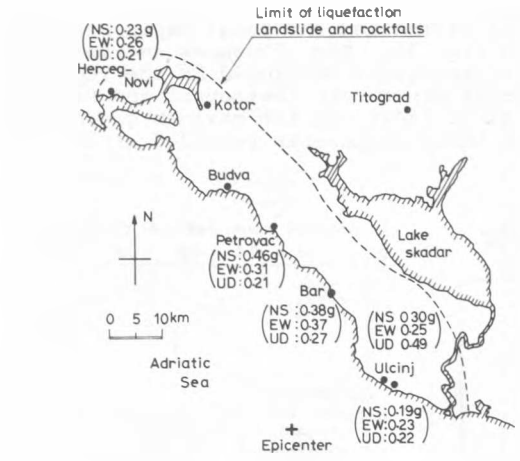

Fig. 70 Area inflicted by the Monte Negro earthquake of April 15, 1979

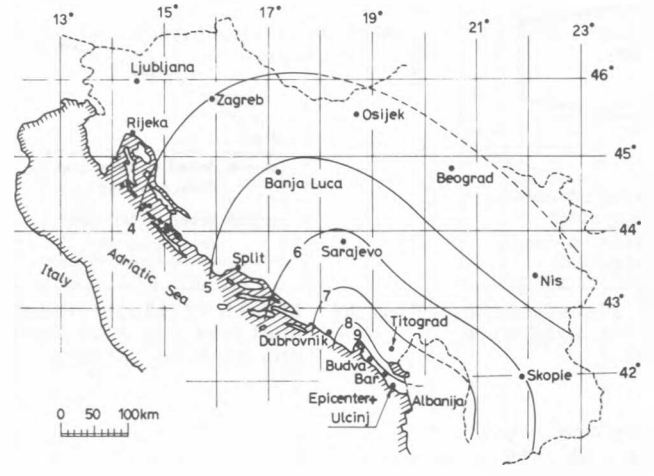

Fig. 71 Seismic intensity distribution in MCS scale of the Monte Negro earthquake of April 15, 1977 (Petrovski-Paskalov, 1981)

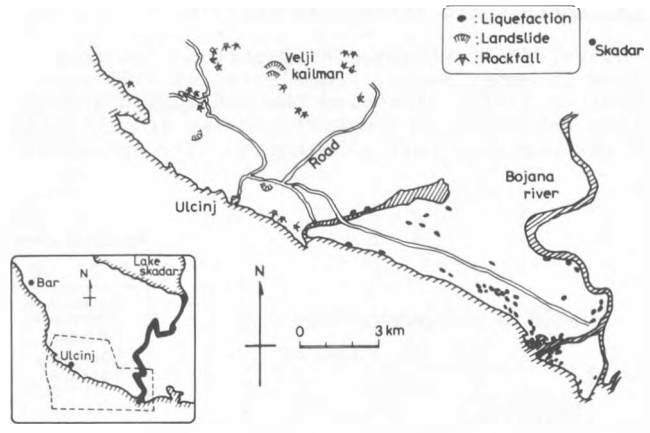

Fig. 72 Ground damage in the region of Ulcinj due to the Monte Negro earthquake of 1979. (Talaganov et al.1981)

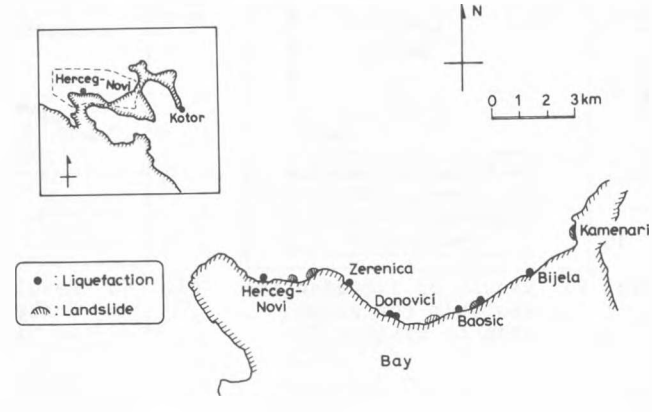

Fig. 73 Sites of ground damage due to liquefaction near Herceg-Novi during the Monte Negro earthquake (Talaganov et al. 1981)

stations located along the Adriatic coast. Among various types of damage to buildings and infrastructure installations, the damage to the ground due to liquefaction, slides in slopes and rockfalls in the limestone mountains were notable. Indicated in Fig. 70 is the approximate boundary showing the area of heaviest damage to the ground and slopes. It may be seen that hardest hit was the littoral belt zone about 15 Km wide inland extending from Ulcinj north to Herceg Novi, where the intensity of shaking was 8 to 9 in the MCS scale with the maximum horizontal ground acceleration greater than approximately 220 gal.

The overall geological regime of the affected zone is described as talus and fluvial deposits underlaid by a kind of claystone called flysch and with limestone constituting the bedrock in this region. In the southern area of Budva, Petrovac and Bar where the mountains rise sheer from the sea, the soft soil deposit is absent and the flysch or limestone formation outcrops directly on the ground surface. In such regions, the ground damage occurred in a limited area in proximity to the waterfront where man-made landfills existed. In the southernmost region near Ulcinj, the damage to the ground and mountain slopes was extensive. As indicated in Fig. 72, landslides and rockfalls took place at a number of places in the mountains north of Ulcinj. Subsidence and lateral spreading caused by liquefaction of a layer of very fine grained sand occurred at many locations along the banks as well as over the delta of the Bojana river on the Yugoslavia-Albania border. The town of Skadar in Albania is reported to have been severely damaged due to the extensive development of liquefaction (Anicic et al. 1980).

In the northern part around the inlet, the damage was more or less associated with liquefaction of the alluvial sand deposit along the coast line. The locations of the ground damage are indicated in Fig. 73 (Talaganov et al. 1984). At Bijela, port and shipyard facilities were heavily damaged due to failure of a man-made landfill. In Kotor, the liquefaction occurred extensively in the deltaic area where the quay, a hotel and a park were located. Lateral displacement and settlements in

the parking lot between tiebacks to the quay wall were of the order of 50 cm in the quay area. An outdoor swimming pool of the hotel floated up about 1 m due to the uplift pressure. An annex building housing an indoor swimming pool collapsed due to lateral spreading of the foundation. A monument in the park tilted noticeably. Almost the entire stretch of beach in this area subsided about 50 cm into the bay. In Kamenari a section of the coast road slid into the bay, due probably to the liquefaction of the sand deposit. A peninsula reportedly extended several tens of meters into the bay at this location before the earthquake. The feature of the slumping is roughly described in Fig. 74. A surveillance of part of the exposed surface indicated that a man-made fill composed of a mixture of silt, sand and stone existed near the ground surface. A sand-rich deposit reportedly underlying this surface fill appears to have liquefied and triggered the slide. In Zelenica, a quay wall constructed of sand and gravel held within a rock retaining wall failed, involving a subsidence of an old two-story warehouse on a slab foundation as shown schematically in Fig. 75. The retaining wall in the area of

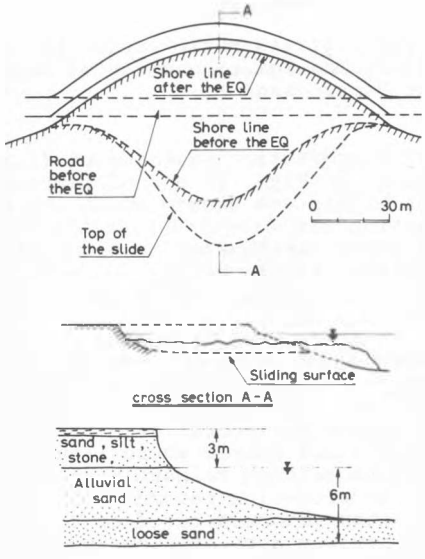

Fig. 74 Kamenari slide during the Monte Negro earthquake of April 15, 1979

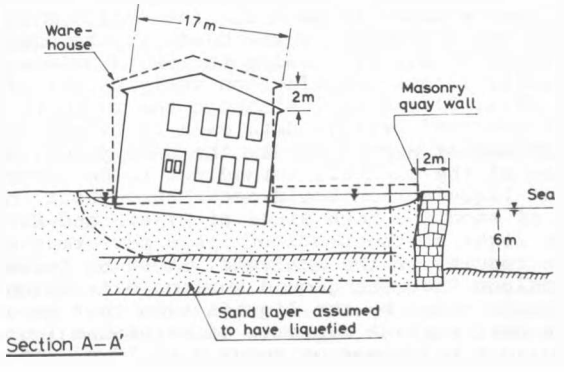

Fig. 75 Damage to a warehouse due to the lateral movement of the quay wall in Zelenica

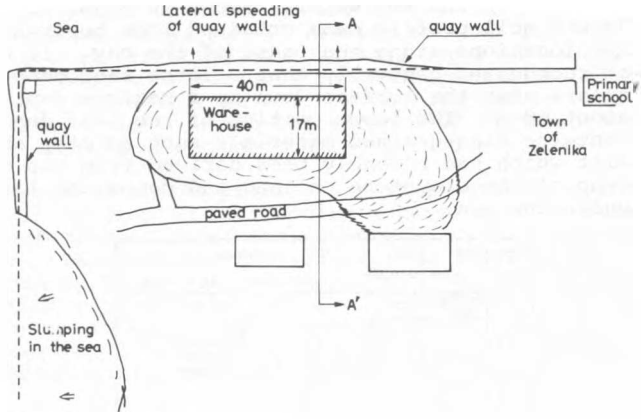

Fig. 76 Damage to the ground and quay wall in Zelenica

soil failure was displaced about 2 m horizontally and a lesser amount vertically. Before the earthquake the quay wall area had extended farther towards the sea about 60 m from the location of the warehouse as illustrated in the plan view of Fig. 76. The most seaward portion of the quay had reportedly slid into the sea for a stretch of more than 100 m as indicated in Fig. 76. About 300 m inland from the warehouse location, there is a primary school building which also suffered a differential settlement of the order of 10 cm. A boring made at the playground of the school disclosed the existence of a sand deposit down to a depth of 20 m having a SPT blow count value of 5 to 10. Since the warehouse is located in the area with the same depositional condition, it is most likely that the liquefaction of the sand underlying the quay had triggered the slide toward the sea.

The overall geological regime in the region of Herceg Novi, Zelenica, Bijela, Kamemari, Kotor and Tivat can be described as consisting of talus deposits underlaid by the baserocks, flysch and limestone. This feature is schematically illustrated in Fig. 77. The colluvial talus is composed of a gravel-rich deposit near the foot of the limestone cliff, but its composition changes coastwards to sand-rich sediment. Near the beach of the bay, a clear pattern of the colluvial deposit had been disturbed by actions of small rivers and waves or

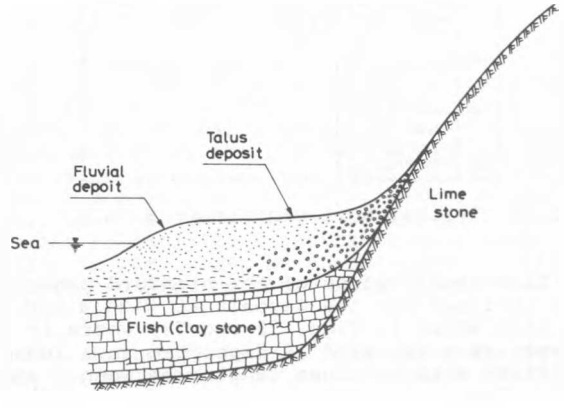

Fig. 77 Schematic illustration of the geological regime in Kotor-Tivat region

currents of the sea water. Shown in Figs. 78 and 79 are soil profile data obtained from borings at two locations along the coast of the bay. It may be recognized generally that a loose sand deposit exists near the surface down to a maximum depth of about 18 m. The lower portion of the sand deposit contains fine-grained materials such as clay and silt which had probably been derived from the outcrop of the claystone on land and deposited later under the sea.

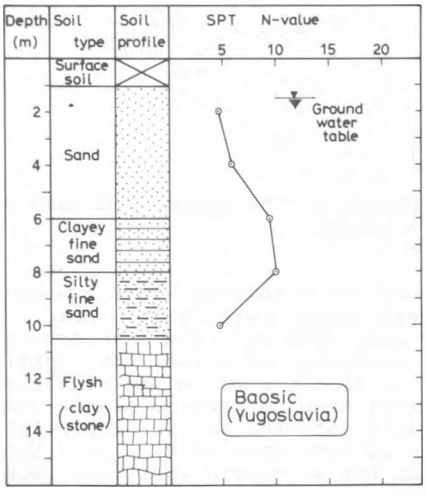

Fig. 78 Typical soil profile at Baosic

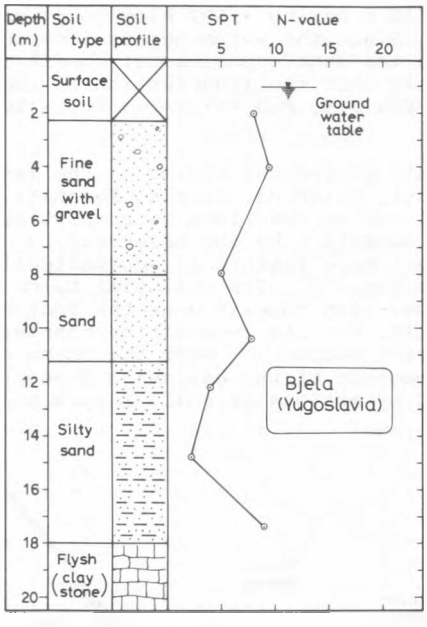

Fig. 79 Typical soil profile at Bijela

The blow count values of the standard penetration test obtained for the deposit at Bijela and Baosic are also shown in Figs. 78 and 79, where it may be seen that the sand is deposited in a loose condition with N-values ranging between 5 and 10. The sand around the bay area was derived from the limestone and as such has a reddish color. The grain size distribution curves of the sand indicate that the gradation is relatively uniform with the mean particle size ranging from D_{50} = 0.15 to 0.45 mm. The results of cyclic triaxial tests on samples reconstituted to relative densities of 42 % and 87 % by the method of pluviation under water are presented in Fig. 80, where it can be seen that the cyclic strength takes a value nearly identical to the average which has been obtained for many other clean sands with similar gradation characteristics.

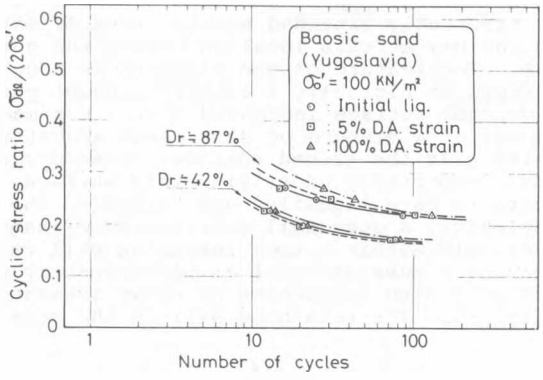

Fig. 80 Cyclic stress ratio versus the number of cycles for reconstituted specimens of Baosic sand

Analysis of liquefaction was made on four soil profiles shown in Figs. 81 and 82 representative of those at Bijela and Baosic where the damage due to liquefaction was disastrous at the time of the 1979 Monte Negro earthquake. Motions of the ground recorded nearest Bijela and Baosic were those at Herceg Novi. Since the maximum horizontal accelerations of 0.26 g and 0.23 g were those monitored on the rock outcrop, the intensity of shaking at the liquefied sites in Bijela and Baosic would have probably been smaller than that in Herceg Novi. Although it is difficult to make an accurate estimate, the maximum horizontal acceleration at the sites of Bijela and Baosic where liquefaction occurred may be assumed to have been approximately 80 % of the acceleration recorded on the rock outcrop. This assumption is based on the comparison between the maximum accelerations ever recorded on rock outcrops and those recorded on sand deposits during major earthquakes in the recent past as summarized in Table 4. In making the analysis, the maximum horizontal acceleration was thus assumed to be 0.21 g. The earth pressure coefficient at rest, K_0, was assumed to be 0.5. The cyclic strength of sand was estimated on the basis of the empirical formula of Eq. (10) using the SPT N-values. The results of the liquefaction analyses are presented in Figs. 81 and 82. Although the analysis was made for two soil profile data each at Bijela and Baosic obtained at approximately the same place, the outcome of the analysis turned out to be identical in that liquefaction could occur throughout the deposit of sand for both sites of Bijela and Baosic. In the light of the observed field performances and the results of the analysis, it seems reasonable to conclude that the ground surface disruption was brought about by the liquefaction that occurred in the near-surface deposits of saturated loose sand having a thickness of about 3 to 18 m. It is noted that, in all cases considered where signs of liquefaction were manifested on the ground surface, the highest elevation of the liquefied zone was

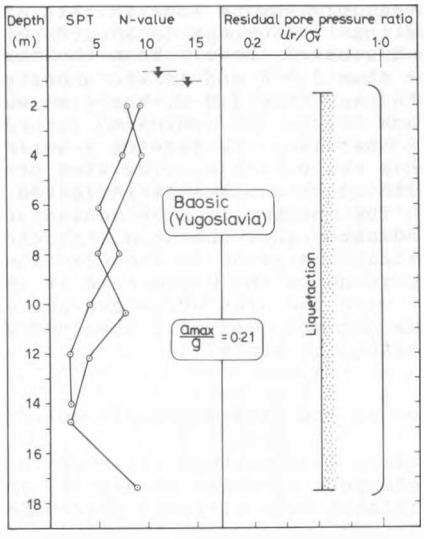

Fig. 81 Result of liquefaction analysis of Bijela

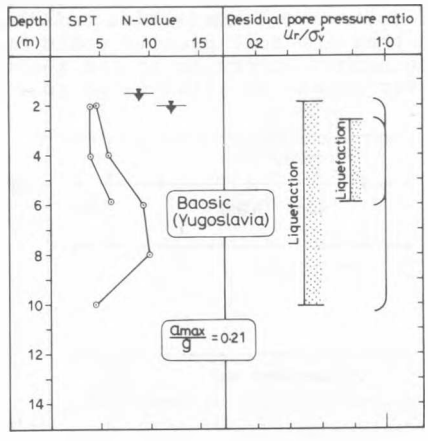

Fig. 82 Result of liquefaction analysis at Baosic

located above the depth of 3 m and the thickness of the liquefied sand layer was greater than about 3 m. The conditions as above in which the effects of liquefaction were manifested on the ground surface are the same as the conditions for the cases of liquefaction encountered in Niigata.

X SITE IDENTIFICATION FOR LIQUEFACTION-INDUCED DAMAGE

10.1 General

Studies of the cases described in the preceding section indicate that the occurrence of liquefaction itself in some layer in the deposit is not necessarily associated with the damage of structures and other installations founded on or near the ground surface. Only when the development of liquefaction is sufficiently extensive through the depth of a deposit and shallow enough in proximity to the ground surface, do the effects of liquefaction become disasterous, leading to sand boiling and ground fissuring with various types of associated damage to structures and underground installations. Therefore, it will be of interest to study conditions under which the effects of liquefaction will or will not appear on the ground surface.

This aspect of the problem has an important bearing in developing microzoning maps with respect to liquefaction-induced damage in area of high seismicity. In executing the microzoning work, it is necessary to have a proper guideline to distinguish whether a given site is to be identified as being prone or immune to liquefaction-induced ground damage for a given intensity of shaking anticipated to occur during an earthquake in the future.

10.2 Factors Influencing the Liquefaction-Induced Ground Damage

One of the factors influencing the surface manifestation of liquefaction would be the thickness of a mantle of unliquefied soils overlying the deposit of sand which is prone to liquefaction. Should the mantle near the ground surface be thin, the pore water pressure from the underlying liquefied sand deposit will be able to easily break through the surface soil layer, thereby bringing about the ground rupture such as sand boiling and fissuring. On the other hand, if the mantle of the subsurface soil is sufficiently thick, the uplift force due to the excess pore water pressure will not be strong enough to cause a breach in the surface layer, and hence, there will be no surface manifestation of liquefaction even if it occurs deep in the deposit. In view of these considerations, the first step for establishing a guideline for site identification of liquefaction-induced damage would be to specify a threshold value on the thickness of the surface soil layer.

The thickness of the liquefiable sand layer itself will also exert a profound influence on the development of the breach in the mantle of surface layer. If the liquefied sand layer is thin, the resulting uplift pressure will not be powerful enough to bring about the collapse in the surface layer. Therefore, the site may need to be identified as being free from the damage due to liquefaction. The opposite effects will be expected to occur if the sand layer is thick enough. Accordingly, the second step for setting up a criterion is to stipulate a threshold on the thickness of the sand layer which is potentially liquefiable.

A guideline in the above context was adopted by Ishihara and Ogawa (1978) in establishing a microzonation map for the area of downtown Tokyo. In that area, the general subsurface stratification is characterized by the presence of a sand deposit of alluvial origin underlying surface fills consisting of a potpourri of clays, loams, sands and cobbles, which are considered immune to liquefaction. The potentially liquefiable sand layer is underlaid in many cases by an alluvium of silt and clay, but sometimes by dense sand deposits of diluvial origin.

To establish the guideline, literature surveys were made on boring data at sites with known field performances during past earthquake in Japan. Over a wide area generally affected by liquefaction, some sites are known to have suffered damage, but

others are known to have shown no evidence of damage. For several sites within such an area, available boring data were examined to seek for the minimum thickness of surface layer required to avoid the ground damage due to liquefaction. The result of this study indicated that the damaging effect of liquefaction is brought about on the ground surface when the thickness of the surface layer is smaller than approximately 3 m. It was also pointed out that, with the thickness of surface layer less than 3 m, the damaging effect of is certainly reinforced, if the thickness of underlying liquefiable layer is larger than about 3 m. It is to be noted that the rule of thumb as above was established for the motions of earthquakes having an intensity of shaking of the order of 200 to 250 gal in terms of maximum horizontal ground acceleration.

10.3 Case Study in the 1977 Vrancea Earthquake

A set of data in support of the above quideline was presented by Perlea (1983) who compiled a number of boring logs obtained on various occasions in a small patch of landfill area along the Dimbovitza river course in the city of Bucharest, Romania. This area suffered extensive ground damage due to liquefaction at the time of the Vrancea earthquake of March 4, 1977, as evidenced by sand spurting and differential settlements of farmhouses (Ishihara-Perlea, 1984). The locations where dozens of sand boils were observed following the earthquake are indicated in Fig. 83. Also

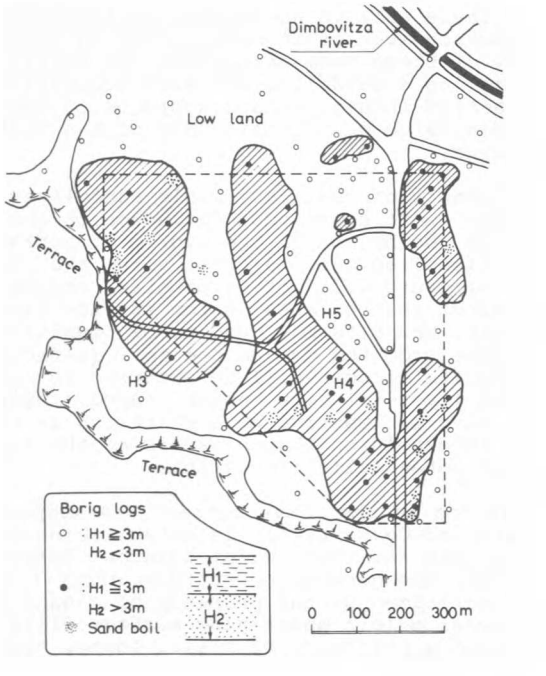

Fig. 83 Sites of liquefaction near the river course in Bucharest during the 1977 Vrancea earthquake, (Perlea, 1983)

indicated are individual locations where borings were performed. The general soil profile in this area is characterized by the presence of an alluvial sand deposit overlaid by a mantle of clayey silt which is not vulnerable to liquefaction.

All the available boring logs in this area were classified into two groups in accordance with the guideline discussed above. When the surface layer is thinner than 3.0 m and if the underlying sand layer is thicker than 3.0 m, the site was labelled with a black circle and indicated accordingly in Fig. 83. Otherwise, the site of a boring is indicated with a white circle. The area predominently studded with black circles is indicated with hatched lines. The outcome of such zoning as shown in Fig. 83 indicates that the area with the soil profile identified as prone to liquefaction-induced damage according to the above rule is approximately coincident with the area where surface evidences of liquefaction were actually observed during the Vrancea earthquake of 1977.

10.4 Cases in the 1983 Nihonkai-chube Earthquake

The earthquake of magnitude 7.7 which occurred in the northern part of Japan on May 26, 1983, furnished an additional body of field performance data which are useful to examine the conditions of occurrence or non-occurrence of ground damage due to liquefaction. Various types of liquefaction-induced damage was incurred to many structures and installations in a widespread area within an epicentral distance of about 120 Km. The boring data collected from many liquefaction-inflicted areas disclosed that the soil profile could be classified into three groups according to the location of the ground water table, as illustrated in Fig. 84.

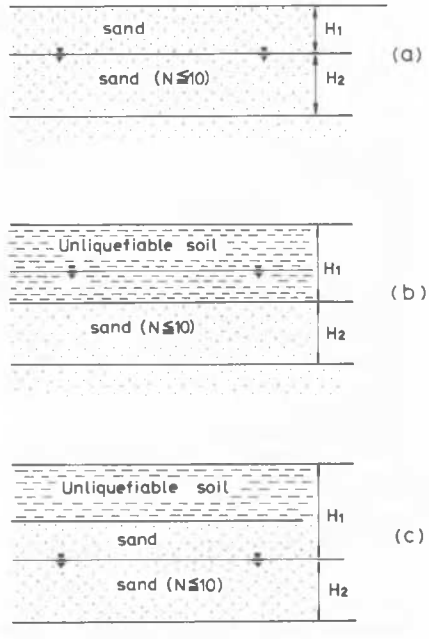

Fig. 84 Definitions of the surface unliquefiable layer and the underlying liquefiable sand layer

The thickness of the surface unliquefiable layer, H_1, was then defined as being equal to the depth of the ground water table if it is located within the sand deposit. Should an unliquefiable cohesive soil exisit to a depth below the ground water table, the value of H_1 was chosen as the thickness of the surface layer itself as illustrated in Fig. 84(b).

The areas inflicted by this earthquake are believed to have undergone a shaking with a horizontal ground acceleration of the order of 200 gal as indicated in Table 4. The simple analysis for liquefaction was made using this acceleration on the basis of the procedure described in Section 8.2. The analysis results indicated that a sand layer with a blow count value less than about 10 would probably have developed liquefaction during the 1983 earthquake. Consequently, the thickness of liquefied sand deposit, H_2, was chosen equal to that of the sand layer satisfying this condition, as accordingly indicated in Fig. 84.

Acting upon the above rule, the thickness of the surface layer, H_1, and the underlying supposedly liquefied layer, H_2 were read off from many boring logs collected from sites within the inflicted area. The collected boring data indicated that the majority of sites inflicted by this earthquake consist predominanly of sand from the ground surface and, therefore, the type of soil profile indicated by Fig. 84(a) is encountered in most cases. The data thus assembled are presented in Fig. 85 by plotting these two layer thicknesses as the ordinate and abscissa. The data from sites of known liquefaction damage are indicated by black circles and those from sites without damage are marked by white circles. It may be seen in Fig. 85 that the data points with known liquefaction damage fall mostly in the zone on the left

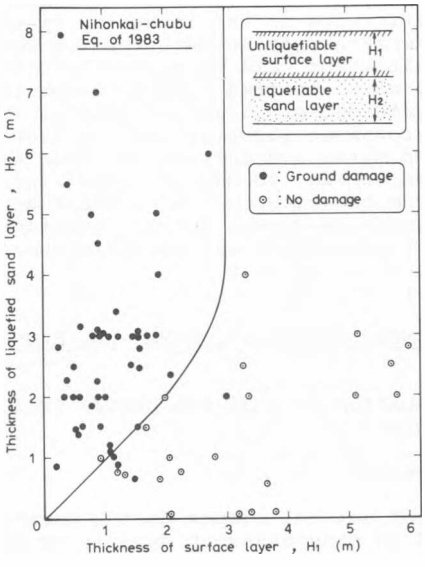

Fig. 85 Conditions of subsurface soil stratification discriminating between occurrence and non-occurrence of ground rupturing due to liquefaction

bounded by H = 3.0m. For the deposits with liquefied sand layer thinner than 3.0 m, the thickness of surface layer required to prevent liquefaction-induced damage appears to decrease, as indicated by a straight line directed to the zero point in Fig. 85. Thus it would appear that, for deposits subjected to an earthquake shaking with an acceleration of the order of 200 gal, the conditions for avoiding liquefaction-induced damage would be to have a mantle of unliquefiable soils thicker than about 3.0 m when the thickness of the underlying liquefiable sand layer is larger than 3.0 m. If the thickness of the liquefiable sand layer is smaller than 3.0 m, the thickness of the surface layer required to prevent damage would be correspondingly reduced. The conditions as above are indicated by a smoothed boundary line in Fig. 85.

10.5 Case Study in the 1976 Tangshan Earthquake

The Tangshan earthquake of July 26, 1976, in China is probably the most catastrophic event to have occurred in recent years. The ground damage due to liquefaction was brought about in a widespread area near the epicenter of the earthquake. The unparalleled degree of destructiveness of this earthquake due to liquefaction is described vividly in several papers by Wang (1981), Wang et al. (1983) and Finn (1982). Among the many areas devastated by the liquefaction, a detailed study was made by Gao et al. (1983) for a limited area north of Tangshan city along the Dou river regarding the soil profile conditions leading to ground damage due to liquefaction. In this area a mantle of sandy clay exists generally near the ground surface underlaid by a loose deposit of fine sand with varying thickness. The SPT N-value of this sand layer ranges between 5 and 24, but mostly below 20 indicating a loose state of deposition susceptible to liquefaction. This area is a flat land and the ground water table is located at an elevation shallower than about 4 m. A total of 226 boring logs was assembled within this area and the soil profile conditions were examined in the light of the ground damage identified by air photographs taken following the earthquake. The results of this investigation are presented in Fig. 86 in which the depth of the surface layer, H_1, is plotted versus the depth to the bottom of

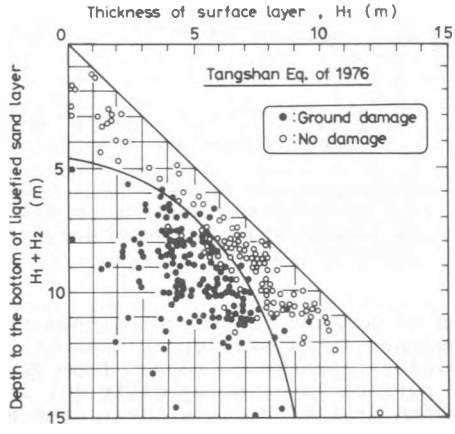

Fig. 86 Conditions of subsurface soil stratification discriminating between occurrence and non-occurrence of ground rupturing due to liquefaction (Gao et al. 1983)

the liquefied sand layer, $H_1 + H_2$. If a site in question is known to have suffered liquefaction-induced damage, it is indicated by a black circle in Fig. 86 and otherwise the data were plotted with white circles. A boundary line was then drawn in Fig. 86 differentiating between the zones of damage and no damage due to liquefaction. It may be seen that the thickness of surface layer

required to avoid damage due to liquefaction is surprisingly large. This fact may need to be interpreted in the light of the extremely strong shaking occurring in this area during the Tangshan earthquake. Since this area is located within 30 Km from the epicenter of the magnitude 7.8 earthquake, the intensity of shaking is believed to have been of the order of 8 to 9 on the Chinese intensity scale. The corresponding ground acceleration is supposed to have been as great as 400 to 500 gal.

In order to compare the results of the two independent studies described above, the boundary curve obtained by Gao et al. (1983) was re-plotted using the same type of presentation as for the diagram in Fig. 85. The two boundary curves thus superimposed are shown in Fig. 87. One of the peculiar features of the curve by Gao et al. (1983) is that, for increasing thickness of liquefiable sand layer, the thickness of surface layer

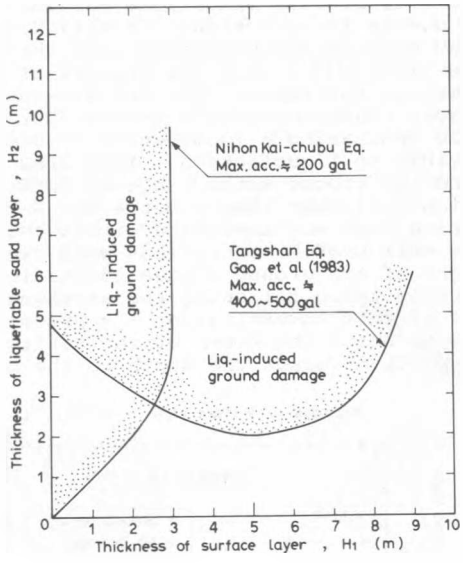

Fig. 87 Comparison of two boundary curves differentiating between conditions of damage and no damage due to liquefaction

required to prevent liquefaction damage tends to decrease when it is smaller than about 5 m. This contradiction appears to result from Gao's definition of surface layer being different from that illustrated in Fig. 84. In their data arrangements, the surface layer thickness appears to be taken simply as the thickness of the sandy clay deposit near the ground surface. However, in cases where the ground water table is located below the bottom of the surface layer as illustrated in Fig. 84(c), the thickness of the unliquefiable surface layer should have been taken as being equal to the depth of the elevation of the ground water table. If such a modification is incorporated in Gao's data interpretation, the boundary curve would probably be corrected as indicated in Fig. 88. Also plotted in Fig. 88 is the boundary curve established in Fig. 85. Comparison of these two curves appears to indicate that the difference emerges mainly from the difference in the intensity of shaking incurred in the investigated areas

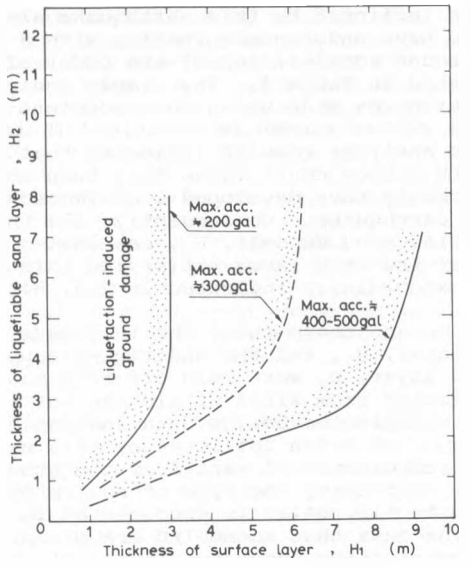

Fig. 88 Proposed boundary curves for site identification of liquefaction-induced damage

during these two earthquakes. Considering the great difference in the intensity of shaking and hence the large gap between the two proposed curves, it might well be possible to draw another boundary curve between them as shown in Fig. 88 for an intermediate level of shaking intensity with a ground acceleration on the order of 300 gal. The three boundary curves thus established and shown in Fig. 88 may be useful for identifying sites from the viewpoint of whether or not the ground sustains damage due to liquefaction during a given intensity of earthquake shaking.

SEISMIC STABILITY OF NATURAL SLOPES

XI EVALUATION OF SOIL PROPERTIES IN SEISMIC LOADING

11.1 General

Failure of natural slopes during earthquakes is governed in many cases by details of geological and hydrological conditions. However, careful scrutiny of the site conditions in many slide areas during past earthquakes has indicated that there always seems to exist a well-defined slip plane in the slide area and that this plane runs through a zone of weakness near the surface of the slope-forming soil deposits. The weak zone is often created by water infiltration into surface layers of residual or weathered soils but there are also many cases where planes of weakness coincide with tectonically disturbed zones such as fault surfaces and contact surfaces between beds or sequences of rock.

Evaluation of seismic stability of natural slopes should, therefore, be made by identifying the potential slip plane and by investigating the properties of the soils constituting the zone of weakness. Since the mode of stress applications

to a soil element beneath a slope is different from that for level ground, somewhat different considerations must be made for evaluating soil properties based on laboratory tests.

11.2 Permanent Displacement and Slope Stability

A soil element beneath a slope is subjected to an initial shear stress, σ_s, due to gravity effects in normal conditions. During an earthquake a sequence of dynamic shear stresses is superimposed on this soil element. If the relative magnitude of this dynamic shear stress is represented by σ_d, the sum of the shear stresses applied during an earthquake shaking is equal to $\sigma_s + \sigma_d$. After the application of the dynamic shear stress, a certain amount of strain or displacement will remain in the soil element. Such a strain will be referred to as a residual strain or permanent strain. The amount of residual strain which occurs in the soil element is a function of the dynamic shear stress plus the initial shear stress, $\sigma_s + \sigma_d$. The ratio of the initial shear stress to the total shear stress may also be a factor influencing the development of the residual shear strain. If a relationship between the shear stress, $\sigma_s + \sigma_d$, and the residual strain, ε_r, is established by tests, either in-situ or in the laboratory, it will become possible to estimate the residual strain for a given value of shear stress assessed through some appropriate procedures.

When a slope is composed of soils with ductile characteristics such as highly plastic clay, the material can sustain increasing magnitudes of seismically induced shear stress without inducing an infinitely large residual strain. The stress-residual strain curve for such a material is schematically shown in Fig. 89. It is then possible and reasonable to assess the residual strain in the soil and hence the permanent deformation of the slope resulting from earthquake shaking. In contrast, if the slope-forming material is characterized by brittle characteristics, such as cemented sand, or with characteristics liable to flow such as loose sand and low-plasticity silt, the residual strain tends to increase indefinitely when the seismically induced shear stress reaches a certain critical value, as illustrated schematically in Fig. 89. In such a case, it becomes potentially difficult to estimate the permanent deformation of the slope with a tolerable degree

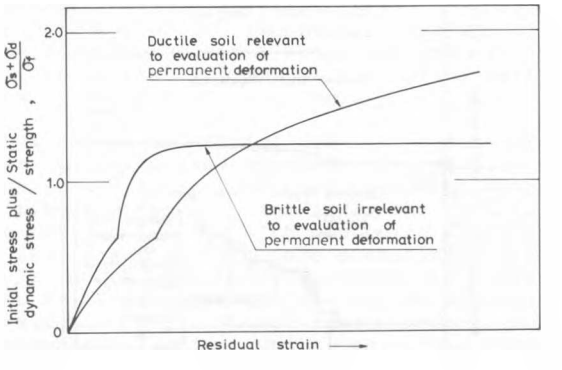

Fig. 89 Illustraion of two different types of soil relevant or irrelevant to the permanent deformation analysis

of accuracy. Therefore it would be appropriate to have recourse to the conventional method of slope stability analysis to examine the degree of stability or instability based on the factor of safety.

11.3 Evaluation of Strength-Permanent Deformation Characteristics for Soils

A conventional method of approach to evaluate the stability of slopes during earthquakes has been the so-called pseudo-static method in which the effect of seismic loading is taken into account by an equivalent static force determined as the product of a seismic coefficient and the weight of the potential sliding mass. This method of approach can be used not only for evaluating the factor of safety as customarily employed but also for assessing the permanent deformation if the stress-residual strain relation can be properly established for key soil deposits associated with sliding.

In evaluating the equivalent force in the above method, one of the concepts would be to consider an entire time history of acceleration and to replace it with a certain number of constant-amplitude accelerations having an effect equivalent to that of the actual time history of earthquake motions. If the analysis is made on this basis, the dynamic component of shear stress as introduced above should be a constant-amplitude cyclic stress with a specified number of cycles in which the variable, σ_d, represents the amplitude. Therefore, the corresponding stress-residual strain relation must be established on the basis of test results employing a constant-amplitude cyclic stress.

An alternative concept for evaluating the equivalent force would be to consider the irregular time history of acceleration as it occurs in the field. In this case, the dynamic component of shear stress should be exactly the same as the irregular time history of acceleration and the peak shear stress in the time history may be taken as the variable, σ_d. When establishing the stress-residual strain relationship based on this concept, the tests on soils must be performed by employing the actual time histories of motions during earthquakes.

The second concept as described above has been adopted by Ishihara et al. (1983, 1984) for evaluating the soil characteristics at several sites of landsliding that occurred in recent earthquakes. In the laboratory test program using a triaxial test equipment, isotropically consolidated specimens were first subjected under drained conditions to a certain level of initial axial stress, σ_s, and then subjected to a series of irregular loads in the axial direction. The dynamic phase of the above tests was conducted by stepwise increasing the amplitude of time history of the irregular loads, σ_d. In each step of the irregular loading tests with varying amplitudes, the residual axial strain, ε_{re}, was measured.

When an irregular time history is transferred to specimens through the up-and-down movement of the triaxial loading piston, one of the loading methods is to orient the stress time change so that the peak can be attained when the piston reaches

the lowest position. This type of test will be referred to as a CM-test. It is also possible to have the peak stress oriented so that it is executed at the highest position of the loading piston. This type of test will be referred to as an EM-test. For each of the wave forms used, both types of test were performed.

The results of one such series of tests performed on undisturbed samples of volcanic clay are presented in Fig. 90. The partially saturated samples used were procured in blocks from an intact surface exposed on a mountain slope which had suffered a large-scale landslide at the time of the 1978 January 14 Izu-Ohshima-Kinkai earthquake (M = 7.0) in Japan. The test was of the CM-type and the strength of specimens from the same sample batch in conventional static loading test was σ_f = 84.4 kN/m^2, where σ_f denotes the axial stress at failure. An initial stress, σ_s, equal to 70 % of the static strength was used in the test. Fig. 90 (a) shows the time history of the EW-component of the acceleration obtained at Muroran at the time of the 1968 Tokachi-oki earthquake in Japan. Fig. 90(b) shows the time history of axial strain recorded in one of the test sequences where the amplitude of peak axial stress was σ_d = 87.5 kN/m^2 in the direction of triaxial compression. It is observed that the residual axial strain produced in the specimen by the application of the irregular load was ε_{re} = 2.12 % in this sequence. Before executing this loading sequence, the test specimen had already undergone a residual strain of ε'_{re} = 1.88 % in a preceding sequence of the test. Fig. 90(c) shows the time history of axial strain recorded in the subsequent test sequence in which the amplitude of the irregular load was raised to σ_d = 110.7 kN/m^2. The specimen having sustained an axial strain of ε'_{re} = 4.0 % in the preceding sequences experienced an additional residual strain of ε_{re} = 5.85 % in the course of this new loading sequence. In the last sequence, the specimen underwent a residual strain as large as 10.9 % as indicated in Fig. 90(d).

An example of similar test sequences employing a reversely oriented wave form (Ew-test) is demonstrated in Fig. 91. The time histories of axial strain for the three test sequences are shown in Fig. 91 in the same way as in the case of the results of the CM-test shown in Fig. 90. It may be noted that the amplitude of the peak σ_d, indicated in Fig. 91 refers to the maximum spike on the side of triaxial compression. In the type of triaxial test procedures described above, the initial shear stress, σ_s, is applied towards the triaxial compression side, and therefore the key phenomena such as residual strains and failure of test specimens are always encountered on the side of triaxial compression. Accordingly, it is considered reasonable to consider the peak stress on the triaxial compression side as a key variable influencing the development of residual strains and failure of the specimens.

To establish the stress-residual strain relationship, values of the total residual strain, ε_{re} + ε'_{re}, accumulated up to the current sequence of irregular loading tests were read off from the test records such as those shown in Figs. 90 and 91, and these values were plotted versus the peak amplitude of the current irregular loading, σ_d, plus the initial axial stress, σ_s. The results of such data compilations for the tests shown in Figs. 90 and 91 are presented in Fig. 92. In this plot, the combined static and dynamic axial stress, σ_s + σ_d, is shown normalized to the static strength, σ_f, in order to discern the effect of dynamic loading as compared with static behavior. In Fig. 92, the data points indicated by arrows are those which were read off directly from the test results shown in Figs. 90 and 91. Also indicated in Fig. 92 are the stress-strain curves for the static phase of loading until the initial axial stress, σ_s, is increased to 70 % of the static strength. The static stress-strain curves which would have been obtained if the loading had been continued further are shown in Fig. 92 by the dashed curves. It may be seen

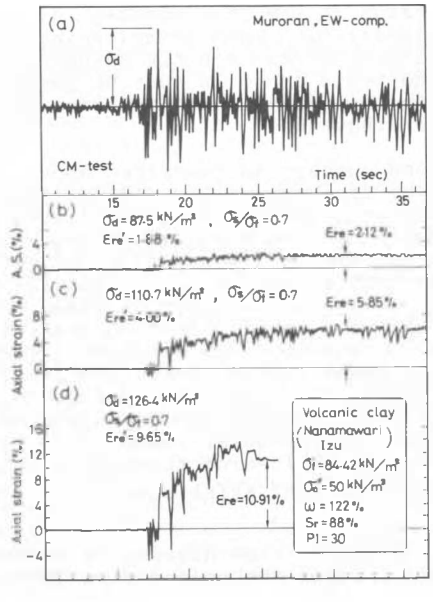

Fig. 90 Evolvement of residual strains in the irregular loading test

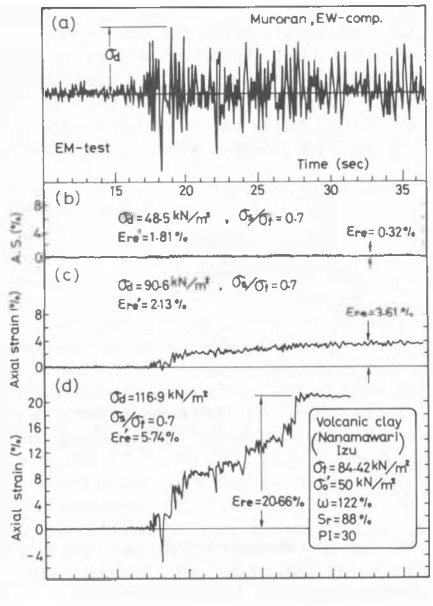

Fig. 91 Evolvement of residual strains in the irregular loading test

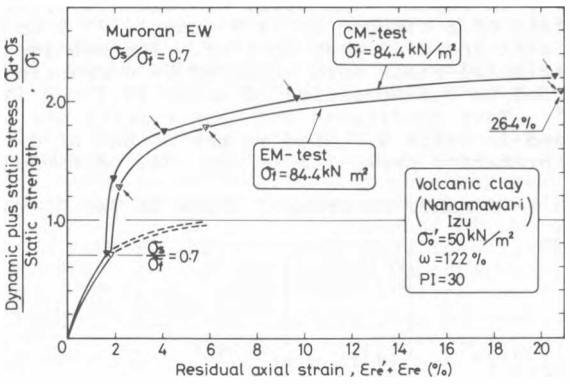

Fig. 92 Shear stress-residual strain relationship

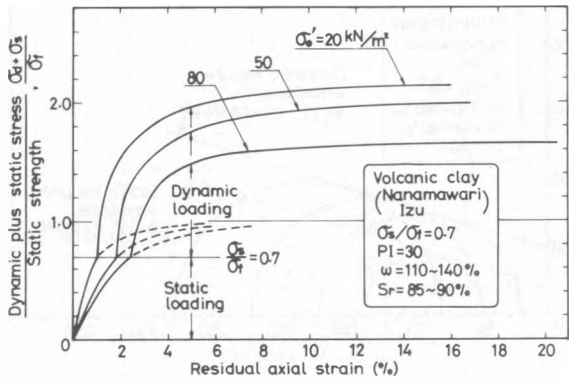

Fig. 93 Shear stress-residual strain relationships for different confining stresses

that the stress-strain curves for the static-dynamic loading is located far above the stress-strain curve for the static loading alone. This fact indicates that if the soil specimen is subjected to a dynamic load after it has deformed statically to some extent, the specimen tends to exhibit a larger stiffness and higher strength than if it is loaded to failure all the way under static conditions. Such an increase in stiffness and strength appears to emerge from the highly rate-dependent nature of cohesive soils when subjected to rapid loads such as those used in the present test scheme. Similar tests in this series employing three other time histories all showed the same tendency in the stress-residual strain relation.

For the purpose of examining the effects of varying initial shear stress on the stress-residual strain relationship, multiple series of similar tests were conducted on the same sample of volcanic clay by employing different initial axial stresses under four irregular time histories of loadings (Ishihara et al. 1983). The results of these tests indicated that the stress-residual strain relationship is not appreciably affected by the initial shear stress, if its value stays within the range of σ_s/σ_f = 0.2 and 0.8, which is generally the case for the conditions in soil deposits under natural slopes. Consequently, the effect of the initial sustained shear stress on the stress-residual strain relation is considered as being of secondary importance, and its effect may be disregarded, if a rough estimate is to be made for the stability of slopes during earthquakes.

Several series of similar triaxial tests were also performed on the same volcanic clay samples by employing different confining pressures under the four time histories of loading. The results of these tests conducted with confining pressures of σ_0' = 20, 50 and 80 kN/m² are summarized in Fig. 93. It can be seen that the effect of confining stress is significant and can not be disregarded in evaluating the residual strain and strength under dynamic loading conditions. This consequence is by no means surprising since the strength of partially saturated cohesive soils under static conditions has been known generally to vary with the magnitude of the confining stress.

The effect of the confining stress on the static strength of soils has been evaluated in terms of the apparent angle of internal friction defined as an angle of slope in the Mohr circle representation of failure state of stress. Therefore, it is of interest to establish a Mohr-Coulomb type of failure criterion for the dynamic loading condition as well and compare it with the conventional failure criterion for the static loading condition. The method adopted herein for establishing the dynamic failure criterion is illustrated in Fig. 94. The value of the confining stress, σ_0', is

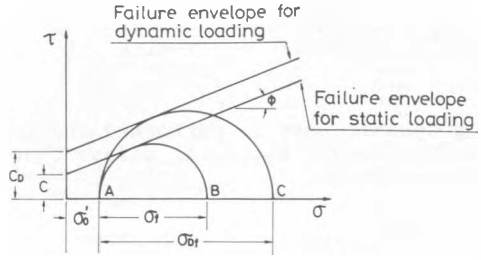

Fig. 94 Construction of Mohr circles and failure envelopes associated with static and dynamic loading

first laid off at point A on the abscissa and the static and dynamic strength values are laid off towards the right as AB and AC, respectively. The circle drawn through points A and B is the Mohr circle associated with failure under static loading. Likewise, the Mohr circle for failure in the dynamic loading can be constructed by drawing a circle through points A and C, as shown in Fig. 94. The Mohr circles drawn in this manner for the test results shown in Fig. 93 are demonstrated in Fig. 95. For the volcanic clay tested, the cohesion component for static loading, C, was 20 kN/m², and the cohesion for dynamic loading, C_D, was 48 kN/m². It is of particular interest to note that the angle of internal friction was practically the same for both the static and dynamic loading conditions. The fact that the effect of dynamic loading on the failure strength is manifested only through the cohesion component may be considered reasonable if one is reminded of the fact that the increase in strength due to rapid loading such as the seismic irregular loading emerges mainly from

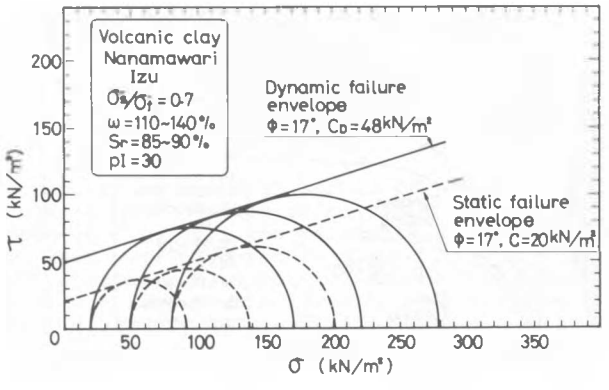

Fig. 95 Failure envelopes obtained from static and dynamic loading test results

the viscous nature of cohesive soils.

On the basis of the oonclusion that the angle of internal friction is identical both in the static and dynamic loading conditions, it becomes possible to deduce some correlation between the strength parameters pertaining to these two loading conditions. Let the angle of internal friction, ϕ, and cohesion, C, in the static loading be known for a given soil ; then the axial stress required to cause failure, σ_f, under a confining stress, σ_0' is given by ;

$$\sigma_f = \frac{2\sin\phi}{1-\sin\phi}\,\sigma_0' + \frac{2C\cos\phi}{1-\sin\phi} \qquad \cdots\cdot(30)$$

When a dynamic test is performed under the same confining stress, the axial stress causing failure, σ_{Df}, is given by

$$\sigma_{Df} = \frac{2\sin\phi}{1-\sin\phi}\,\sigma_0' + \frac{2C_D\cos\phi}{1-\sin\phi} \qquad \cdots\cdot(31)$$

Combining Eqs. (30) and (31), one obtains

$$\frac{C_D}{C} - 1 = \left(1+\frac{\sigma_0'}{C\cot\phi}\right)\left(\frac{\sigma_{Df}}{\sigma_f} - 1\right) \qquad \cdots\cdot(32)$$

Thus, knowing the static strength parameters, C and ϕ, one can estimate the dynamic cohesion value, C_D, from Eq. (32), if a single dynamic test is run to determine the value of the dynamic strength, σ_{Df}, under an appropriate confining stress. Once the value of the dynamic cohesion is thus known, it becomes possible to estimate the dynamic strength for any other value of the confining stress through the use of Eq. (31).

The dynamic test program as described above has been implemented for another cohesive soil obtained from a site of man-made fills at Shiroishi which had suffered a large-scale landslide at the time of the 1978, June 12 Miyagiken-oki earthquake (M=7.4) in Japan. The soil, of volcanic origin, consists of a mixture of 13 % gravel, 47 % of sand, 12 % silt and 28 % clay content. The specimens for the triaxial tests were prepared by compacting the material to two densities of about 18.7 and 19.0 kN/m^3. Test conditions and test results are summarized in Table 6, based on the method of data interpretation presented in Fig. 94. Although no definitive conclusion can be drawn from the tests on only two clays, it may be noted that the clay with higher plasticity index exhibits a larger percentage of increase in cohesion under dynamic loading over that for the static loading as compared to a clay with lower plasticity index.

Table 6 SUMMARY OF DYNAMIC TESTS ON TWO CLAYS

	Volcanic clay(Izu)	Volcanic sandy clay (Shiroishi)	Volcanic sandy clay (Shiroishi)
Unit weight γ_t(kN/m^3)	13.3	18.7	19.0
Water content ω(%)	110 ~ 140	22 ~ 23	20 ~ 21
Saturation ratio S_r(%)	85 ~ 90	82 ~ 84	82 ~ 84
Plasticity Index PI	30	18	18
Static cohesion C(kN/m^2)	20	28	32
Angle of int. friction φ(degree)	17	14	16
Dynamic cohesion C_D (kN/m^2)	48	52	51
C_D/C	2.4	1.86	1.59

XII EFFECTS OF TOPOGRAPHY ON GROUND MOTIONS

Many of landslides and rockfalls during earthquakes take place in areas near topographical prominences such as steep slopes, mountain walls and roadcuts. The ground motions in such an area can be expected to differ significantly from those on level ground for which extensive studies have been made thus far. The effects of topography on earthquake ground motions have been highlighted as an issue of practical importance since a series of in-situ measurements was made for the motions of aftershocks following the San Fernando earthquake of February 9, 1971. On the basis of several sets of field data recorded during earthquakes on the crest, flank and base of mountains, Davis and West (1973) demonstrated the fact that the peak amplitude of acceleration at the crest of mountains could be greater in many cases than that at the base. Chang (1976) indicated that the topographical effects on the ground motion could be interpreted in a simple manner as a function of elevation and direction of wave transmission path for the case of San Fernando area where the topography

has its highest elevation at the epicentral region and decreases in elevation to the surrounding area. It was pointed out that the peak amplitude of recorded accelerations increased approximately in proportion to the elevation of the mountains.

Although the field data are not yet sufficiently comprehensive to lead to any quantitative conclusion, there is no doubt that topography plays a significant role and is an important consideration in determining the seismic response of the ground in mountainous areas. Since many landslides and rockfalls occur in the area of topographical prominences, it will be necessary to allow for this effect in evaluating the intensity of shaking or seismic coefficient to be incorporated into the stability analysis of natural slopes during earthquakes.

XIII CASE STUDIES OF FAILURE OF NATURAL SLOPES

13.1 Failure of Slopes in Residual soils

On January 14, 1978, a destructive earthquake of magnitude 7.0 shock the south-eastern area of the Izu peninsula which is located about 120 Km southwest of Tokyo, Japan (Fig. 96). The epicenter of the main shock was located about 15 Km off the east coast of the peninsula, midway between the peninsula and Ohshima island. Lacking any data on recorded motions, a comprehensive in-situ survey was conducted by Ohashi et al. (1978) over the damage feature of tombstones at 44 cemetry yards near the epicentral area. On the basis of this survey, approximate values of maximum horizontal acceleration were inferred at each cemetry yard and contour lines connecting locations of equal acceleration were drawn as displayed in Fig. 97.

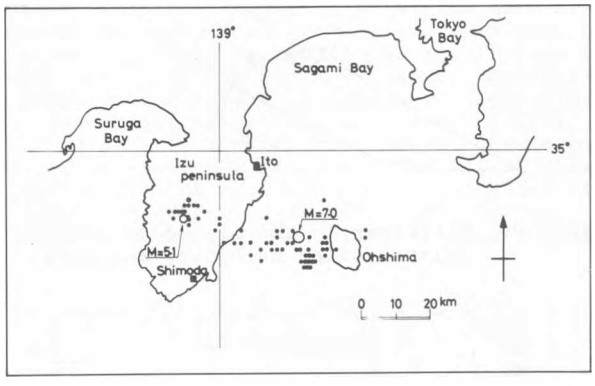

Fig. 96 Epicenter of the 1978 Izu-Ohshima-Kinkai earthquake

(a) Landslide at Hokkawa Site

Dozens of landslides and rockfalls took place during the earthquake on steep slopes, mountain walls and roadcuts along the east coast of the peninsula. The highway and railway running along the east coast were crosscut at many places by slides and slide debris. The location of one of the slides which was investigated in detail is shown in Fig. 98, where it may be seen that the debris amounting to approximately 1000 m^3 slid down the steep slope, burying the highway and spreading over the beach

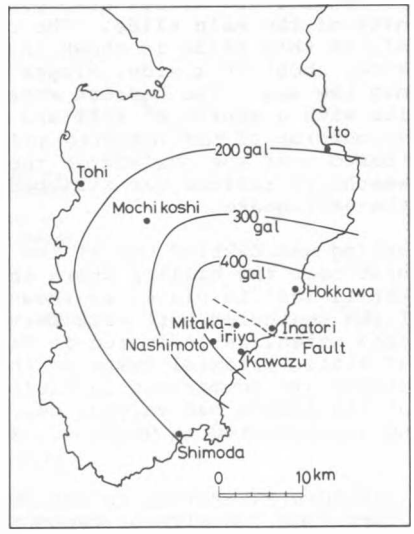

Fig. 97 Distribution of maximum horizontal accelerations during the 1978 Izu-Ohshima-Kinkai earthquake (Ohashi et al. 1978)

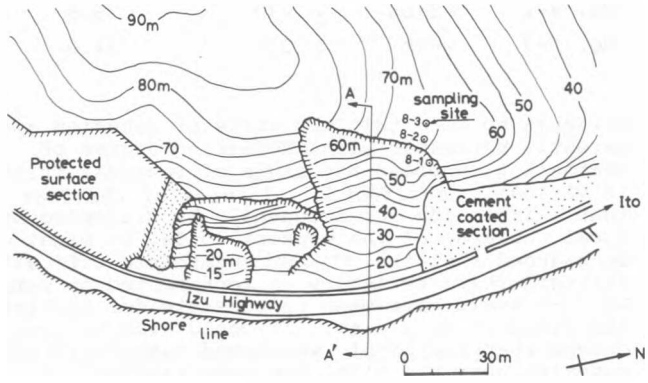

Fig. 98 Slides on the hillside at Hokkawa, Izu

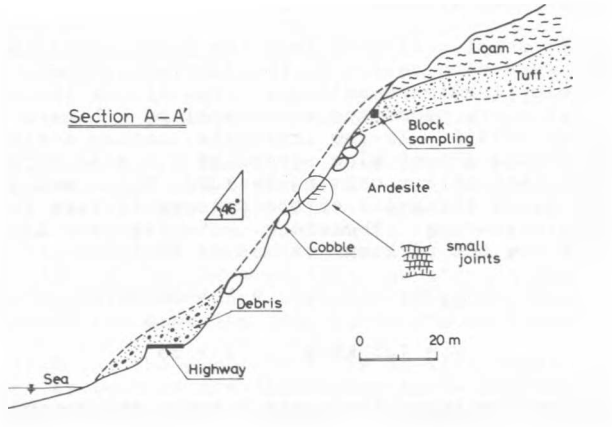

Fig. 99 Cross section of the landslide at Hokkawa

downhill. Small scale slides also occurred in the vicinity of the main slide. The cross-section, A-A', of this slide is shown in Fig. 99. The hillside. about 50 m wide. slopes at an angle of 46° into the sea. The bedrock consists mainly of andesite with a mantle of tuff and volcanic loam. The outcrop of the andesite and tuff had been weathered near the surface of the cliff, and the weathered surface was stripped off at the time of the earthquake.

Block sampling was carried out at the scarp of the tuff deposit near the hilltop where the weathered tuff was still left in place. as shown in Fig. 99. Blocks of the weathered tuff were carved out of three nearby sites, as indicated in Fig. 98. The results of static triaxial tests on these undisturbed samples are summarized in Table 7. Three batches of the sample had varying degrees of weathering as indicated in Table 7. It is of

Table 7 STRENGTH PARAMETERS OF THE WEATHERED TUFF FROM THE SITE OF LANDSLIDE AT HOKKAWA, IZU

Sampling location	Degree of weathering	Cohesion C, (kN/m²)	Angle of internal friction, φ, (degree)
No. 8-1	strong	125	35.0
No. 8-2	medium	230	35.5
No. 8-3	weak	305	34.0

interest to note that the value of cohesion apparently decreases with increasing degree of weathering, whereas the angle of internal friction is virtually unaffected. In view of the fact that a landslide can frequently be triggered by local collapse of the weakest soils, it might well be assumed that the strongly weathered tuff with strength characteristics as represented by sample No. 8-1 could have been responsible for initiating the slide at this site. It could also be conceived that the highly weathered mantle of the andesite near the cliff had been involved in triggering the slide, but in the absence of any information on the strength of this material, it will be assumed in the present study that the weathered tuff with the smallest strength parameters will represent the general characteristics of the soils associated with the initiation of the slide.

Small samples trimmed from the block sample No. 8-1 were also tested in the laboratory under irregular loading conditions. Details of the test results are presented in a paper by Ishihara and Nagao (1981). In the irregular loading tests employing a confining stress of $\sigma_0' = 50$ kN/m², the axial stress causing failure, σ_{Df}, was about 1.5 times the axial stress causing failure in the static loading. Therefore, entering into Eq. (32) with the set of known values as follows,

$$\sigma_{Df}/\sigma_f = 1.5, \quad \sigma_0' = 50 \text{ kN/m}^2$$

$$C = 125 \text{ kN/m}^2, \quad \phi = 35°$$

one can evaluate the ratio between the dynamic cohesion and static cohesion as,

$$C_{D/C} = 1.64, \quad C_D = 205 \text{ kN/m}^2$$

Using the strength parameters thus obtained for the seismic loading condition, the stability analysis was made for the sliding surface actually observed during the Izu-Ohshima-Kinkai earthquake. The factor of safety, F_d, was calculated for different values of the maximum acceleration, a_{max}, using the following formula,

$$F_d = \frac{\Sigma\left[W\tan\phi + C_D \ell\cos\alpha\right] / \left[\cos^2\alpha\,(1+\tan\alpha\cdot\tan\phi/F_d)\right]}{\Sigma\left[W\tan\alpha + \frac{a_{max}}{g} W\right]} \quad \cdots\cdots(33)$$

where W, ℓ, and α denote, respectively, the total weight, the length and the inclination of the sliding plane for each slice as illustrated in Fig. 100. This formula is modified version of the formula originally proposed by Janbu (1955). The computed factors of safety are plotted in Fig. 101 versus the maximum acceleration. Values of the factor of safety incorporating the static cohesion value were also computed and shown in Fig. 101. It may be seen in this figure that when using the static cohesion the computed factor of safety becomes equal to unity for an acceleration of 230 gal, whereas an acceleration as high as 550 gal is required to bring the factor of safety down to unity, if the dynamic cohesion is used in the stability analysis.

On the other hand, it is observed in Fig. 97 that the site of the Hokkawa landslide is located in the area where the estimated maximum acceleration

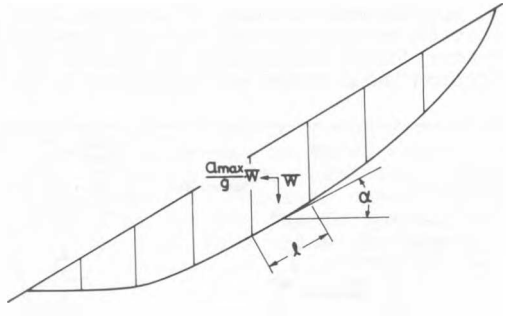

Fig. 100 Notations in the sliced method of seismic slope stability analysis

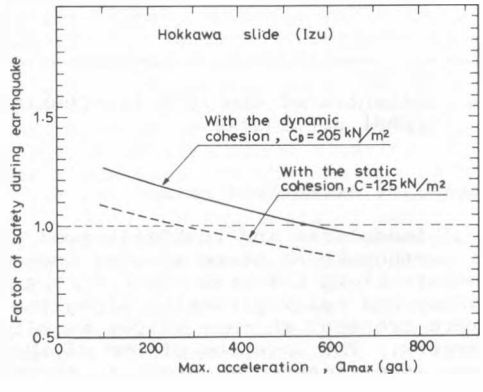

Fig. 101 Computed factors of safety versus maximum ground acceleration

is greater than 400 gal. In view of the topography at the site of the landslide, involving a steeply sloping hillside, it is reasonable to believe that the intensity of motions during the earthquake might have been significantly amplified near the hilltop and, therefore, the actual value of the maximum acceleration encountered at the landslide site might have been well over 400 gal. From these considerations, it would appear that for these types of soil, stability analyses based on the conventionally used static strength leads to an understimate of the factor of safety and that if the strength parameters are properly chosen allowing for the effect of dynamic loading, the computed factor of safety becomes more coincident with what was actually encountered in the field during the earthquake.

The test results in the laboratory on the undisturbed weathered tuff indicated that the magnitude of axial strain at failure in dynamic loading was as small as about 1 % reflecting the brittle characteristics of a weathered rock. When the stability is to be examined for slopes with such brittle materials, the method of approach to estimate permanent displacements loses its potential merit and the stability must be discussed in terms of the safety factor indicating whether or not a given slope will slide under a specified intensity of earthquake motions. This point of view was discussed in the preceding section with reference to Fig. 89.

(b) Landslide at Nashimoto site

Traffic was paralyzed by the large-scale landsliding which occurred at several sites along the mountain highway crossing the Izu peninsula. The most destructive of these was the slide that took place at Nashimoto some 10 Km inland from the east coast as indicated in Fig. 97. A plan view of the landslide site is shown in Fig. 102. In this area, two slides occurred on the slopes uphill from the highway and one on the downhill side. To clarify the cause of the slides, an extensive investigation was carried out by Iwasaki et al. (1980) involving in-situ Swedish cone tests, static cone penetration tests and standard penetration tests. Two cross sections investigated for detailed study are indicated in Fig. 102. The cross section, B - B' was selected on the slope with no damage,

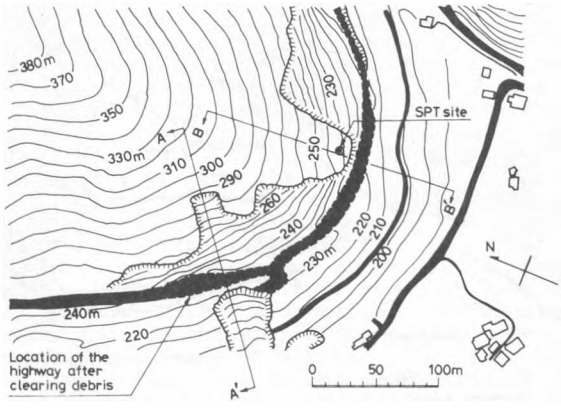

Fig. 102 Slides on the mountain flank at Nashimoto, Izu, (Iwasaki et al 1980)

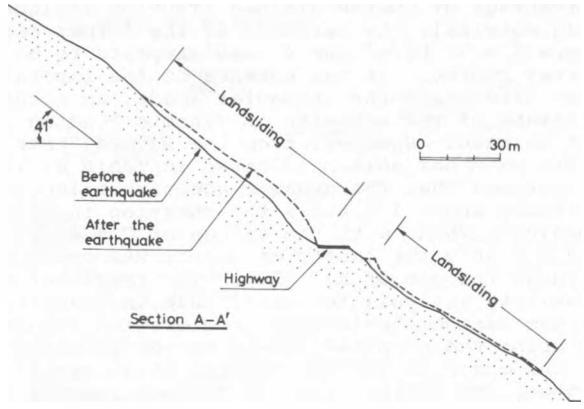

Fig. 103 Cross section of the slide area in Nishimoto, Izu

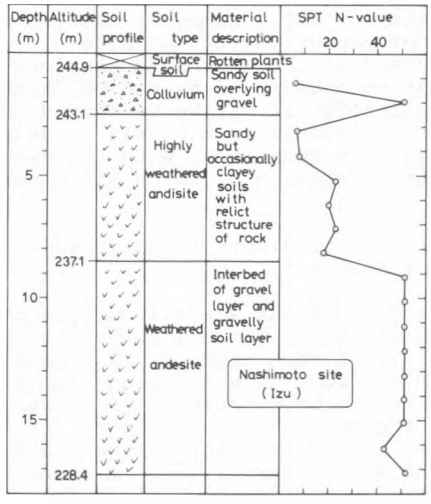

Fig. 104 Soil profile at the landslide site at Nashimoto

and the cross section, A - A', is located on the slope damaged by the landslides both uphill and downhill from the highway. The cross section, A - A', is shown in Fig. 103. On the basis of the standard penetration tests performed on the slope along the cross section, B' - B', (Fig. 102), the soil profile was established as shown in Fig. 104, where it may be seen that a mantle of colluvium overlies the weathered andesite formation. It should be noted that, at a depth of 3 to 4 m, a highly weathered andesite layer exists with a blow count value of the order of 8. The colluvium beneath the surface organic soil appears to be the debris resulting from previous slides high up on the slope. From the cross section, A - A', shown in Fig. 103, it can be seen that the sliding plane runs for the most part through the highly weathered layer of the andesite just below the colluvium.

Considering the results of the in-situ penetration tests as well as the laboratory tests on soils recovered nearby, the strength parameters for the weathered andesite were estimated to be C = 30 kN/m^2 and ϕ = 30° for one case and C = 50 kN/m^2 and ϕ = 0 for another. However, in view of the fairly large

percentage of coarse-grained fraction included in this material, the estimate of the former case where C = 30 kN/m^2 and ϕ = 30° appears to be a better choice. In the absence of the laboratory test data using the irregular loads, an accurate estimate of the cohesion in dynamic loading can not be made. However, from the several test results on other soils indicated in Table 6, it may be assumed that the dynamic cohesion value was probably about 1.5 times the cohesion in static loading. Then, with the values of C = 45 kN/m^2, and ϕ = 30°, the factor of safety was computed through the use of Eq. (33). The result of the stability analysis indicated that the magnitude of the maximum horizontal acceleration required to bring the computed safety factor to unity was on the order of 450 gal for the slide uphill the highway and on the order of 500 gal for the slide downhill from the highway. The distribution of the maximum acceleration shown in Fig. 97 indicates on the other hand that this area might have probably been shaken with a maximum acceleration of 400 gal at the time of the Izu-Ohshima-Kinkai earthquake of 1978. However, in view of the effects of topography at the site of landsliding as discussed in the foregoing section, the maximum acceleration appears to have been larger than 400 gal. Therefore, it may be concluded that the results of the stability analysis as described above are roughly in conformity with the estimate of the intensity of shaking based on other considerations.

13.2 Failure of Slopes in Interbedded Sandstones and Shales

The island of Taiwan was shaken by a strong earthquake known as the Chia-yi earthquake on December 17, 1941. Its magnitude of 7.1 with a focal depth of 10 Km placed this event among the greatest earthquakes to have occurred in Taiwan in recent years. The epicenter was located about 10 Km southeast of Chia-yi city in the southwest part of Taiwan as shown in Fig. 105. A number of landslides and rockslides took place in the mountains within an area of about 50 Km from the epicenter. The main features of the destructiveness of this event are described by Hung (1977, 1980). By far the most destructive and geologically alluring aspect of this earthquake was a cataclysmic landslide that occurred in the mountain of Tsaoling. This landslide appears to be an event that, in terms of the scale and volume, far exceeds any landslide known to have occurred in historic time.

The topography in this mountain area before the 1941 earthquake is shown in Fig. 106. In the valley south of the mountain, the Chinshui river flows from east to west. A stretch of a small scarp about 800 m long had existed at an altitude of about 800 m before the earthquake. This scarp was purported to have been formed by an earthquake which hit this area in 1862. At the time of the 1941 event, a cataclysmic rockslide took place with a deafening noise on the southern flank of the mountain. The length of the slide area was as long as 800 Km at the top and about 2 Km at the toe. The total amount of debris involved was estimated to be approximately 100 million m^3. A topographic map published 3 months after the earthquake is shown in Fig. 107. The slide debris moved down the mountain slope and over the colluvium onto the other side of the Chingshui river. The stream blocked by the slide debris formed a lake thereby changing the river course. The

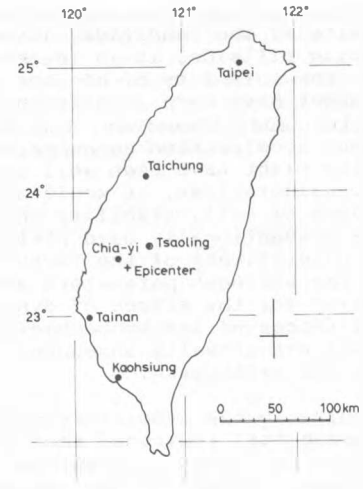

Fig. 105 Location of Tsaoling slide area

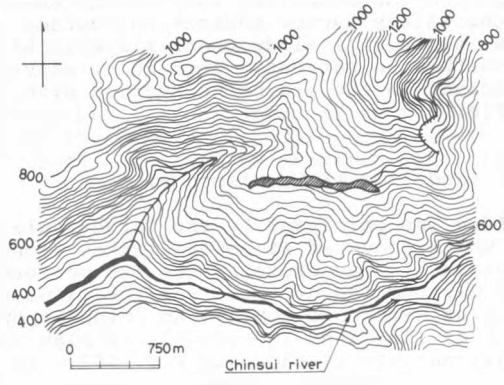

Fig. 106 Tsaoling mountain slope before the 1941 earthquake (Hung, 1977)

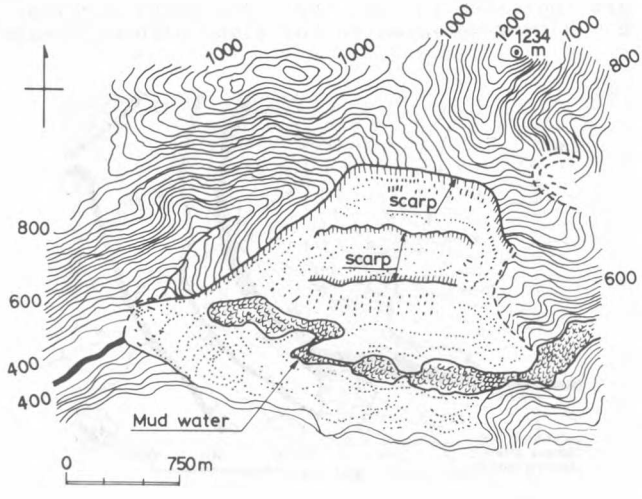

Fig. 107 Tsaoling mountain slope after 1941 earthquake (Hung, 1977)

natural earthdam thus formed was estimated to be about 140 m high above the riverbed and about 200 m wide at the crest elevation. On August 10, 1942, the slide area suffered heavy rainfall and another round of sliding took place on the same slope involving the movement of about 150 million m^3 of debris. As a result of the second slide, the topography in the slide area was changed to some extent and the elevation of the natural dam was raised about 30 m and the width was enlarged by about 100 m at the crest level. On August 15, 1979, a third round of landslides took place on the same slope as a result of further heavy rainfall, but the essential feature of the topography remained unchanged.

Following the third landslide, some in-situ investigation was carried out by Hung et al. (1981), including surveying and boring at two sites. The locations of the borings and a more detailed topographic map are shown in Fig. 108. The approximate geological profile through the cross section, A - A', is presented in Fig. 109(c), where it may

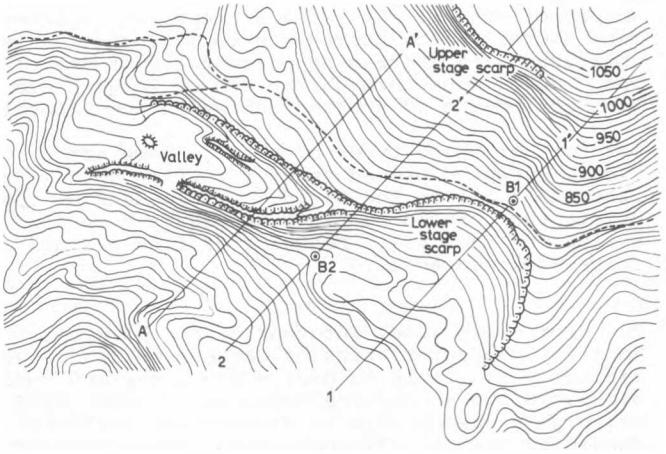

Fig. 108 Tsaoling mountain slope in 1980

be seen that the bedrock consists of interbedded shales and sandstones dipping towards the river at an angle of about 12°. The topographical map in Fig. 108 indicates that the huge landslide initially triggered by the 1941 earthquake consisted of two parts which occurred at different altitudes. It is speculated that a slide was first triggered from the old scarp at the altitude of about 800 m indicated in Fig. 106 which corresponds to the lower stage scarp shown in Fig. 108. This slide was followed by the second slide starting from the upper stage scarp at the altitude of about 1000 m indicated in Fig. 108. The chain of events involved in the sliding along the cross section A - A' in Fig. 108 may be speculated as illustrated in Fig. 109. It appears likely that a huge block of rock first slid down from the lower stage scarp through a distance of about 100 m thereby forming a graben behind it as shown in Fig. 109 (b). The rock existing downslope was pushed downward and brought to the river site where it collapsed into scree or debris. The first slide might have induced the second slide upslope leaving the upper stage scarp at the elevation of about 1000 m. The direct cause of this second slide appears to be the undercutting at the altitude of 800 m resulting from the first slide below

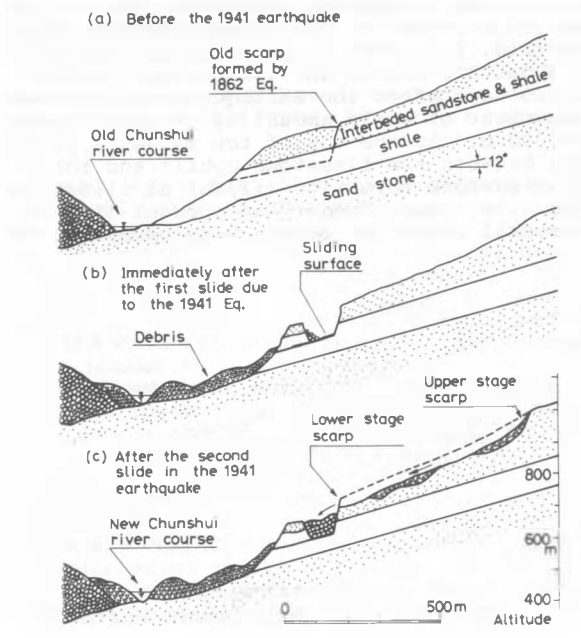

Fig. 109 Schematic picture of progressive failure in the Tsaoling landslide in 1941 at cross-section A - A'

this elevation. Following the chain of sliding as above a large amount of muddy water was reportedly seen coming out of the debris near the sliding surface as indicated in Fig. 107. It may be speculated, therefore, that the first slide must have been initiated in the layer of shale overlying the sandstone formation. The shale unit might have probably been saturated with water which had infiltrated through the cracks formed at the time of the 1862 earthquake. Thus, by the time of the 1941 earthquake, seams of mylonite might have been formed in the shale unit, thereby reducing the strength of the material. The aggravated conditions as above must have been a direct cause of the deep-seated slide which occurred at the elevation of 800 m in Tsaoling. The frequent occurrence of this type of slide is pointed out by Deere and Patton (1971). The second slide took place in the near-surface rock formation consisting of interbedded sandstones and shales, as illustrated in Fig. 109(c). Thus it appears likely that in this case also, saturated sandstone beds or seams of mylonite shales dipping downwards created a series of sliding planes, releasing a huge volume of debris over the mountain slope.

In the absence of any data on the strength of the weathered sandstones and the mylonite shales, it is impossible at present to discuss the cause of the slides quantitatively, but the overall considerations discussed above indicate that the stability of interbedded sandstone and shales during earthquakes should be examined with the help of knowledge on the geological and hydrological conditions at the site.

13.3 Failure of Slopes in Colluvium

The biggest event in scale at the time of the Monte Negro earthquake of 1979 was a landslide

that occurred in the village of Kaliman located about 10 Km inland in the rugged coastal mountain range (Fig. 72). The slide which covered a slope area about 300 m wide and 700 m long, was initiated two days after the earthquake and involved the movement of soils amounting to approximately 1,200,000 m. At the top of the slide, a junction exists between the limestone uphill and the underlying claystone formation (flysh) as illustrated in Fig. 110. According to an account of a villager, several series of cracks were opened at the

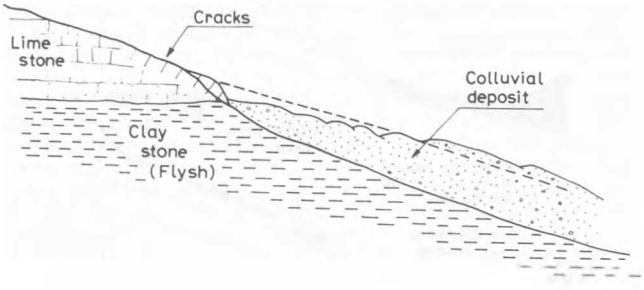

Fig. 110 Profile of landsliding at Velji Kaliman, 1979 Monte Negro earthquake

junction during the earthquake, and following the rainfall two days later, the soil mass started gradually to move downhill, leaving scarps about 5 m high at the top of the slide. It is speculated that the development of the cracks might have altered seepage paths under the ground, making it easier for the rain water to seep into the debris near the surface. With a supply of more water, the debris about 5 to 15 m thick consisting of weathered limestone and claystone well have become water-saturated and softer, leading to the massive earth flow through a distance of about 50 to 100 m.

The experience in the Kaliman landslide indicates that while the earthquake shaking may not have been the direct cause of the slide, it altered the ground water conditions by local ruptures thereby enhancing the susceptibility to a large-scale earth flow which took place following the earthquake.

CONCLUDING REMARKS

Now that two decades have passed since the devastating earthquakes in Niigata and Alaska, the subject of soil liquefaction has grown into a major field in soil dynamics for which a vast amount of knowledge both in research and practice has been accumulated. It appears that the basic aspects of the soil liquefaction phenomenon such as the triggering mechanisms, influencing factors and predictive methods have been throughly investigated, but there still remain many issues open to question and also novel features yet to be explored with respect to fundamentals and practice of liquefaction during earthquakes.

The presentation in the foregoing pages is intended to identify focal points of controversy and uncertainty in the present state of knowledge and practice in the subject area of this address.

The main points derived from the overview of the current state-of-the-art may be summarized as follows.

1. The liquefaction and cyclic mobility characteristics of soils other than clean sands have not been the subject of comprehensive investigation or discussion. Evaluation of the liquefaction potential of fine-grained soils and coarse-grained soils are important problems requiring further investigation. With respect to fine-grained soils, clay or silt with low plasticity index such as tailings material has been found to be as vulnerable to liquefaction as are loose clean sands. However, little is known about the liquefaction potential of clay or silt with high plasticity index. Since the physical properties of these soils are strongly affected by local conditions of deposition, efforts should be made to test local soils both in the laboratory or in-situ to supplement information in this regard.

With regard to coarse-grained soils, the possibility of liquefaction exists for sand containing some amount of gravel. It appears necessary to determine therefore how resistance to liquefaction is increased with increasing percentages of gravel. This may be done through the use of large-scale test equipments or shaking tables in the laboratory.

For both of these types of soil , there are no widely accepted procedures for testing both in the laboratory and in the field. Development of appropriate test procedures is a necessary step for evaluating the cyclic behavior of fine-grained and coarse-grained soils.

2. For clean sand, information on the cyclic mobility characteristics of dense sand is not sufficiently available to derive any clear-cut conclusions. Since undisturbed samples of dense sand are highly susceptible to disturbance, efforts should be make to eliminate this deleterious effect and to determine the real behavior of in-situ dense sands by means of laboratory tests.

3. The development of liquefaction during earthquakes in some layer of the ground does not always mean that ground damage such as sand boiling and fissuring will result. If a thick layer of unliquefiable soil exists near the ground surface and if the thickness of the underlying layer of liquefied sand is thin, then the damaging effects of liquefaction will not be manifested at the ground surface. Therefore, there appear to be some threshold thicknesses of the surface layer and underlying liquefiable sand layer differentiating between conditions producing damage and no damage at the ground surface. A correlation between these threshold thicknesses is useful to identify a site with a given soil profile from the viewpoint of whether or not surface damage is likely to be brought about as a result of liquefaction. This problem also requires further investigation, since it is necessary for carrying out microzoning work in a particular area.

4. Analysis of liquefaction is generally made using the simple procedure based on the total stress principle. In this method, shear stresses induced by motions during earthquakes are roughly

estimated from a force equilibrium relation for soil column located near the ground surface or they can be more accurately determined by wave propagation analysis which takes into account the effects of soil deformability. However because pore pressure build-up in the soil is not directly considered in total stress analysis, the computed shear stresses are sometimes greater than those actually developed, particularly when the soil is deformed to a state of near-failure. In order to eliminate this error, a more exact method of approach has been developed in recent years based on the effective stress principle. This approach requires a more complete modelling of soil behavior under cyclic loading conditions about which many points of controversy still exist. In view of the great interest in this aspect of the liquefaction phenomenon, it is highly desirable to have further discussions of this subject.

5. In contrast to the comprehensive efforts in the study of soil liquefaction, problems of seismic stability of natural slopes have not been investigated or discussed extensively. One reason for this lack of interest would probably lie in the difficulty of assessing strength characteristics of slope-forming soil materials under seismic loading conditions. Generally slopes are composed on partially saturated cohesive soils for which it is difficult to evaluate soil characteristics in a unified fashion. The other reason would be that sliding of slopes occurs in many cases in mountain areas where needs for engineering consideration are not stringent.

The first step towards coping with slope stability problem during earthquakes will thus be to develop a methodology to define strength-deformation characteristics of natural soil deposits under slopes. One possible approach to this goal has been suggested in the preceding pages of this paper and other methods will undoubtedly be used for this purpose. For further progress, the aquisition of more test data on soil properties appears to be a necessary prerequisite.

6. As is the case with the conventional slope stability problems, the assessment of the seismic stability of slopes can not be successfully made unless detailed consideration is given to local geological and hydrological conditions prevailing in areas of landsliding. In view of this, studies of individual cases of earthquake-triggered landslides are extremely important to obtain a better understanding of the phenomena and to develop a truly realistic and meaningful state-of-the-art in this subject area. It is suggested herein that the most frequently encountered cases are landsliding in areas of residual soils such as weathered shales, weathered limestones and volcanic soils. Case studies of slope failures in these areas during earthquakes should be encouraged.

ACKNOWLEDGEMENTS

During the review of literatures and evaluation of case records, the writer has received much help from Professor K. Talaganov, University of Kiril and Methodij, Skopje, Yugoslavia ; Professor, J. U. Hung of National Taiwan University, Taipei ; Dr. V. Perlea of Research Institute of Hydraulic Engineering, Bucharest, Romania ; Mrs. Liu Huishan of Central Research Institute of Building and Construction, Ministry of Metallurgy Industry, Beijing, China ; Professor L. T. Youd of Brigham Young University and Dr. K. Kawashima of Public Works Research Institute, Ministry of Construction, Japan.

Professor Y. Yoshimi of Tokyo Institute of Technology kindly offered the information on liquefaction case records and Professor L. W. D. Finn of University of British Columbia provided invaluable suggestion on the writing of this report. The kindest offer was provided by Professor H. B. Seed of University of California for the enormous work to review the original manuscript of this paper.

Most of the recent test data introduced in this paper are those obtained by K. Haga for his batchelor degree and by H. Nagase for his PhD dissertation at the University of Tokyo.

The author wishes to express his deep and sincere thanks to all the persons as above for their kindnesses and overall cooporations. Thanks are also to be expressed to the colleague, Mr. K. Sugo, for his enormous work for drawing all the figures demonstrated in this paper.

REFERENCES

Anicic, D., Berz, G., Boore, D., Bouwkamp, J., Hakenbeck, U., McGuire, R., Sims, J. and Wieczorek, G. (1980), "Reconnaissance Report, Monte Negro, Yugoslavia Earthquake April 15, 1979," Earthquake Engineering Research Institute, Berkeley, California.

Arulanandan, K., Harvey, S. J. and Chak, J. S. (1981), "Electrical Characterization of Soil for In-Situ Measurement of Liquefaction Potential," International Conference on Recent Advances in Geotechnical Earthquake Engineering and Soil Dynamics," St. Louis, Vol. III, pp. 1223-1229.

Botea, E., Perlea, V and Perlea, M. (1980), "Liquefaction Susceptibility of Sand Deposits in the Danube Flood Plain," Proc. 6th Danube-European Conference on Soil Mechanics and Foundation Engineering, Varna, Bulgaria, pp.51-64.

Casagrande A. (1933), "Research on the Atterberg Limits of Soils," Public Roads, Vol. 13, pp. 121-136.

Castro, G. (1975), "Liquefaction and Cyclic Mobility of Saturated Sands," Proc. ASCE, Vol. 101, GT6, pp.551-569.

Chang, F. K. (1976), "An Empirical Interpretation of the Effects of Topography on Ground Motion of the San Fernando, California, Earthquake, 9 February 1971," Miscellaneous paper S-76-1, U. S. Army Engineer Waterways Experiment Station, Vicksburg, Miss.

Coulter, H. W. and Migliaccio, R. R. (1966), " "Effects of the Earthquake of March 7, 1964 at Valdez, Alaska," Geological Survey Professional Papers 542-C, U.S. Department of the Interior.

Davis, L. L. and West, L. R. (1973), "Observed Effects of Topography on Ground Motion," Bulletin of the Seismological Society of America, Vol. 63, No.1, pp.283-298.

Deere, D. U. and Patton (1971), "Slope Stability in Residual Soils," Proc. 4th Panamerican Conference on Soil Mechanics and Foundation Engineering, Puerto Rico, Vol. 1, pp.87-170

Dixon, S. J. and Burke, J. W. (1973), "Liquefaction Case History," Proc. ASCE, Vol. 99, SM11, pp.921-937

Dobry, R., Powell, D. J., Yokel, F. Y. and Ladd R. S. (1980), "Liquefaction potential of Saturated Sand-The Stiffness Methos," Proc. 7th World Conference on Earthquake Engineering, Istanbul, Vol. 3, pp.25-32.

Espana, C., Chaney, R. C. and Duffy, D. (1978), "Cyclic Strengths Compared for Two Sampling Methods," Soil Sampling and its Importance to Dynamic Laboratory Testing, ASCE National Convention. Chicago, pp.287-319.

Finn, W. D. L. (1981), "Liquefaction Potential ; Developments Since 1976," International Conference on Recent Advances in Geotechnical Engineering and Soil Dyanmics, St. Louis, Vol. Vol. 2, pp.655-681.

Finn, W. D. L. (1982), "Soil Liquefaction Studies in the People's Republic of China," Soil Mechanics-Transient and Cyclic Loads, John Wiley and Sons Ltd. pp.609-626.

Frydman, S., Hendron, D., Horn, H., Steinbach, J., Baker, R. and Shaal, B. (1980), "Liquefaction Study of Cemented Sand," Proc. ASCE, Vol. 106, GT.3, pp.275-297.

Gao, Z., Hu, B. and Chang, D. (1983), "Some Geological Considerations for the damage during the Tangshan Earthquake," North China Earthquake Sciences, Vol.1, pp.64-72 (In Chinese).

Haga, K. (1984), "Shaking Table Tests for Liquefaction of Gravel-Containing Sand," Bachelor Thesis, Department of Civil Engineering, University of Tokyo, (In Japanese).

Horn, H. (1978), "North American Experience in Soil Sampling and its Influence on Dynamic Laboratory Testing," Soil Sampling and Its Importance to Dynamic Laboratory Testing, ASCE National Convention, Chicago, Illinois, pp.113-178.

Hung, J. (1977), "General Report on Rock Slides in Taiwan," Proc. Advisory Meeting on Earthquake Engineering and Landslides, Taipei, pp.126-142.

Hung, J. (1980), "A Study on Tsaoling Rockslides, Taiwan," Journal of Engineering Environment, No.1, pp.29-39.

Ishihara, K. (1977), "Simple Method of Analysis for Liquefaction of Sand Deposits during Earthquakes," Soils and Foundations, Vol. 17, No.3,pp.1-17.

Ishihara, K. (1979), "Evaluation of Liquefaction Potential in the Tokyo Bay Area," Report to Metropolitan Office

Ishihara, K. and Ogawa, K. (1978), "Liquefaction Susceptibility Map of Downtown Tokyo," Proc. 2nd Inbernational Conference on Microzonation for Safer Construction, Vol. 2, pp.897-910.

Ishihara, K. and Koga, Y. (1981), "Case Studies of Liquefaction in the 1964 Niigata Earthquake," Soils and Foundations," Vol. 21, No.3, pp.35-52

Ishihara, K. and Koyamachi, N. and Kasuda, K. (1984), "Strength of a Cohesive Soil in Irregular Loading," Proc. 8th World Conference on Earthquake Engineering, San Francisco, Vol. 3, pp.7-14.

Ishihara, K. and Nagao, A. (1981), "Strength of Weathered Tuff under Irregular Dynamic Loading Conditions," Proc. International Symposium on Weak Rock, Tokyo, Vol. 2, pp.1217-1222.

Ishihara, K. and Nagao, A. and Mano, R. (1983), "Residual Strain and Strength of Clay under Seismic Loading," Proc. 4th Canadian Conference on Earthquake Engineering, pp.602-613.

Ishihara, K. and Perlea, V. (1984), "Liquefaction-Associated Ground Damage during the Vrancea Earthquake of March 4, 1977," Soils and Foundations. Vol. 24, No.1, pp.90-112.

Ishihara, K. and Silver, M. L. (1977), "Large Diameter Sand Sampling to Provide Specimens for Liquefaction Testing," Soil Sampling, 9th International Conference on Soil Mechanics and Foundation Engineering, Tokyo, pp.1-6.

Ishihara, K. and Silver, M. L. and Kitagawa, H. (1978), "Cyclic Strengths of Undisturbed Sands Obtained by Large Diameter Sampling," Soils and Foundations, Vol. 18, No.4, pp.61-76.

Ishihara, K. Silver, M. L. and Kitagawa, H. (1979), "Cyclic Strength of Undisturbed Sands Obtained by a Piston Sampler," Soils and Foundations, Vol. 19, No.3, pp.61-76.

Ishihara, K., Tatsuoka, F., and Yasuda, S. (1975), "Undrained Deformation and Liquefaction of Sand under Cyclic Stresses," Soils and Foundations," Vol. 15, No.1, pp.29-44.

Ishihara, K., Troncoso, J., Kawase, Y. and Takahashi, Y. (1980), "Cyclic Strength Characteristics of Tailings Materials," Soils and Foundations, Vol. 20, No.4, pp.127-142.

Ishihara, K. and Yamazaki, F. (1980), "Cyclic Simple Shear Tests on Saturated Sand in Multi-Directional Loading," Soils and Foundations, Vol. 20, No.1, pp.45-59.

Ishihara, K. and Yasuda, S. (1973), "Sand Liquefaction under Random Earthquake Loading Condition," Proc. 5th World Conference on Earthquake Engineering, Rome Session 1D, 38.

Ishihara, K. and Yasuda, S. (1975), "Sand Liquefaction in Hollow Cylinder Torsion under Irregular Excitation," Soils and Foundations, Vol. 15, No.1, pp.45-59.

Ishihara, L, Yasuda, S., and Yokota, K. (1981), "Cyclic Strength of Undisturbed Mine Tailings," International Conference on Recent Advances in Geotechnical Earthquake Engineering and Soil Dynamics, St. Louis. Vol. 1, pp.53-58.

Iwasaki, T., Kawashima, K. T., Asae and K. Nadano (1980), "Seismic Stability Analysis of Slopes in Road Cuts, Report ISSN 0386-5878, Public Works Research Institute, Ministry of Construction of Japan. (In Japanese).

Iwasaki, T., Tatsuoka, F., Tokida, K. and Yasuda, S. (1978), "A practical Method for Assessing Soil Liquefaction Potential Based on Case Studies at Various Sites in Japan," Proc. 2nd International Conference on Microzonation for Safer Construction-Research and Application. Vol. 2, pp.885-896.

Janbu, N. (1955), "Application of Composite Slip Surface for Stability Analysis," Proc. European Conference on Stability of Earth Slopes, Stockholm, (3), pp.43-49.

Japan Highway Association (1980), Seismic Design Code of Highway Bridge.

Kishida, H. (1966), "Damage to Reinforced Concrete Buildings in Niigata City with Special Reference to Foundation Engineering," Soil and Foundation, Vol. 6, No.1, pp.71-88.

Koizumi, Y. (1966), "Changes in Density of Sand Subsoil Caused by the Niigata Earthquake," Soil and Foundation, Vol. 6, No.2, pp.38-44.

Kokusho, T., Yoshida, Y., Nishi, K. and Esashi, Y. (1983a), "Evaluation of Seismic Stability of Dense Sand Layer (Part 1) - Dynamic Strength Characteristics of Dense Sand," Report 383025. Electric Power Central Research Institute, Japan (In Japanese).

Kokusho, T., Yoshida, Y. and Esashi, Y. (1983b), "Evaluation of Seismic Stability of Dense Sand Layer (part 2) - Evaluation Method by standard Penetration Test," Report 383026, Electric Power Central Research Institute, Japan (In Japanese).

Kvasnicke, P. (1984), Private Communication at the University of Zagreb, Yugoslavia.

Luong, M. P. (1980), "Stress-Strain Aspect of Cohesionless Soils under Cyclic and Transient Loading," International Symposium on Soils under Cyclic and Transient Loading, Swansea, Balkema, Vol. 1, pp.315-324.

Mandrescu, N. (1978), "The Vrancea Earthquake of March 4, 1977 and the Seismic Microzonation of Bucharest," Proc. 2nd International Conference on Microzonation for Safer Construction-Research and Application, San Francisco, Vol. 1, pp. 399-411.

Mandrescu, N. (1981), "The Romanian Earthquake of March 4, 1977 ; Aspects of Soil Behavior," Revue Roumaine de Geologie Geophysique et Geographie, Vol. 25, pp.35-56, (In Romanian).

Marcuson, W. F. and Franklin, A. G. (1979), "State of-the-Art of Undisturbed Sampling of Cohesionless Soils,' Proc. International Symposium on Soil Sampling, Singapore, pp.57-71.

Meyerhof, G. G. (1957), Discussion, Proc. 4th International Conference on Soil Mechanics and Foundation Engineering, Vol. 3, p.110.

Mori, H. and Koreeda, K. (1979), "State-of-the Art Report on the Current Practice of Sand Sampling," Proc. International Symposium on Soil Sampling, Singapore, pp.73-93.

Mori, K. and Ishihara, K. (1979), "Undisturbed Block Sampling of Niigata Sand," Proc. 6th Asian Regional Conference of Soil Mechanics and Foundation Engineering, Singapore, Vol. 1, pp.39-42.

Nagase, H. (1985), "Behavior of Sand in Multi-directional Irregular Loading," PhD dissertation, Department of Civil Engineering, University of Tokyo (In Japanese).

Ohashi, A., Iwasaki, T. and Kawashima, K. (1978), "Estimate of Shaking Intensity during the January 1978 Izu-Ohshima-Kinkai Earthquake Based on Overturning of Tomb Stones," Report of the Public Works Research Institute of Japan, No.1399. (In Japanese).

Ohsaki, Y. (1966), "Niigata Earthquake, 1964 Building Damage and Condition," Soil and Foundation, Vol. 6, No.2, pp.14-37.

Osterberg, J. O. (1952), "New Piston Type Soil Sampler," Engineering News Records, April 24, pp.77-78.

Peck R. B., Hanson, W. E. and Thornburn, T. H. (1974), Foundation Engineering, 2nd Ed. Wiley, New York, pp.113-115.

Perlea, V. (1981), Penel Discussion, Proc. 10th International Conference on Soil Mechanics and Foundation Engineering, Stockholm, Vol. 4, pp.872-876.

Perlea, V. (1983), Private Communication

Petrovski, J. and Paskalov, T. (1981), "The Monte Negro, Yugoslavia Earthquake of April 15, 1979," Institute of Earthquake Engineering and Engineering Seismology, University "Kiril and Methodij" Stopje, Yugoslavia.

Pyke, R. M., Seed, H. B. and Chan, C. K. (1975), "Settlement of Sands under Multi-Directional Shaking," Proc. ASCE, GT4, Vol. 101, pp.370-398.

Seed, H. B. (1979), "Soil Liquefaction and Cyclic Mobility Evaluation for Level Ground during Earthquakes," Proc. ASCE, Vol. 105, GT2, pp. 201-255.

Seed, H. B., Arango, I., Chan, C. K., and Ascoli, R. G. (1981), "Earthquake-Induced Liquefaction Near Lake Amatitlan, Guatemala," Proc. ASCE, Vol. 107, GT4, pp.501-518.

Seed, H. B. and Idriss, I. M. (1971), "Simplified Procedures for Evaluating Soil Liquefaction Potential," Proc. of ASCE, Vol. 97, SM9, pp. 1249-1273.

Seed, H. B. and Idriss, I. N. (1981), "Evaluation of Liquefaction Potential of Sand Deposits Based on Observations of Performance in Previous Earthquake," Preprint 81-544, In-Situ Testing

to Evaluate Liquefaction Susceptibility ASCE National Convention. St. Louis.

Seed, H. B., Idriss, I. M., and Arango, I. (1983), "Evaluation of Liquefaction Potential Using Field Performance Data," Proc. ASCE, Vol. 109, GT3, pp.458-482.

Seed, H. B. and Lee, K. L. (1966), "Liquefaction of Saturated Sand during Cyclic Loading," Proc. ASCE, Vol. 91, SM6, pp.105-134.

Seed, H. B., Lee, K. L., Idriss, I. M., and Makdisi, F. I. (1975), "The Slides in the San Fernando Dams during the Earthquake of February 9, 1971," Proc. ASCE, Vol. 101, GT7, pp.651-688.

Seed, H. B., Pyke, R. M. and Martin, G. R. (1978), "Effect of Multi-Directional Shaking on Pore Pressure Development of Sands," Proc, ASCE, GT1, Vol. 104, pp.27-44.

Shi Zhaoji (1984), "Formulae for Identifying Liquefiability of Clayey Sands," Report 84-013, Institute of Engineering Mechanics, Academia Sinica, Hafbin (In Chinese).

Shibata, T. (1981), "Relations between N-value and Liquefaction Potential of Sand Deposits," Proc. 16th Annual Convention of Japanese Society of Soil Mechanics and Foundation Engineering, pp.621-624, (In Japanese).

Talaganov, K. and Aleksovski (1984), "Soil Stability and Urban Design Case Study," Proc. 8th World Conference on Earthquake Engineering, San Francisco, Vol. 3, pp.453-460.

Talaganov, K., Galbov, S. and Bogoevski, T. (1981), "Characteristics of Liquefied Sands during the April 15, 1978 Monte Negro Earthquake," Proc. 15th National Conference of Yugoslavian Society of Soil Mechanics and Foundation Engineering, Ohrid, pp.119-134, (In Macedonian).

Tatsuoka, F., Iwasaki, T., Tokida, K., Yasuda, S., Hirose, M., Imai, T. and Kon-no, M. (1980), "Standard Penetration Tests and Soil Liquefaction Potential Evaluation," Soils and Foundations, Vol. 20, No. 4, pp. 95-111.

Tohno, I. and Yasuda, S. (1981), "Liquefaction of the Ground during the 1978 Miyagiken-oko Earthquake," Soils and Foundations, Vol. 21, No. 3, pp. 18-34.

Tokimatsu, K. and Yoshimi, Y. (1983), "Empirical Correlation of Soil Liquefaction Based on SPT N-Value and Fines Content," Soils and Foundations, Vol.23, No.4, pp.56-74.

Tsuchida, (1970), "Prediction and Countermeasure against the Liquefaction in Sand Deposits," Abstract of the Seminar in the Port and Harbor Research Institute, pp.3.1, 3.33 (In Japanese).

Wang Wenshao (1984), "Earthquake Damages to Earth Dams and Levees in Relation to Soil Liquefaction and Weakness in Soft Clays," Proc. of the International Conference on Case Histories in Geotechnical Vol. 1, pp.511-521.

Wang, Z. Q. (1981), "Macroscopic Approach to Soil Liquefaction," Proc. International Conference on Recent Advances in Geotechnical Earthquake Engineering and Soil Dynamics, St. Louis, Vol. 1, pp.179-185.

Wang, Z. Q., Fang, H. Q. and Zhao, S. D. (1983), "Macroscopic Features of Earthquake-Induced Soil Liquefaction and its Influence on Ground Damage," Canadian Geotechnical Journal, Vol. 20, No.1, pp.61-68.

Wong, R. T., Seed, H. B. and Chan, C. K. (1975), "Cyclic Loading Liquefaction of Gravelly Soils," Proc. ASCE, GT6, pp.571-583.

Xie, Junfei. (1979), "Empirical Criteria of Sand Liquefaction," Special Session on Earthquake Engineering in China, 2nd U.S. National Conference on Earthquake Engineering, Stanford University, pp.22-24.

Yamazaki, A. (1984), "Wave-Induced Liquefaction in the Seabed Deposit," Master thesis, Department of Civil Engineering, University of Tokyo.

Yoshimi, Y., Hatanaka, M. and Oh-Oka, H. (1978), "Undisturbed Sampling of Saturated Sands by Freezing," Soils and Foundations," Vol. 18, No.3, pp.59-73.

Yoshimi, Y., Richart, F. E., Prakash, S., Balkan, D. D., and Ilyichev (1977), "Soil Dynamics and its Application to Foundation Engineering," State-of-the-Art Report, Proc, 9th International Conference on Soil Mechanics and Foundation Engineering, Tokyo, Vol. 2, pp.605-650.

Yoshimi, Y., Tokimatsu, K. and Ohoka, H. (1983), "On the Earthquake Resistant Strength of Saturated In-Situ Sand," Proc. Japan National Symposium on the Ground Damage during Earthquakes, pp.113-118, (In Japanese).

Youd, T. L. and Bennett, M. J. (1983), "Liquefaction Sites, Imperial Valley, California," Proc. ASCE, Vol. 109, GT3, pp.440-457.